

2009

# Development of a Rate of Injection Bench and Constant Volume Combustion Chamber for Diesel Spray Diagnostics

Anthony Phan  
Iowa State University

Follow this and additional works at: <https://lib.dr.iastate.edu/etd>

 Part of the [Mechanical Engineering Commons](#)

## Recommended Citation

Phan, Anthony, "Development of a Rate of Injection Bench and Constant Volume Combustion Chamber for Diesel Spray Diagnostics" (2009). *Graduate Theses and Dissertations*. 10691.  
<https://lib.dr.iastate.edu/etd/10691>

This Thesis is brought to you for free and open access by the Iowa State University Capstones, Theses and Dissertations at Iowa State University Digital Repository. It has been accepted for inclusion in Graduate Theses and Dissertations by an authorized administrator of Iowa State University Digital Repository. For more information, please contact [digirep@iastate.edu](mailto:digirep@iastate.edu).

**Development of a rate of injection bench and constant volume combustion chamber for  
diesel spray diagnostics**

by

**Anthony Phan**

A thesis submitted to the graduate faculty  
in partial fulfillment of the requirements for the degree of  
MASTER OF SCIENCE

Major: Mechanical Engineering

Program of Study Committee:  
Song-Charng Kong, Co-major Professor  
Terrence Meyer, Co-major Professor  
Thomas Brumm

Iowa State University

Ames, Iowa

2009

## TABLE OF CONTENTS

LIST OF FIGURES	iv
LIST OF TABLES	vi
ACKNOWLEDGEMENTS	vii
ABSTRACT	viii
CHAPTER 1. INTRODUCTION	1
1.1 Motivation	1
1.2 Objective	3
CHAPTER 2. REVIEW OF LITERATURE	4
2.1 Introduction	4
2.2 Rate of Injection Metering	4
2.2.1 Importance of Rate of Injection	4
2.2.2 Rate of Injection Measurements	5
2.2 Optical Combustion Simulations	10
2.2.1 Combustion Simulation Techniques	10
2.2.2 Premixed Gaseous Combustion in CVPC	16
2.3 Diagnostics	19
2.3.1 Diesel Spray and Combustion	19
CHAPTER 3. METHODS AND PROCEDURES	21
3.1 Introduction	21
3.2 Rate of Injection Bench System Design	21
3.2.1 High Pressure Common Rail System and Controls	21
3.2.2 Rate of Injection Components	26
3.3 Rate of Injection Bench Testing Method	30
3.3.1 Pressure Measurement System Calibration	30
3.3.2 Data Acquisition and Control System	31
3.3.3 Rate of Injection Validation Study	32
3.4 Combustion Chamber System Design	39
3.4.1 CVHC Previous Test Setup	39
3.4.1 Redesigning of Window Seals	41
3.4.2 Premixed Combustion and Mixing Fan	42
3.4.3 Spark Ignition System	47
3.4.4 Data Acquisitions and Controls	48
CHAPTER 4. RESULTS AND DISCUSSIONS	53
4.1 Introduction	53
4.2 Rate of Injection Bench	53
4.2.1 High Pressure Common Rail System Injection Delay	53
4.2.2 Diesel Rate of Injections Using Baseline Injector	56
4.2.3 Biodiesel and Biodiesel Blend Rates of Injection	59
4.2.4 Rates of Injection for Different Injectors	60
4.2.5 Rate of Injection of Double Injection Scheme	62

4.3 Constant Volume Combustion Chamber	63
4.3.1 Ultra Fast Frame Rate PLIF Diesel Spray Revisit	63
4.3.2 Filling Process	68
4.3.3 Premixed Combustion	72
CHAPTER 5. CONCLUSIONS AND RECOMMENDATIONS	75
5.1 Conclusions	75
5.2 Future Recommendations	77
5.2.1 Injection Bench	77
5.2.2 Constant Volume Pre-Combustion Cell	77
APPENDIX A1. INJECTION BENCH OPERATING PROCEDURES	79
APPENDIX A2. INJECTION BENCH POST PROCESSING CODES	84
APPENDIX B1. DIESEL SPRAY IMAGING CODES	95
BIBLIOGRAPHY	98

## LIST OF FIGURES

Figure 2.1 - Bosch rate of injection metering schematic. ....	6
Figure 2.2 - Zuech rate of injection schematics. ....	8
Figure 2.3 - A comparison of the injection rate shape from the Bosch and Zuech rate of injection meter. ....	10
Figure 2.4 - Shell Thornton Research Centre rapid compression machine. ....	11
Figure 2.5 - Constant volume hot cell (CVHC) at Iowa State University. ....	12
Figure 2.6 - Sandia National Laboratory's CVPC. ....	13
Figure 2.7 - Sandia National Laboratory's ORE. ....	14
Figure 2.8 - Comparison of operating range of different optical test setup in simulating a heavy duty compression ignition engine. ....	15
Figure 2.9 - Schematic of the chamber (left) and inside the chamber (right) of Sandia National Laboratory CVPC. ....	17
Figure 2.10 - Pressure history of typical CVPC. ....	18
Figure 3.1 - Schematic of Denso common rail system. ....	22
Figure 3.2 - USB CAN2 250 adapter used to connect to L14 ECU/EDU. ....	23
Figure 3.3 - Sample generated crank and cam signal simulating 1000 rpm engine speed. ....	24
Figure 3.4 - Injection supply pump, AC motor and drive system (left), frequency inverter (right). ....	25
Figure 3.5 - Fuel supply pump and fuel filter (left), hand valve and dial gauges (right). ....	26
Figure 3.6 - Scaled, sectioned CAD drawing of the fuel passage side view cutaway(left) and top view cutaway(right). ....	27
Figure 3.7 - Injection bench meter with system components and high pressure injection system notions. ....	29
Figure 3.8 - Kistler 6125B pressure sensor with PCB 464A charge amplifier system calibration. ....	31
Figure 3.9 - Injection bench data acquisition and control system LabView front panel. ....	32
Figure 3.10 - Raw vs. corrected signal for double injection event. ....	34
Figure 3.11 - Bower and Foster observed fuel line pressure trace and rate of injection trace. ....	35
Figure 3.12 - PLIF images of diesel spray evolution using a single-hole nozzle injector with solenoid energizing time of 2 milliseconds. ....	36
Figure 3.13 - Validation study comparing integrated vs. weighted injected mass per injection event. ....	38
Figure 3.14 - CAD assembly of Chamber (left), exploited view of chamber assembly (right). ....	40
Figure 3.15 - Window cap with redesigned o-ring seal isometric view (left) and cutaway view with quartz window (right). ....	42
Figure 3.16 - Gaseous cylinders with air actuated valves. ....	44
Figure 3.17 - CAD renderings of the multipurpose housing assembly (left), cutaway view showing the motor, cooling coil, ball bearing, and shaft (middle), and isometric cutaway view (right). ....	46
Figure 3.18 - Multipurpose housing installed to the chamber with component notions (top) and Conax power lead glands (bottom). ....	47

Figure 3.19 - Spark ignition system: coils, ignition wires, and spark plugs (left) and fast SSR (right).	48
Figure 3.20 - PCB 1704M02 system calibration.	50
Figure 3.21 - Setra 280E system calibration.	50
Figure 3.22 - DAQ system and controls.	51
Figure 3.23 - Combustion vessel DAQ and control VI front panel.	52
Figure 4.1 - 6x133x800 injector characteristics with injection delay, energizing time, and injection duration definitions.	54
Figure 4.2- Common rail pressure fluctuation.	56
Figure 4.3 - 6x133x800 injector characteristics, effects of backpressure.	57
Figure 4.4 - 6x133x800 injector characteristics, effects of injector energizing time.	58
Figure 4.5 - 6x133x800 injector characteristics, effects of rail pressure.	59
Figure 4.6 - 6x133x800 injector rates of injection comparison using No 2 diesel, B20, and B100 with injection pressure of 100 MPa, 6.21 MPa back pressure, and 0.8 ms injector energizing time.	60
Figure 4.7 - Diesel rate of injection comparison for different injectors at 100 MPa injection pressure, 6.21 MPa back pressure, and 0.8 ms injector energizing time.	62
Figure 4.8 - Diesel rate of injection of double injection scheme.	63
Figure 4.9 - Scaled single-hole nozzle diesel spray PLIF images collected at 10 kHz with the CVHC temperature of 300 K and pressure of 3.5 MPa and with injection pressure of 100 MPa.	64
Figure 4.10 - Optical layout for burst-mode laser imaging of diesel sprays.	64
Figure 4.11 - Scaled single-hole nozzle diesel spray PLIF images collected at 10 kHz with the CVHC at ambient condition and with injection pressure of 100 MPa.	65
Figure 4.12 - Colorized raw image showing cuevette and spray PLIF (left) and setup for simultaneously imaging cuevette and diesel spray (right).	66
Figure 4.13 - Raw and colorized diesel PLIF with 355 nm wavelength (left) and with 266 nm wavelength (right).	67
Figure 4.14 - Linearization test using laser power meter detection.	68
Figure 4.15 - Linearization test using photodiode detection.	68
Figure 4.16 - Low pressure leak test using nitrogen.	69
Figure 4.17 - High pressure leak test using nitrogen.	70
Figure 4.18 - Pressure history of the filling process.	71
Figure 4.19 - Pressure and temperature traces acquired during premixed combustion with an input mixture of 689 kPa.	73
Figure 4.20 - Pressure trace acquired during premixed combustion at high acquisition rate with an input mixture pressure of 345 kPa.	74

**LIST OF TABLES**

Table 2.1 - Quality attributes of different optical test rigs.....	15
Table 3.1 - 6125B technical data. ....	28
Table 3.2 - Speed of sound correlations.....	33
Table 4.1 - Injection delay study results. ....	55

## ACKNOWLEDGEMENTS

I would like to first thank my major professors, Dr. Song-Chang Kong and Dr. Terrence Meyer for the unique opportunity to work in such special environments. Throughout my academic experience, they have provided exceptional support and guidance. I would also like to thank Dr. Thomas Brumm for taking the time to serve as my committee member.

This study was primarily funded by John Deere. I would like to acknowledge John Deere for providing funding and engineering support. In addition, I want to recognize Jim Dautremont and Larry Couture for providing their wealth of experience and knowledge.

I would like to thank all the graduate students in Dr. Kong's group and Dr. Meyer's group. In particular, I would like show appreciation to Matthias Veltman, Qingluan Xue, Justin Callies, Joseph Fuller, Aravind Vaidyanathan, and Joseph Miller. I would like to also thank the undergraduate research assistants in Dr. Kong's group: James Slawson, Nathan Gibilisco, Dan Apperson, Lukas Shea, and Dmitry Altshul. All of their support and friendship have made my experience at Iowa State University truly an enjoyable one.

Finally, I would like to thank my family and Pauline Nguyen. I will never forget the many sacrifices that were made to get me where I am today.

## ABSTRACT

To help understand the complex fuel spray combustion phenomena in modern diesel engine using high injection pressure, a fuel injection test bench and a constant volume combustion chamber were developed and demonstrated in this study for diesel spray diagnostics. Both facilities are significant when linking between spray injection and combustion dynamics and engine performance. This link is important to determine changes needed in order to optimize the performance of a diesel engine.

Combustion and emissions of a diesel engine are influenced by the rate of fuel injection which, in turn, is determined by the injection pressure, nozzle geometry, and fuel type. The rate of injection bench capable of studying a modern common-rail injection system was designed, fabricated, and demonstrated in this study. Experimental apparatus included a high pressure fuel pump, a fuel rail, a transient pressure transducer, and a data acquisition and control system. The rates of injection of different injectors with various nozzle diameters and spray angles injecting different types of fuel under different injection schemes were investigated. Results of this study showed that for the same injector, the differences in the rates of injection were negligible under the same injection conditions with variations only in the back pressure from 2.07 MPa to 6.21 MPa. When injection pressure was increased from 75 MPa, to 100 MPa, and to 150 MPa more fuel was injected and the rise and decay of the injection rate also increased. This indicated that fuel exited the nozzle at a faster rate. Subsequently, as injection pressure was increased, a higher peak injection rate was seen. If the same fuel quantity was desired, injection duration was shortened. When comparing the rate of injection for diesel and biodiesel blend (i.e, B20 and B100), the rates of injection were comparable but the injected mass of biodiesel was slightly higher because biodiesel has a slightly higher density. On the other hand, the difference in the

delay between the electronic injection signal and the onset of injection was negligible for diesel and biodiesel blends using the current common-rail system. Additionally, the rate of injection for the double injection scheme was also studied and results showed that the shape of individual injection in the multiple injection schemes was similar to that of single injection.

To further understand the engine in-cylinder combustion process, a constant volume combustion chamber was also developed and demonstrated in this study. With optical access provided by quartz windows, experiments using modern laser imaging and spectroscopy were performed to further understand high-speed diesel fuel jet development. The previous experiment was revisited using a superior camera to capture higher quality images to study the diesel spray structure. The previous constant volume heated chamber was then converted to a constant volume pre-combustion chamber. During this conversion, seals were redesigned and new O-rings seals were utilized. In addition, a high speed mixing fan, powerful ignition system, and data acquisition and control system were implemented. After the conversion, it was demonstrated that the new combustion chamber could attain temperature up to 919 K while showing negligible leaks. Even higher temperature and pressure could be attained if more combustible gas mixture was inputted. The combustion chamber developed in this study can be readily utilized to study high-speed diesel jet combustion under high-pressure and high-temperature environments.

## CHAPTER 1. INTRODUCTION

### 1.1 Motivation

The topics of reducing oil dependence, climate change, and operating cost, and increasing energy sustainability have been the prime drivers in the automotive industry. With the diminishing world oil supplies, harmful greenhouses gaseous emission, desire to increase efficiency and becoming more energy dependent, everyone is forced to rethink how things are done on a fundamental level. With recent and stricter changes to government mandates, these foci are more transparent than ever.

Ever since the internal combustion (IC) engine concept was envisioned and developed in the late 1800s, it has significantly impacted our world. Due to its relatively low cost, straightforward and robust characteristics, relatively high efficiency, and favorable power to weight ratio, the application of the IC engine has become the dominant prime mover technology in many applications such as vehicular, railroad, marine, aircraft, home use and stationary power generation (Ferguson and Kirkpatrick, 2001). The IC engine can be characterized as either spark ignition or compression ignition. Either class has had over a century of research and development and has been considered by some to have reached its peak and to have little potential for further improvement remaining (Heywood, 1988). However, this is not the case. Due to continuing and significant improvements in materials, technologies and combustion strategies, there are substantial improvements that can be made in efficiency, power, and emission controls. For example, the typical gaseous emissions during 1970s for a four-stroke, naturally aspirated diesel engine were 6.7-12.7 g/kWh, 2.1-4.5 g/kWh, and 3.5-5.5 g/kWh for

NO<sub>x</sub>, HC, and CO, respectively (Majewski and Khair, 2006). As of 1990s, the gaseous emissions for the same type of engine have drastically reduced by approximately 98% in NO<sub>x</sub>, 95% in HC, and 40% in CO (Majewski and Khair, 2006). These reduction percentages are only better as of today and going into the future. As we continue to put efforts in broadening our understanding through ongoing researches such remarkable improvements will continue.

The motivation behind fabricating and developing a rate of injection bench was to quantify the injection velocity profile of a diesel injector. Data obtained from the injection bench can be used to correlate injection profiles with signals obtained during engine testing. In addition, injection bench data are useful inputs for computational fluid dynamic (CFD) modeling programs and can provide the required fuel injection data for the constant volume combustion chamber testing as will be described below.

On the other hand, it is of great importance to explore the details of spray combustion process. A constant volume combustion chamber can provide a simulated environment for studying the spray structures. The combustion chamber, coupled with the state-of-art imaging and spectroscopy technologies have proven to be a very useful tool for understanding what really happens inside a diesel engine. Both the injection bench and the combustion chamber are valuable tools for researchers to understand the complex spray combustion mechanism powering the compression ignition engine. While the knowledge gained from the injection bench and combustion chamber studies may have diminutive or substantial impact to our understanding of the IC engine, it may be reminded that only a small gain in engine performance and tailpipe emission is needed in order to make an enormous impact in reducing oil dependency, reducing climate change, reducing operating cost, and increasing energy sustainability.

## 1.2 Objective

The objective of this study was to design and develop an injection metering bench to obtain the fuel injection profiles. After completion, validation was carried out and injection profiles of different injectors using different types of fuels with various nozzle diameters, spray angles, and flow numbers were obtained to investigate the effects of back pressure, fuel quantity, and the injection pressure on the injection profile. The injection rate data can be used for computer simulation and can also provide detailed fuel injection characteristics during engine operation. The other objective was to implement a constant volume chamber that could simulate the engine in-cylinder high temperature and high pressure conditions. The chamber is expected to be used with modern laser and spectroscopy techniques to understand many important spray combustion and emission formation mechanisms.

Although useful, data from traditional engine testing do not typically provide visual and/or sufficient information about the injection and in-cylinder combustion events. By characterizing the rates of injection and diagnosing the in-cylinder combustion process, researchers can really understand what happens inside the engine. It is important to link between injection and combustion dynamics and engine performance to determine changes needed in order to optimize the performance of an engine.

## CHAPTER 2. REVIEW OF LITERATURE

### 2.1 Introduction

Government regulations have become a major driving force for diesel engine research and development. As regulations become more stringent, the fundamental knowledge about fuel spray behaviors and combustion mechanisms becomes more critical. To understand these phenomena, researchers must critically analyze what really happens inside an engine. Due to the significant amount of work performed by researchers in the past, this section only highlights spray and combustion literature relevant to the progression of the present study.

### 2.2 Rate of Injection Metering

#### 2.2.1 Importance of Rate of Injection

Emission mandates have driven many researches and the development of many new high pressure injection systems as a way to improving the combustion process in the compression ignition engine. The process of mixing fuel with air is determined by the injection characteristic, air movement, and the combustion chamber. Out of all these factors, injection characteristic is the most important factor since fuel carries high momentum and kinetic energy as it exits the injector nozzle to promote mixing. With higher injection pressure, fuel exits the injector better atomized for enhanced mixing, which can result in less PM (particulate matters) after combustion (e.g., Karra and Kong). The rate of injection is therefore an important parameter to obtain because it characterizes the injection event. This is the strongest precursor for combustion.

Moreover, many researchers have demonstrated the use of multiple injection strategies and the use of different injector nozzles with different flow characteristics in different scenarios to optimize combustion (Karra and Kong, 2008; Kim and Lee, 2007). As a result, better understanding for the rate of injection is considered essential. Data from the injection bench not only can provide rates of injection but also can provide detailed timing characteristics between injection events of multiple injection strategies.

Furthermore, with the popular use of alternative fuels, there is higher significance in obtaining the rate of injection. Alternative fuels such as biofuel made from vegetables and animal fats have become increasingly popular because they offer reduced energy dependency from foreign oil. However, due to significance differences in fluid properties when compared to the conventional diesel fuel, the rates of injection from these alternative fuels are necessary to optimize its combustion process in the compression ignition engine.

### **2.2.2 Rate of Injection Measurements**

The rate of injection, also known as the injection profile, is defined as the shape of instantaneous mass flow rate over a period of time. There are two popular methodologies to characterize the injection profile. The first is the Bosch type, which has been the standard measurement tool since the development of the Bosch injection system (Bosch, 1966). The second is the Zuech type (Takamura, Fukushima, and Omori, 1989).

The most frequently applied method of measuring the injection rate today is the Bosch measuring method (Marcic, 2003). This method has overcome scrutiny by many researchers. The most conclusive one was done by Bower and Foster (1991) where they compared the Bosch and Zuech injection benches and concluded that both systems predict the same magnitude and

shape of injection. The principle of the Bosch rate of injection meter is to measure pressure wave that is produced when an injector injects compressible fluid to correlate an injection profile using the pressure-velocity equation valid for a single pressure wave. A schematic of the Bosch rate of injection metering can be seen in Figure 2.1 (Bower and Foster, 1989).

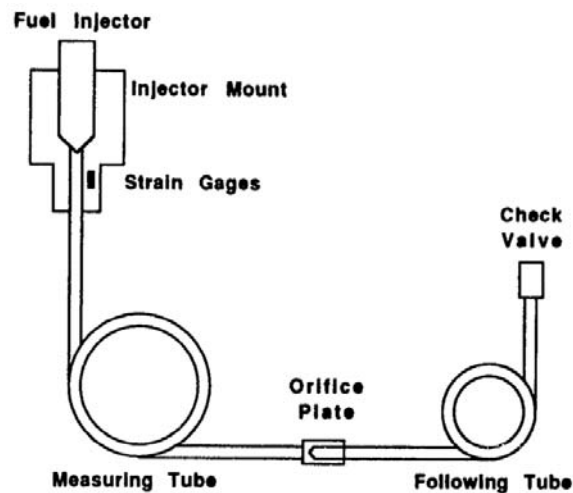


**Figure 2.1 - Bosch rate of injection metering schematic.**

Fuel fed to the injector is driven by a high pressure injection system and the injector is mounted into the injector mount so that the tip is at the beginning of the measuring tube. As the fluid is injected, a pressure wave is created and measured by a pressure sensor that is also mounted on the injector housing. Between the measuring and the following tube is an orifice plate. The size of the orifice controls what portion of the pressure wave is reflected and what portion enters the following tube. When too much fuel enters the following tube, a negative pressure wave will be reflected into the measuring tubing and the opposite is true if not enough fuel enters the following tube. Both will produce undesirable and unreal rate of injection. The

theory behind the Bosch rate of injection measurement is the pressure-velocity equation valid for a single wave in nonstationary flow (Bower and Foster, 1991). This equation makes the assumption of one dimensional motion but was later investigated by Matsuoka to hold true (Matsuoka, 1996). This equation is given below in Eq. (2.1). When Eq. (2.1) is combined with the conservation of mass equation, Eq. (2.2), the governing equation for the Bosch rate of injection meter is derived, i.e., Eq. (2.3). The integration of Eq. (2.3) will equate the injected mass,  $m$ .

$$P = c \times \rho \times u \quad (2.1)$$

$$\frac{dm}{dt} = \rho \times u \times A \quad (2.2)$$

$$\frac{dm}{dt} = \frac{A}{c} \times P \quad (2.3)$$

where:

$P$  = Pressure

$c$  = Speed of Sound in Fluid

$\rho$  = Density of Fluid

$u$  = Flow Velocity

$m$  = Mass of Fuel

$A$  = Area

Different from the Bosch concept of obtaining the rate of injection, the Zuech concept relies on an internal pressure measurement of a constant volume chamber into which fuel is injected in order to correlate the injection profile. As the mass of the fuel enters the chamber, the internal pressure of the chamber must increase. Using the derivative of the constant volume chamber pressure, the injection rate shape was obtained. A schematic of the Zuech rate of injection meter can be seen below in Figure 2.2 (Bower and Foster, 1991).

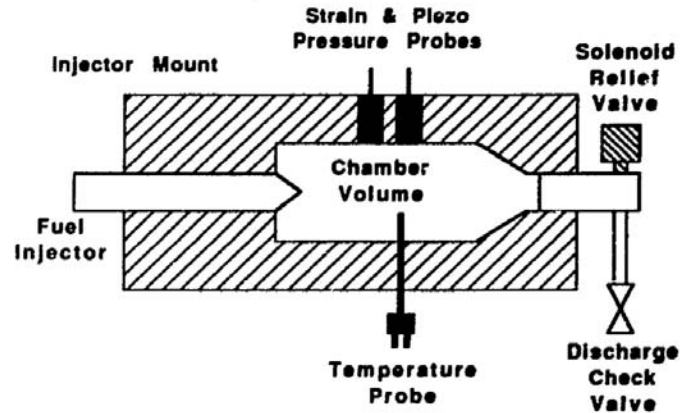


**Figure 2.2 - Zuech rate of injection schematics.**

Along with a high pressure injection system to feed fuel to an injector, the Zuech rate of injection meter consists of a chamber equipped with pressure and temperature instrumentations and a solenoid relief valve. The injector is mounted so that the tip is at the beginning of the chamber volume. Before injection, the chamber is filled with fuel and the solenoid valve is then closed. As fuel enters the chamber through the injector nozzle, the pressure inside the chamber increases proportionally to the injection quantity. Consequently, the injection rate is measured by detecting the volume of fuel injected into the chamber of a known and fixed volume. After the end of the injection event, the solenoid valve opens and discharges the fuel along with the pressure buildup. To understanding the governing equation of the Zuech type meter, the bulk modulus of the fuel needs to be define. The bulk modulus of the fuel is a function of pressure and temperature and is define as the change in pressure due to the change in volume multiple by the original volume, Eq. (2.4), (Takamura, Fukushima, and Omori, 1989). The fuel bulk modulus values must be known to a high degree of accuracy to produce a correct rate of injection because the temperature in the chamber changes as a result of compression work during injection (Bower

and Foster, 1991). When combining the fuel bulk modulus with the conservation of mass, Eq. (2.2), the governing equation for the Zuech rate of injection meter is derived, i.e., Eq. (2.5).

$$K = V \times \frac{dP}{dt} \quad (2.4)$$

$$\frac{dm}{dt} = \rho \times \frac{V}{K} \times \frac{dP}{dt} \quad (2.5)$$

where:

$K$  = Bulk Modulus of the Fuel

$V$  = Chamber Volume

When compared to the Bosch type rate of injection meter, the Zuech type was more accurate at predicting injected volumes (Bower and Foster, 1991). However, signals obtained from the Bosch injection meter were much smoother. Signals from the Zuech injection rate meter need high frequency noise elimination from filters such as the Bessel low-pass filter (Takamura, Fukushima, and Omori, 1989). This can be seen in Figure 2.3. To reduce noise and improve accuracy, injection profile obtained from the Zuech type meter are typically ensemble averaged over many injection events. Conclusively, both systems predict the same magnitude and shape of injection. The Zuech type meter requires a time phasing between the injection event and the solenoid valve operation while the Bosch type meter requires no timing between the injection system and rate of injection meter (Bower and Foster, 1991).

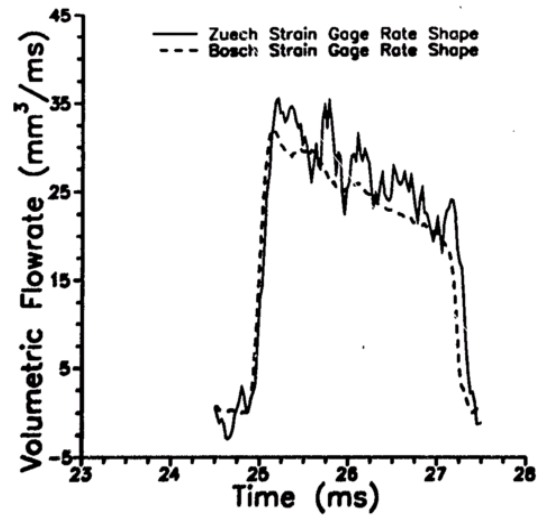


**Figure 2.3 - A comparison of the injection rate shape from the Bosch and Zuech rate of injection meter.**

## 2.2 Optical Combustion Simulations

### 2.2.1 Combustion Simulation Techniques

The ability to look inside the engine to diagnose the combustion process is a decisive and key path in maximizing the overall performance of the engine. There are many solutions which offer this ability and are as follow: rapid compression machines (RCM), rapid cycling machines (RCYM), constant pressure flow rigs (CPFR), constant volume hot cells (CVHC), constant volume pre-combustion cell (CVPC), and optical research engines (ORE). Each method will be described briefly below.

The RCM utilized a single compression stroke and a constant volume combustion event to model combustion in reciprocating engines. Figure 2.4 is a RCM at Shell's Thornton Research Centre. RCM has been used by many researchers to simulate a diesel engine (e.g., Kobayashi,

Kamimoto, and Matsuoka, 1981; Rife and Heywood, 1974). Though accurately simulating the in-cylinder combustion process, RCM are difficult and often costly to fabricate and operate. Notably, at the end of the compression stroke the machine undergoes strong vibrations which make it complicated to impose undistributed laser or imaging diagnostics.

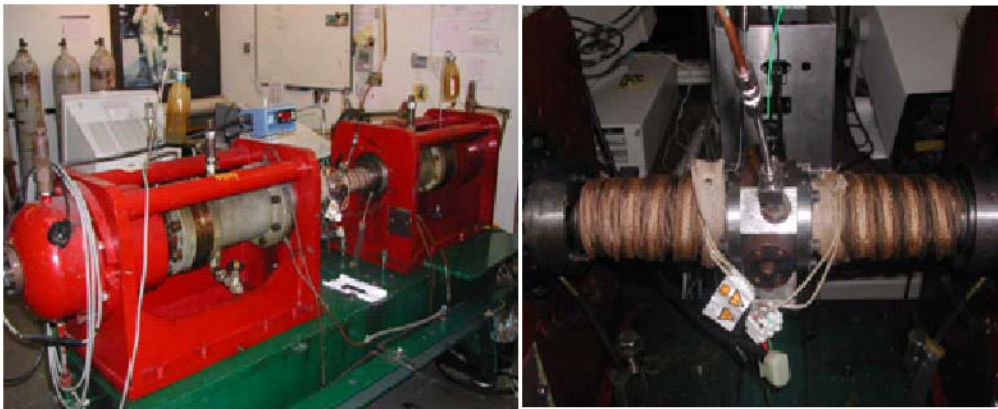


**Figure 2.4 - Shell Thornton Research Centre rapid compression machine.**

On the other hand, the rapid cycling machine (RCYM) uses a regular piston engine design and extends the combustion volume. This is typically achieved with a cylindrical combustion chamber that is part of the modified cylinder head. This extension chamber is made optically accessible to which diagnoses are made. Nonetheless, this small volume suffers from very small confinement and offers limited optical accessibility (Baert et al., 2009).

Differently, the constant pressure flow rig (CPFR) offers unconfined diesel combustion simulation (Negus et al., 1987). In this test setup a constant flow of hot, pressurized gas is set up in an optically accessible pipe. When fuel is injected parallel and against the flow, combustion would occur due to the high pressure and temperature environment. This method offers great

optical accessibility. However, the test setup is limited by a maximum pressure and temperature due to the pipe mechanics of material limitation. In addition, a powerful clean air compressing and heating system to simulate high pressure and temperature flow condition are needed (Baert et al., 2009).

Alternatively is the constant volume chamber method which can be separated into two categories CVHC and CVPC. In the CVHC, seen in Figure 2.5, pressurized air enters the chamber and is heated using heating elements. Fuel injection is triggered when the desired temperature and pressure is attained. A drawback of CVHC is the lengthy time needed to settle a target environment condition. Due to the length of time required, cooling for the injector is required in order to prevent damage and radiation heat transfer from the hot walls become a factor to the combustion process. Additionally, often there is an upper temperature limitation without a secondary heating source due to the heating element limitation.



**Figure 2.5 - Constant volume hot cell (CVHC) at Iowa State University.**

This temperature limitation does not exist with the more popular CVPC. In CVPC, a lean, premixed combustion (Oren, Wahiduzzaman, and Ferguson, 1984) is burnt raising the temperature and pressure of the chamber. In a sense, chemical energy release by combustion aids in setting the desirable environment for diesel combustion. By controlling the pressure, temperature, and composition of the premixed combustion constituents a very wide range of pressure and temperature prior to diesel fuel injection can be attained. For the same reason, this method is also able to simulate different levels of EGR. Seen in Figure 2.6 is Sandia National Laboratory's CVPC (Pickett, 2007). Conversely, both CVHC and CVPC suffer from having a different pressure history during combustion and fuel-air mixing than that of a real engine due to having a fixed volume. In addition, there are absences from spray/wall, spray/piston, and spray/spray interactions.

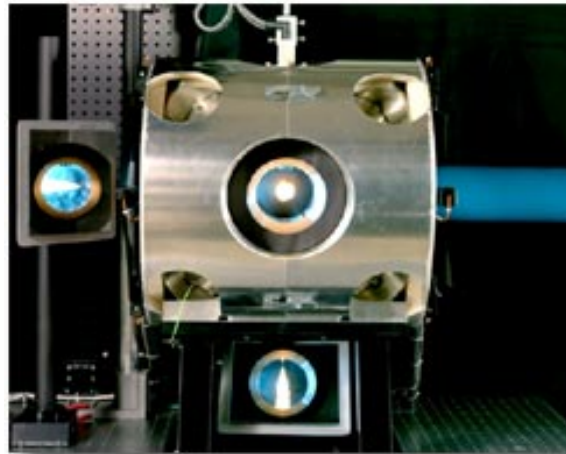


**Figure 2.6 - Sandia National Laboratory's CVPC.**

Finally, the ORE offers the spray/wall, spray/piston, and spray/spray interactions and resembles closest to the actual engine out of all the mentioned methods. Seen in Figure 2.7, optical accessibilities are provided in and on top of the extended cylinder head housing (Dec, 1997). However, due to the complexity of these engines, ORE are difficult to acquire or build and adapt diagnostic without careful design.

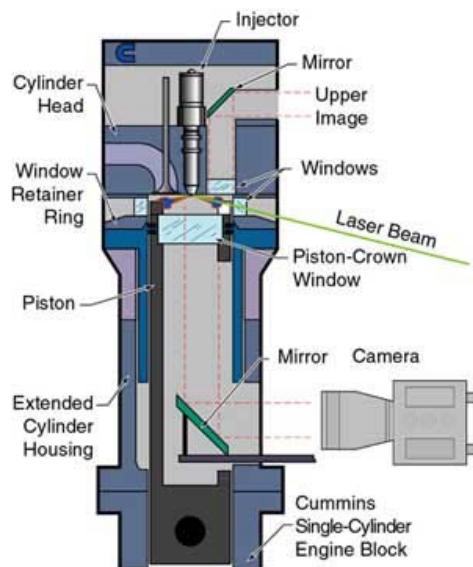


**Figure 2.7 - Sandia National Laboratory's ORE.**

Baert et al (2009) compared strengths and weaknesses of the mentioned optical methods for simulating diesel combustion. Taken directly from their publication, Figure 2.8 and Table 2.1 are presented below. In Figure 2.8, the operating ranges for different optical test setup are given. ORE1 and ORE2 refer to the two optical research engines at Sandia National Laboratory (Espey and Dec, 1993; Upatnieks, Mueller, and Martin, 2005). It can be noted that the CVPC covers the entire range of Figure 2.8 and is only limited by the mechanic of materials out of which the CVPC is built. Furthermore, Table 2.1 summarizes the quality attributes of each optical test

setup. The notations “0”=neutral, “+”=better, and “-”=worse. As mentioned, the ORE is the best test setup to simulate the running engine condition. However, all methods are suited for basic research of free spray combustion. In order to make a selection out of all the methods, it really depends on the topics of interest.

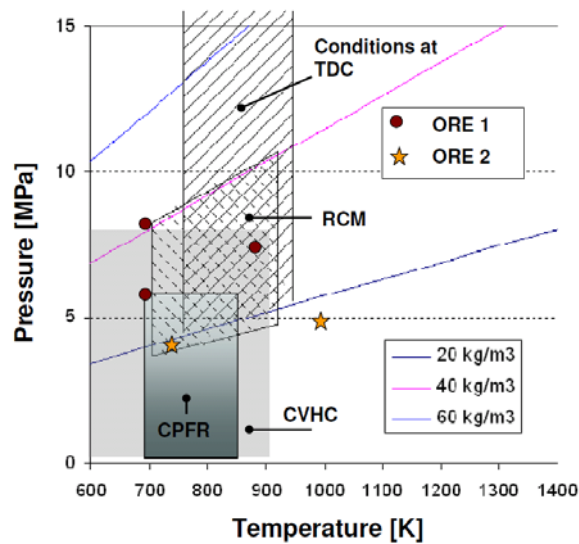


**Figure 2.8 - Comparison of operating range of different optical test setup in simulating a heavy duty compression ignition engine.**

**Table 2.1 - Quality attributes of different optical test rigs**

Type of optical test rig	ORE	RCM	RCYM	CPFR	CVHC	CVPC
Optical accessibility	0	0	++	++	-	+
Similarity to the real engine situation	0	-	--	--	--	--
Free spray penetration distance	0	+	+	+++	++	++
Control on trapped gas p / T	0	+	0	++	++	++
Control on trapped gas composition (i.e. EGR)	0	-	0	+	++	+++
Flow field impact on combustion	--	-(-)	-	0	-	-
Test facility volume	0	+	0	0	++	++
Time to switch between operating conditions (i.e. T)	0	0	0	0	--	++
Time between tests [s] (*)	1	120-600	1	1-3	60	600

“0”=neutral, “+”=better, and “-”=worse

## 2.2.2 Premixed Gaseous Combustion in CVPC

Iowa State University Internal Combustion Engine Laboratory and Multiphase Reacting Laboratory currently share a CVHC test setup seen in Figure 2.5. Diesel spray was studied using ultra high frame-rate planar laser-induced fluorescence imaging for a single-hole nozzle at elevated temperature and pressure using both air and nitrogen filled environment (Fuller, 2009). However, due to the limited heating source capability and the lengthy time required to achieve the desired environment condition, the current CVHC setup was adapted to become a CVPC. For this reason, the CVPC test setup has been researched in detail.

Since early 1990s, Sandia National Laboratory has developed a constant volume combustion chamber for direct injection spray and combustion research. Although there are more CVPCs implemented at other facilities; most are very similar to that of Sandia's. Figure 2.9 is a schematic of Sandia's combustion vessel with notations to its components and Figure 2.6 is photo of the vessel. From their website (Pickett, 2007), it is mentioned that there are four optical accesses provided by four 102 mm sapphire windows. Eight other 19 mm diameter access ports are located on the corners of the cubical shaped constant volume combustion vessel. The injector is located on the side while two spark plugs and a mixing fan are located at the top. To simulate engine wall temperature and to prevent condensation on the window surface during combustion events the chamber walls are heated electrically. Also notably is a mixing fan in Figure 2.9. The three main functions of the mixing fan are:

- To insure rapid equilibrium of the gas temperature with the vessel wall temperature during the premixed gas fill process
- To increase the flame speed during the premixed burn

- To keep the temperature in the vessel uniform after the premixed combustion

The fan is spinning throughout the experiment but is argued by Pickett (2007) that the gas velocities induced by the fan ( $\sim 1$  m/s) are insignificant when compared with the velocity of the dense liquid fuel spray (250 to 600 m/s).

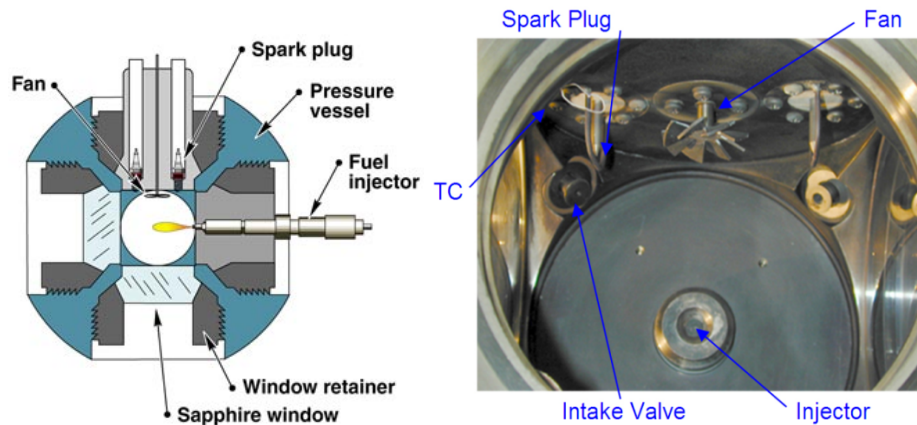


**Figure 2.9 - Schematic of the chamber (left) and inside the chamber (right) of Sandia National Laboratory CVPC.**

A premixed and combustible gas fills the chamber and is ignited with two spark plugs to create a high temperature, high pressure environment. After some time the mixture cools down due to heat transfer to the vessel walls and thus pressure slowly decreases. When the desired pressure is obtained the diesel fuel is injected into the chamber. Auto ignition will occur and the combustion process begins. Figure 2.10 is the pressure history illustrating the diesel combustion simulation procedure in Sandia's CVPC. Prior to time zero the vessel was heated to 458K to simulate the approximate temperature of combustible gases prior to spark ignition and the combustible premixed gases fill the chamber. At time zero, sparks are created by the spark plugs and the premixed combustion occurs from time zero to about 0.2 seconds. The cool down

process occurs from about 0.2 seconds to 1.65 seconds. Then at approximately at 1.65 seconds, a sharp rise in pressure denotes the beginning of the diesel combustion process.

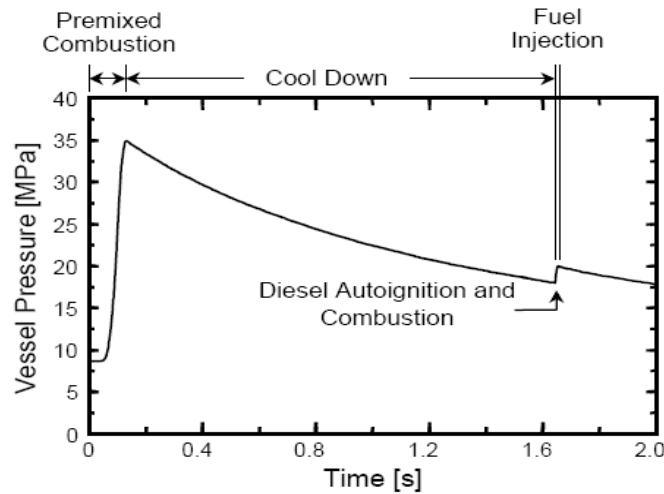
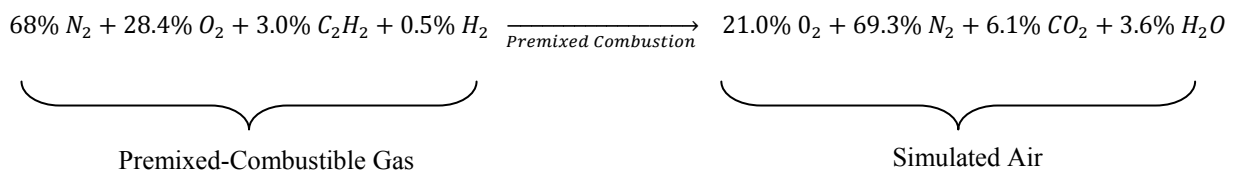


**Figure 2.10 - Pressure history of typical CVPC.**

Combustible gases were carefully chosen for premixed combustion which consists of nitrogen, oxygen, acetylene, and hydrogen. This premixed combustible gas composition was selected to obtain the product composition of oxygen and the molecular weight similar to that of air, 21% and 29.47 g/mol, respectively. Through experiments and CFD modeling, it was argued that the simulated air and actual air showed negligible results on a diesel jet process (Pickett, 2007). The overall premixed combustion process can be described in the following reaction:



(2.6)

## 2.3 Diagnostics

### 2.3.1 Diesel Spray and Combustion

Fuel injection pressure in a typical diesel engine today can exceed 240 MPa. At this pressure, fuel exits the nozzle with high kinetic energy, which can result in high turbulent velocity, and makes it very difficult to study. Today's modern laser diagnostic and spectroscopy offers an excellent and nonintrusive method. Analyses of diesel spray have been studied by many researchers. Diagnostics used include shadowgraphy/schlieren imaging (e.g., Myong et al., 2004; Siebers, 1998), chemiluminescence (e.g., Pickett, Siebers, and Idicheria, 2005), reflection and scattering (e.g., Higgins, Mueller, and Siebers, 1999; Myong et al., 2004), laser induced fluorescence (e.g., Fuller, 2009) and ballistic imaging (e.g., Linne and Parker, 2006).

Planar laser induced fluorescence (PLIF) is a popular diagnostic tool when studying diesel spray and one of the most common method used for exploiting the spectroscopic properties of molecules. To simplify, the setup of a PLIF include a source of light, an arrangement of sheet forming optics, a fluorescent media, and a detector. As light from the source strikes the media, energy is transferred which then causes it to fluoresce. These emissions of photons are then capture by a detector.

Typical PLIF images of diesel spray evolution in the past have been compiled using many images captured at different time of many injection events. Due to the fact that there are cycle-to-cycle differences, the structure of the spray may be lost from one injection event to the next. The latest and notable work was done by Fuller (2009) where a PLIF technique for spatially and temporally resolving a single diesel injection was demonstrated. With the aid of a

high-frequency laser operating in burst-mode (Miller et al., 2008), Fuller (2009) was able to trace the spray penetration and structure evolution in a single injection event.

Not only can laser diagnostics be used to study spray but it can also be used to study spray combustion. Analyses of diesel spray combustion have been studied by many researchers (e.g., Dec, 1997; Dec and Canaan, 1997; Idicheria and Pickett, 2005; Mueller et al., 2004; Pickett, Kook, and Williams, 2009; Pickett and Lopez, 2005; Pickett and Siebers, 2004; Pickett, Siebers, and Idicheria, 2005). As the flame front moves irregularly, the need to implement a high-frequency laser operating in burst-mode is of more importance. When taking a time average, the flame profile can appear relatively thick, forming a “turbulence flame brush” (Ferguson and Kirkpatrick, 2001). Fuller’s (2009) outcomes, along with others mentioned, are conclusive and prove that the CVPC, when coupled with modern laser imaging and spectroscopy technique, can offer an excellent avenue to understanding the complex diesel spray and the spray combustion mechanism.

## **CHAPTER 3. METHODS AND PROCEDURES**

### **3.1 Introduction**

This chapter summarizes the methods and procedures used to carry out this study. It is divided into two subsections. The first section consists of the design and testing method of the rate of injection. The second section describes the design concept of the constant volume combustion chamber.

### **3.2 Rate of Injection Bench System Design**

As mentioned previously, there are two main methodologies in obtaining the rate of injection. The Bosch system was favored over the Zuech system for its ease in operation and smoother rate of injection output. The Bosch type meter requires no timing between the fuel injection system and rate of injection meter. To reiterate, the Bosch rate of injection meter consists of an injector/pressure sensor mount, measuring and following tube, an orifice plate, and a pressure relief valve. Each component will be discussed. In addition to the meter components, a high pressure injection system and control system is needed in order to provide fuel into the injector and to trigger injection. This will be described foremost.

#### **3.2.1 High Pressure Common Rail System and Controls**

Originally developed by Denso Corporation in 1995, the typical high pressure common rail system in a modern diesel engine was used. Particularly, this system can be found in John Deere's Tier 3 and Tier 4 medium-duty electronic controlled diesel engines. When launched in

2002, these injection systems were capable of injection pressure of 180 MPa and up to five multiple injections with high accuracy. Today, an injection pressure of 240 MPa can be attained with the correct fuel supply pump, pressure sensor, and control system. A schematic of Denso high pressure common rail system is presented in Figure 3.1 (Denso, 2005).

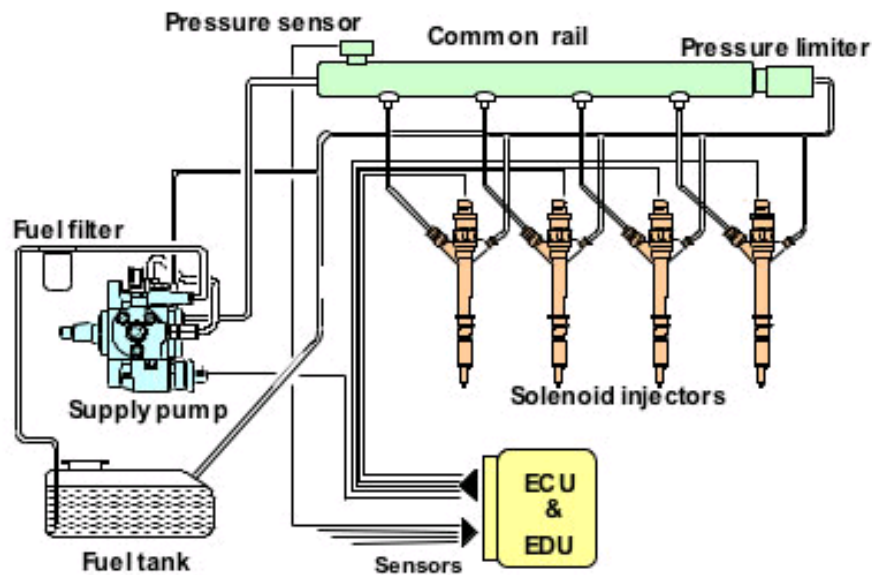


**Figure 3.1 - Schematic of Denso common rail system.**

The Denso solenoid injectors and supply pump are also noted in Figure 3.1. The supply pump rotates to pressurize the fuel and sends the fuel to the common rail. The fuel pressure is detected by the high pressure sensor and is controlled by adjusting an electromagnetic valve of the supply pump. This is done within the electronic control unit (ECU).

There are three available types of fuel supply pumps. The HP-3 is for passenger cars and light-duty vehicles; the HP-4 is for medium-duty vehicles; the HP-0 is for heavy-duty vehicle. All three are very similar in design. The differences exist in size which is based on fuel demand. Since only low flow rate was expected to be tested, the HP-3 supply pump was chosen. When

fuel injection is desired, the electronic driving unit (EDU) sends out a current signal energizing the solenoid injector, and the rail pressure pilot opens the injector needle. De-energizing the solenoid triggers the end of the injection event.

The L14 ECU and electronics found in John Deere's Tier 3 and Tier 4 medium-duty electronically controlled diesel engine were used. The EDU is located inside the ECU. To provide power to the ECU, a conventional 12 VDC automotive battery was kept charged through a trickle battery charger. DevX 1.0, a proprietary program of John Deere, was installed on a PC and connected to the ECU via a USB CAN2 250 adapter (Figure 3.2) to interface and control the inputs and outputs of the ECU. The communication protocol exchange is controller–area network (CAN-bus).



**Figure 3.2 - USB CAN2 250 adapter used to connect to L14 ECU/EDU.**

On a typical engine the ECU detects engine speed with a crank and cam signal pickups and detects throttle position with a throttle position sensor. When the engine is running, the crank and cam signals are square waveforms. The frequency of these waveforms, along with the intersection with respect to each other, corresponds to the engine speed and cylinder 1 position with respect to top dead center (TDC). Since the high pressure injection system was not mounted

on the typical engine setup and the EDU does not operate until the ECU receives engine speed signals and throttle position signal, signal generations were required.

National Instrument LabView 8.2 was installed on the same PC. The NI PCI-6251, a 16-bit multifunction data acquisition card from National Instrument (NI), was used to simulate engine speed signals. This card has two analog outputs (2.8 MS/s), 16 analog input channels (1 MS/s) and 24 digital input/output channels. This card has a NIST-traceable calibration certificate and was used in junction with the NI SCB-68 pin shielded connector box. Engine speed signals were captured during engine experiment and a library was created for engine speed from 1000 to 2400 rpm in 50 rpm intervals. When running the injection bench, one of the files was read and was continuously outputted to simulate engine speed. Figure 3.3 shows the engine speed signal waveform simulating 1000 rpm. The distinct break in cam and crank signal signifies that cylinder 1 position is approaching TDC. To simulated throttle position at 100%, a 4.2K ohms resistor was placed across the respective ECU pinouts. The fuel/speed map inside the ECU was adjusted in DevX 1.0 to adjust the amount of relative fuel injected per injection,

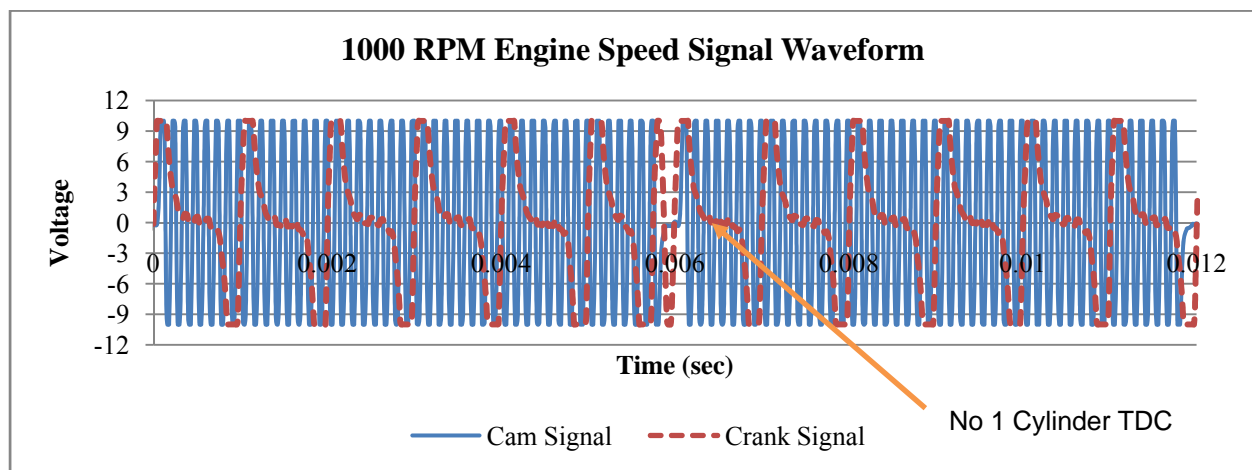


**Figure 3.3 - Sample generated crank and cam signal simulating 1000 rpm engine speed.**

A three-phase 15 hp AC motor was used to rotate the HP-3 supply pump. However, since the required rotational pump speed was different for different simulated engine speed, a Hitachi frequency inverter was coupled to the motor. The frequency inverter was controlled remotely through an Ethernet connection. A timing belt and timing pulleys along with a belt tensioner were used to connect the motor to the supply pump illustrated in Figure 3.4. This setup allowed for slight misalignment and excellent work transfer from the AC motor to the supply pump without slippage.

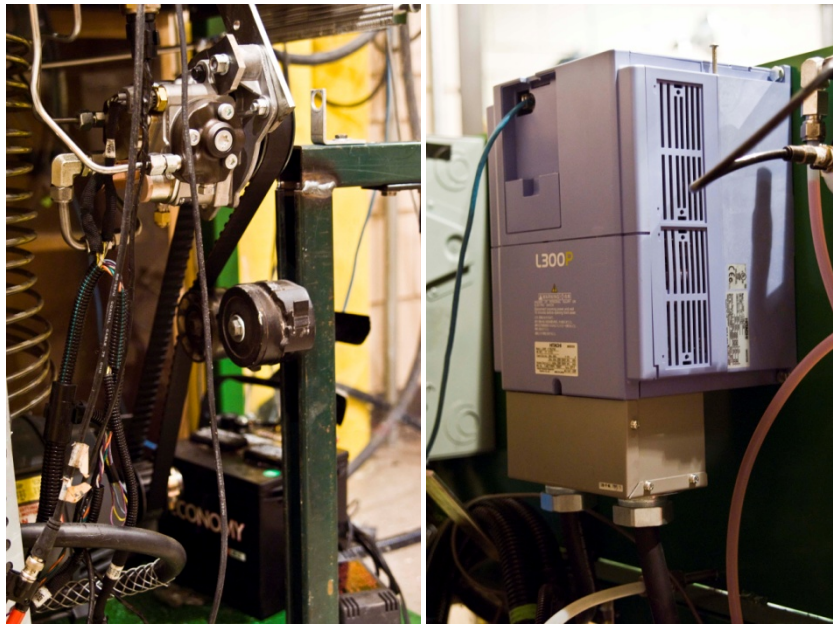


**Figure 3.4 - Injection supply pump, AC motor and drive system (left), frequency inverter (right).**

Fuel was fed to the HP-3 supply pump by an electric fuel pickup pump drawing fuel from the fuel storage tank. Before fuel entered the pump, the fuel was filtered using a 40-micron automotive fuel filter. The fuel supply pressure was controlled with a hand valve throttling the returned fuel and monitored through a mechanical dial gauge. This is seen in Figure 3.5. John

Deere recommended that the fuel pressure to the HP-3 supply pump must be greater than 24 kPa. In addition, a forced air convection cooler was used to cool the returned fuel during the supply pump compression work. With the cooler inlined, the supply fuel to the injection pump was kept at a temperature of 30-40 degrees Celsius.

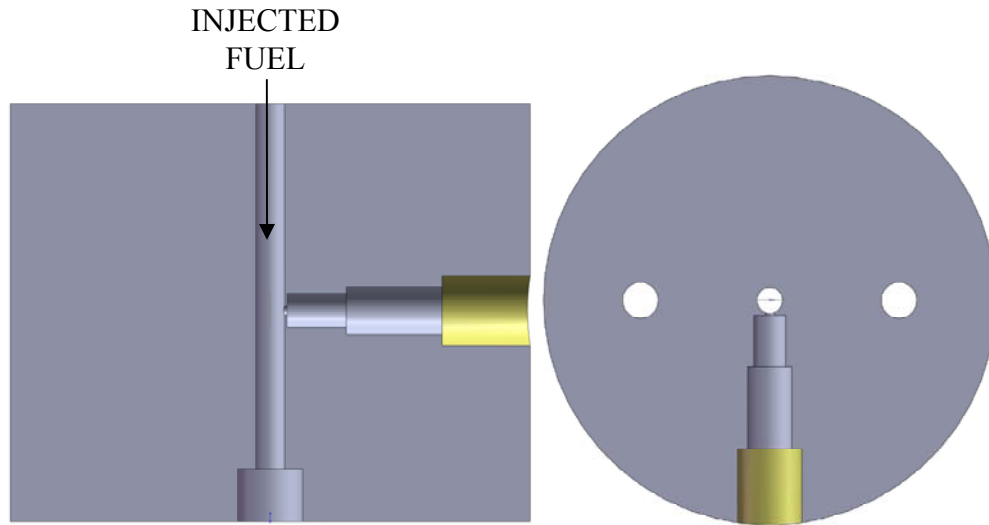


**Figure 3.5 - Fuel supply pump and fuel filter (left), hand valve and dial gauges (right).**

### 3.2.2 Rate of Injection Components

The most critical part of the Bosch rate of injection meter is the injector/pressure transducer mount. In order to accurately measure the pressure wave a constant diameter where the fuel is injected into is important and the pressure transducer should be placed in a way that is nonintrusive to the path of the pressure wave. Figure 3.6 is a scaled drawing of the fuel passage

showing the position of the pressure transducer location. The cross sectional diameter of the fuel pathway is 0.120 inches.



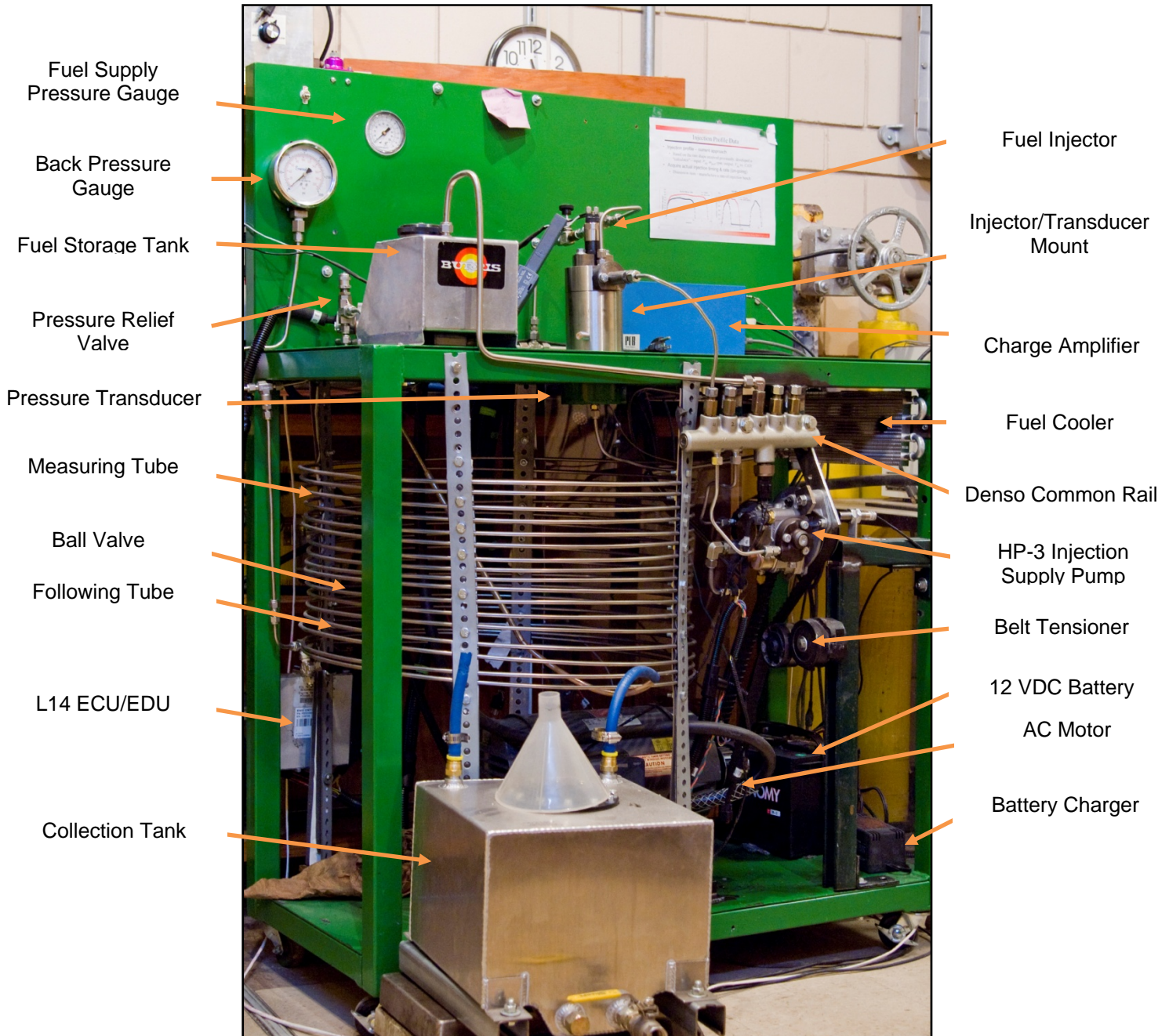
**Figure 3.6 - Scaled, sectioned CAD drawing of the fuel passage side view cutaway(left) and top view cutaway(right).**

Figure 3.6 shows that the pressure transducer was located orthogonal to the fuel passage. A Kistler 6125B piezoelectric pressure sensor was chosen to detect the pressure wave because of great linearity, low hysteresis, and high responsiveness. The technical characteristic of the pressure sensor is given in Table 3.1. Figure 3.6 also shows that the pressure sensor was approximately flush mounted to the passage of the fuel with only a small opening exposing the transducer to the fuel passage. The distance from the edge of the fuel passage to the tip of pressure sensor was minimized to reduced signal delay and the diameter of the opening was miniature to keep a circular fuel passage in order to keep the 1-D assumption mentioned previously. The signal from this pressure sensor was amplified using a PCB 464A charge amplifier to a 0-10 VDC signal and filtered using a 180 kHz low pass filter.

**Table 3.1 - 6125B technical data.**

Range	bar	0 ... 250
Calibrated partial range	bar	0 ... 50
Overload	bar	300
Sensitivity	pC/bar	$\approx 1/6$
Natural frequency	kHz	$\approx 75$
Linearity, all ranges	%FSO	$\leq \pm 0,5$
Acceleration sensitivity		
axial	bar/g	<0,002
radial	bar/g	<0,003
Operating temperature range	°C	-50 ... 350
Sensitivity shift		
200 ... $\pm 150$ °C	%	$\leq \pm 2$
200 ... $\pm 50$ °C	%	$\leq \pm 1$

As the fuel exits the injector/transducer mount, the fuel enters the measuring tube. The inside diameter of the measuring tube was 0.120 inches and the outside diameter was 0.125 inches. The transition from the injector/transducer mount to the measuring tube was with a ¼ inch NTP to ¼ inch compression tube fitting adapter. This ID of this adapter was drilled out so that the beginning of the measuring tube stuck into the injector/transducer mount. As a result, a constant cross sectional diameter of 0.120 inches was maintained. The length of the measuring tube was approximately 80 ft. The orifice was provided by a ball valve which allowed for size change on-the-fly while observing the pressure wave during experiment. The following tube had the same ID and OD dimension as the measuring tube with a shorter length of approximately 20 ft. A pressure regulating relief valve was installed at the end of the following tube to control the back pressure. Back pressure was read by a mechanical pressure gauge installed in between the following tube and the pressure regulating relief valve. After the relief valve fuel was dumped into a collection tank. The material of the mount, measuring tube, ball valve, following tube, and pressure relief valve was of stainless steel alloys for its excellent yield strength and great corrosion resistivity. Figure 3.7 is a picture of the completed rate of injection bench with notions to its components.



**Figure 3.7 - Injection bench meter with system components and high pressure injection system notions.**

### 3.3 Rate of Injection Bench Testing Method

Once fabrication and construction of the rate of injection bench was completed, a pressure measurement system calibration was carried out. In addition, a data acquisition and control system was designed and implemented and validation for rate of injection bench was performed. These methods will be described in the following sections.

#### 3.3.1 Pressure Measurement System Calibration

Although, the manufacturer provided a degree of certainty in accuracy and linearity for the pressure sensor, a system calibration was necessary in order to confirm that the pressure sensor was in working order. It was also necessary to verify that the combination of the pressure sensor and charge amplifier would yield accurate results. An Amthor dead weight tester was used to test for accurate static pressure measurement and for linearity. This dead weight testing procedure did not test for system responsiveness. To test for any hysteresis, a downward calibration was also performed. In this testing procedure, a known pressure was applied by the Amthor dead weight tester on the pressure sensor and voltage was read after the charge amplifier using the same NI PCI-6251 data acquisition card mentioned previously. Figure 3.8 is the pressure measurement system calibration using the Kistler 6125B and PCB 464A charge amplifier. A linear curve was fitted on the upward calibration and was found to have an excellent linear regression,  $R^2=0.9996$ . By comparing the downward calibration and the upward calibration of the pressure measurement system, one can observe that the hysteresis was very minimal. After the calibration on the pressure measurement was completed, the pressure measurement was used with great confidence. For further confirmation, similar calibrations were

carried out throughout the experiments and the calibration results confirmed that there were negligible drift.

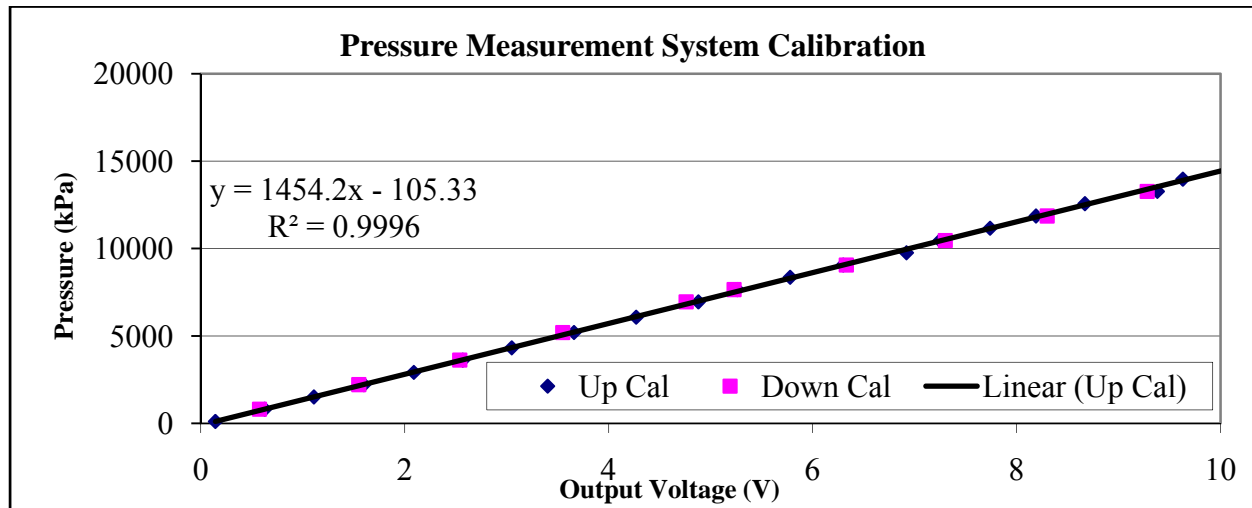


**Figure 3.8 - Kistler 6125B pressure sensor with PCB 464A charge amplifier system calibration.**

### 3.3.2 Data Acquisition and Control System

A data acquisition (DAQ) and control system was designed using LabView 8.2 and a NI PCI-6251 data acquisition card. In this LabView virtual instrument (VI), a file was selected from the engine speed library and signals were generated continuously to simulate the desired engine speed. After the motor pressurized the common rail, injections occurred when the “Start Injection” button was depressed. The pressure trace and the inductive pickup trace, used to capture the current going into the injector, were recorded in specified file at a user specified rate. This VI ran on a user specified timer and also counted the number of injections that occurred during the experiment. Each injection event was saved in a specific file and MATLAB was used for post processing. The front panel to this VI can be seen in Figure 3.9.

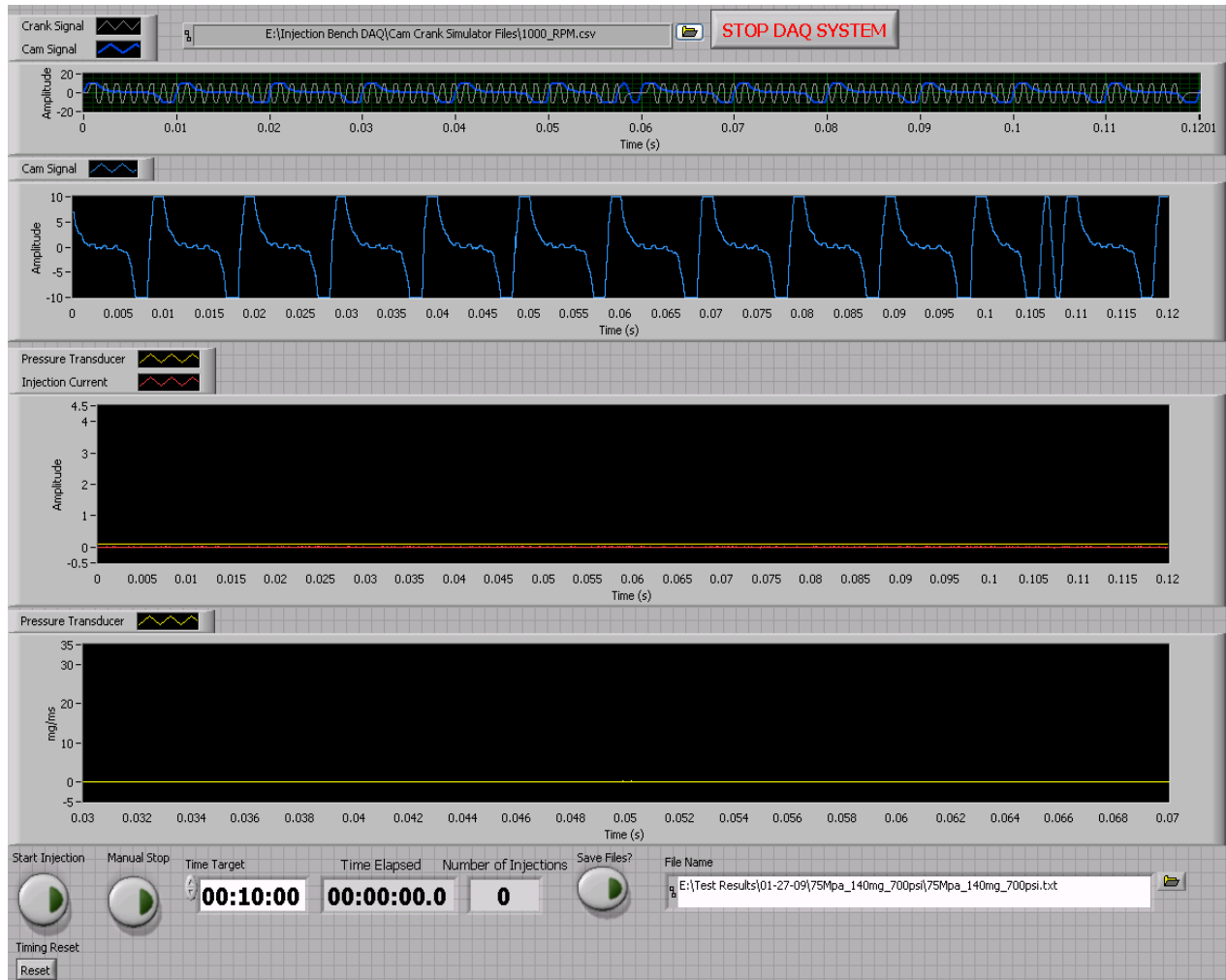


**Figure 3.9 - Injection bench data acquisition and control system LabView front panel.**

### 3.3.3 Rate of Injection Validation Study

With the completion of the pressure sensor system calibration and the design and implementation of the DAQ and control system, validation on the bench accuracy was performed. However, the speed of sound in fluid was required to convert the pressure trace into an instantaneous mass flow rate. Many researchers in the past have used a speed of sound in

diesel of 1355 m/s at 2.76 MPa. This pressure was the typical in-cylinder pressure at the start of fuel injection in the past. Although this value was close, the study by Tat and Van Gerpen (2002) concluded that the speed of sound in fluid was actually 1410 m/s at 2.76 MPa with fuel temperature of 300 degree Kelvins. In their study, the effects of biodiesel blend level on the fuel mixture density, speed of sound, and isentropic bulk modulus at higher pressures for 20 °C and 40 °C were investigated (Tat and Van Gerpen, 2002). From their study the speed of sound correlation was based on different fuel blends, fuel temperature, and back pressure. This correlation which is presented in Table 3.2 was used in this study throughout the different experiments to calculate the speeds of sound in fluid.

**Table 3.2 - Speed of sound correlations.**

Samples	C <sub>1</sub>	C <sub>2</sub>	C <sub>3</sub> ×10	C <sub>4</sub> ×10 <sup>2</sup>	C <sub>5</sub> ×10 <sup>3</sup>	C <sub>6</sub> ×10 <sup>2</sup>	C <sub>7</sub> ×10 <sup>4</sup>	C <sub>8</sub> ×10 <sup>-3</sup>
No. 2 Blends	-3.5972	4.6849	2.3682	1.4412	-3.9664	-1.6236	8.8429	1.4570
No. 1 Blends	-3.7043	5.0232	6.5479	1.4958	-6.9146	-1.7425	11.8120	1.4147
$\text{Speed of Sound (m/s)} = C_1 \times T(^{\circ}\text{C}) + C_2 \times P(\text{MPa}) + C_3 \times \%(\text{Biodiesel Percentage}) + C_4 \times T \times P + C_5 \times P \times \% + C_6 \times P^2 + C_7 \times \%^2 + C_8$								

Subsequently, a selective sweep in rail pressure, injector energizing time, back pressure, and single/double injections using the baseline injector was selected to form the test matrix for the validation study. Validation of bench accuracy was done by comparing the integrated mass, which was averaged over many cycles with a high accuracy weight scale measuring the injected fuel mass. However, the raw signal obtained from the rate of injection bench needed to be corrected due to a slow rate of decay. This is illustrated in Figure 3.10. After trying many settings on the charge amplifier including adjusting the response time setting and using a different charge amplifier, the slower than expected decay rate was still present. The present

pressure sensor operated on a piezoelectric effect to measure pressure. As the quartz crystal inside the transducer deforms due to pressure changes, an electric charge was generated. This charge was amplified and converted into a voltage after the charge amplifier. The transfer of the electric charge from the transducer to the amplifier was slower at lower electric potential, which was believed to have resulted in a slower than expected decay rate. Small cavitations may have been present due the positioning of the pressure sensor with respect to the pathway of the fuel which could have affected the deformation of the pressure sensor crystal and resulted in a slow than normal rate of decay.

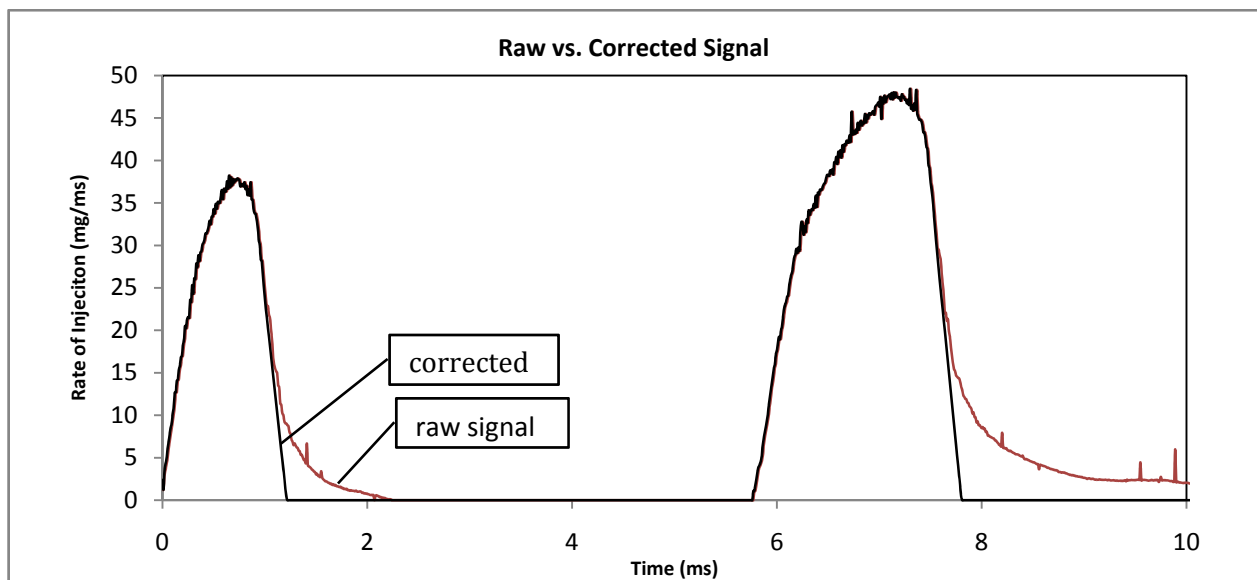


**Figure 3.10 - Raw vs. corrected signal for double injection event.**

Similar effect was also seen by Bower and Foster (1989). In their study, pressure trace on the fuel line was acquired during testing along with the rate of injection trace. In Figure 3.11 their pressure and rate of injection traces showed the slower than normal decay rate (Bower and Foster, 1989). They argued that if cavitations were occurring one would expect to see steps in the

fuel line pressure trace as bubbles formed and collapsed. They concluded that the slow decay phenomenon was due to some noise related to the injection operation. However, in this experimental setup careful considerations were taken to eliminate noise from interrupting the measurement. The pressure sensor had a ground insulated design which would have avoided electrical interferences due to ground loop and shielded cables were used from the transducer to the DAQ card.

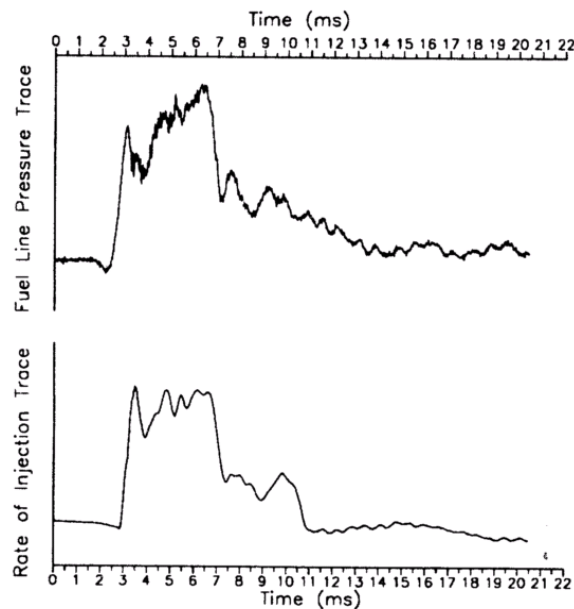


**Figure 3.11 - Bower and Foster observed fuel line pressure trace and rate of injection trace.**

With the optical accesses provided by the constant volume combustion chamber, which will be mentioned in greater detail, a sequence of PLIF images were taken and compiled to study the evolution of the diesel spray using a similar Denso high pressure common rail injection system. Figure 3.12 shows that the spray was fully developed at approximately 325 microseconds after start of injection (ASOI). After 2 ms, the injector solenoid was de-energized

which marked the closing of the injector needle. Approximately a few microseconds after 725 microseconds, there was completely no fuel. Although this study was conducted using a single-hole nozzle injector and cases from the injection bench used a multiple-hole nozzle, the number of holes would have negligible effect because the same type of injector was used. The slow rate of decay seen in Figure 3.10 was concluded to be unreal. The slow rate of decay could have been caused by a slow transfer of electric charge at lower electric potential and/or it could have been due to small cavitations in the space between the pressure transducer and the fuel pathway. Correcting the rate of decay was chosen and proceeded based on continuing the most dominate decay rate until it reached zero.

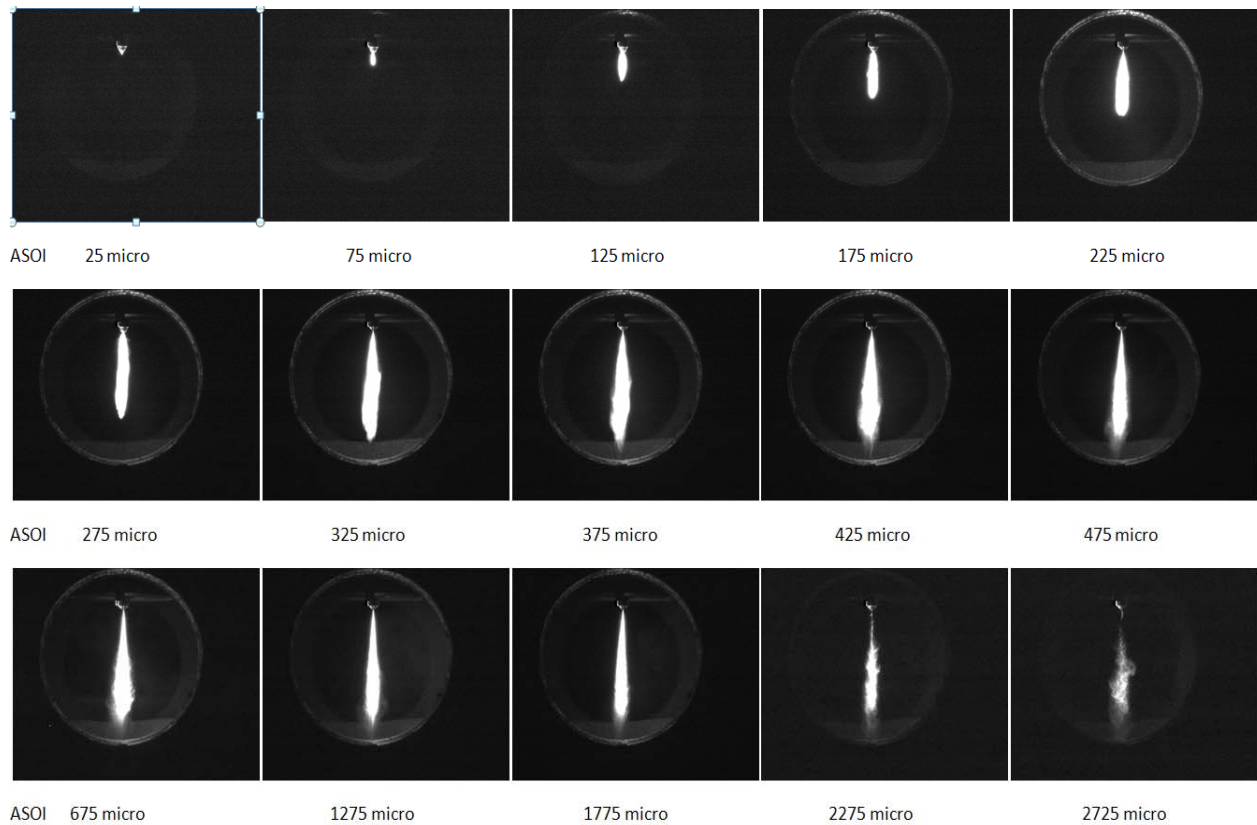


**Figure 3.12 - PLIF images of diesel spray evolution using a single-hole nozzle injector with solenoid energizing time of 2 milliseconds.**

Validation of the injection bench accuracy was continued by correcting the slow decay rate in the injection profile. Again, to validate the bench accuracy the injection profiles of many injection events were ensemble-averaged (typically more than 100 cycles) and integrated to find fuel mass injected per injection. Many cycles were recorded and averaged to eliminate any cycle-to-cycle variation in the individual injection event. Based on engine experiments, it was decided that ten minutes per experimental case would be enough time for sufficient fuel to be injected and weighted by the scale to obtain good accuracy and resolution when divided by the total number of injections to find individual injected mass per injection event. In addition, any residual fuel that was left behind inside the tubing could be considered negligible. After running the injection bench for ten minutes there were approximately 4877 injection events when 1000 rpm simulated engine speed was chosen. Figure 3.13 is the result from the validation study graphing the percent differences when comparing the integrated mass from the injection profile and to the injected mass measured by the weight scale per injection event. There were 30 cases with injection pressure ranging from 75 to 150 MPa and injector solenoid energizing time from 0.5 ms to 3.2 ms using the baseline injector testing with both diesel and biodiesel blend with a back pressure of 6.21 MPa. The injection pressure and ranges were chosen based on observations during engine experiments. The back pressure was chosen because this was the typical in-cylinder pressure at the time of fuel injection in a modern diesel engine.

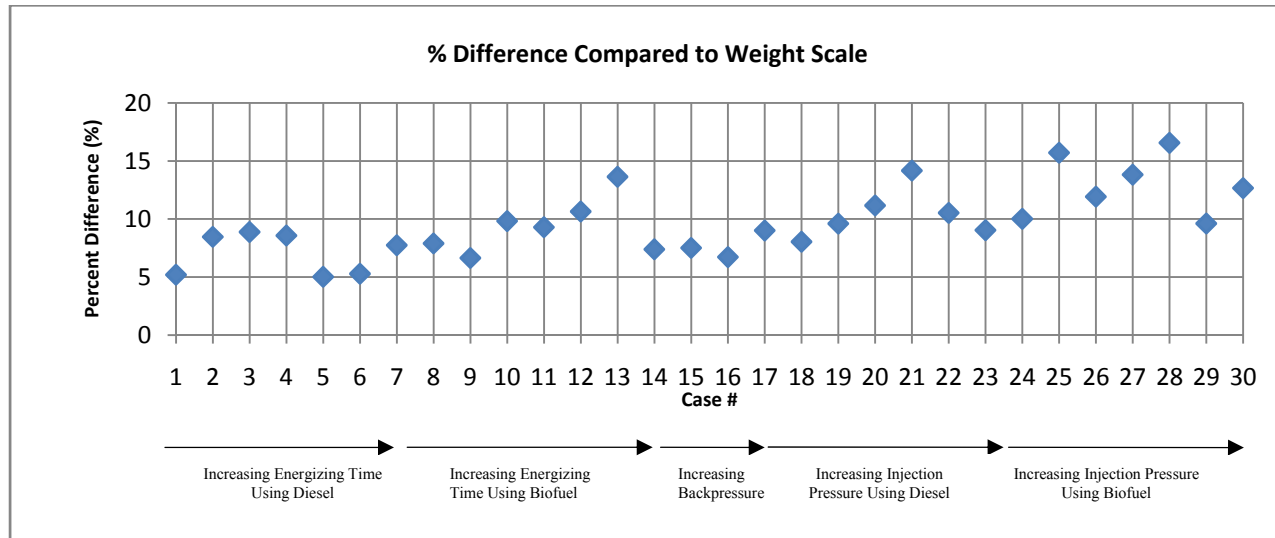


**Figure 3.13 - Validation study comparing integrated vs. weighted injected mass per injection event.**

After correcting the slow rate of decay the injection profiles obtained from the injection bench looked very similar to that of other injection benches. However, when compared to the weight scale the injection bench consistently under quantified the injected fuel mass by approximately 10%. Nonetheless, this was similarly seen by Bower and Foster (1991) as well. Figure 2.3 again was their results comparing the rates of injection obtained from the Bosch type injection meter and from the Zuech type injection meter. When integrating results from both injection benches, the Bosch type meter would yield a lower injected mass. After the validation study, similar results were observed to that of Bower and Foster (1991) and to that of other injection benches. Though the injection bench consistently under quantified the total injected mass by approximately 10%, the shape of the injection profiles were similar to that of other systems of injection metering and were smooth.

### 3.4 Combustion Chamber System Design

Aforementioned, the Internal Combustion Engine Laboratory and Multiphase Reacting Laboratory currently share a CVHC test setup. However, due to the limiting heating source capability and the lengthy time required to achieve the desired chamber conditions the CVHC setup was modified and became a CVPC. In addition, sealing on the four optical windows was revisited due to leaks that were seen in previous experiments. This section will detail the design process.

#### 3.4.1 CVHC Previous Test Setup

Figure 3.14 are CAD renderings of the constant volume hot cell assembly. The CVHC had four optical accesses through four UV optical grade quartz windows. On each of the end cap there was a 2 kW heating element used to heat the internal air to raise the temperature and pressure to the desired conditions. On the top of the chamber was an injector mount to position the injector. The injector mount had an internal cooling chamber to prevent heat from damaging the injector. A Denso high pressure common rail injection system similar to that used in the injection bench was used to provide high pressure fuel to the injector. Between each mating surfaces was copper gasket that were used to seal the chamber. The nickel chromoly steel (AISI 4340) chamber was found to have a pressure not-to-exceed at 473 K uniform wall temperatures of 20.6 MPa. This work was done by Fuller (2009) using the finite element analysis package in Solidworks as well as using the classical ASME boiler and pressure vessel calculations.

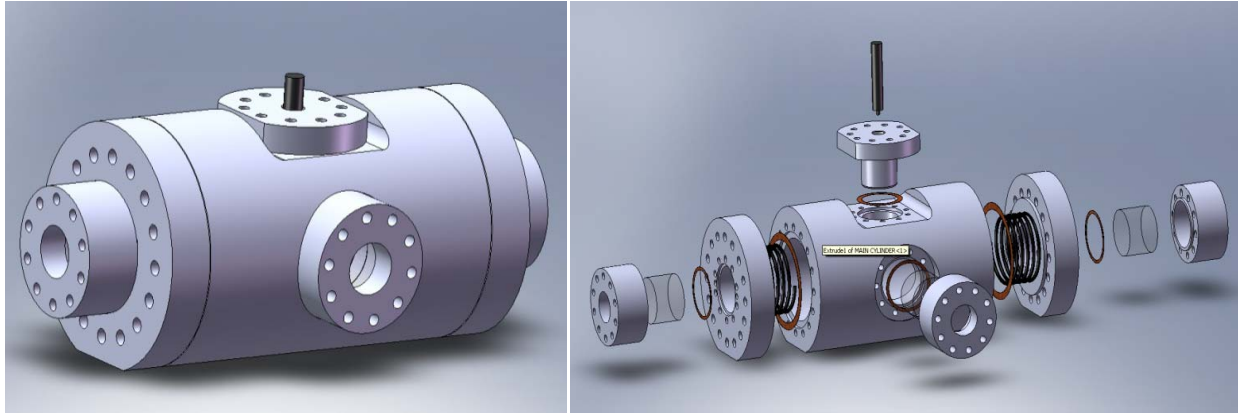


**Figure 3.14 - CAD assembly of Chamber (left), exploited view of chamber assembly (right).**

Fuller (2009) used this chamber to study diesel spray structure evolution using a high-frequency laser operating in burst-mode at elevated pressure and temperature using both air and nitrogen filled environment. Though successful at studying diesel spray, many drawbacks to this chamber were discovered while running the experiments. First, despite the fact that the 4 kW inconel heating elements offered good heating source to heat the internal temperature of the chamber, only a maximum temperature of 600 K was attained. The auto-ignition temperature of No. 2 diesel is 523–558K (Elert, 2005). With an air-filled environment temperature of 600 K at elevated pressure diesel flame could not propagate although auto-ignition sparks were observed. At 600 K, auto-ignition occurred at the edge of the dense fuel jet but flame could not propagate due to low local air temperature. Secondly, the time for heating the internal temperature to 600 K exceeded 15 minutes. The internal pressure suffered from leaks thus losing initial air mass in the chamber as a result from the lengthy time requirement.

### 3.4.1 Redesigning of Window Seals

The previous method for sealing the chamber was through using copper gaskets. Although this was a suitable approach for sealing two metal surfaces, this technique did not performed well for sealing the quartz windows. If too much torque was applied on the fasteners when mating the window to the chamber, the window would suffer from mechanical defects and cracks would occur. However, if not enough torque was applied the chamber would experience leaks at high pressure due to the gaps formed in between the relatively uneven surface of the copper gaskets and windows. To combat this problem, high temperature RTV silicone was used around the outside edge of the window to fill in gaps when light torque was applied. This procedure proved effective. However, the pliable RTV needed time to solidify in order to work. If the chamber needed to be taken apart for cleaning the task proved to be a complicated and prolonged.

It was desired for a new sealing approach for better sealing and for a more seamless operation when the chamber needed to be taken apart. The solution was to use O-rings. O-Ring glands were machined on the four end caps and silicone O-rings were matched. Silicone O-rings were selected because of its high temperature resistance (up to 533 K) and great chemical compatibility. Figure 3.15 are CAD renderings of the end cap with the O-rings installed. As pressure inside the chamber builds up, nominal force will exert on the window crushing the o-ring and makes for even a better seal. It was designed for the O-ring seal to withstand an internal pressure of 40 MPa ("Parker O-Ring Handbook ORD 5700," 2007).

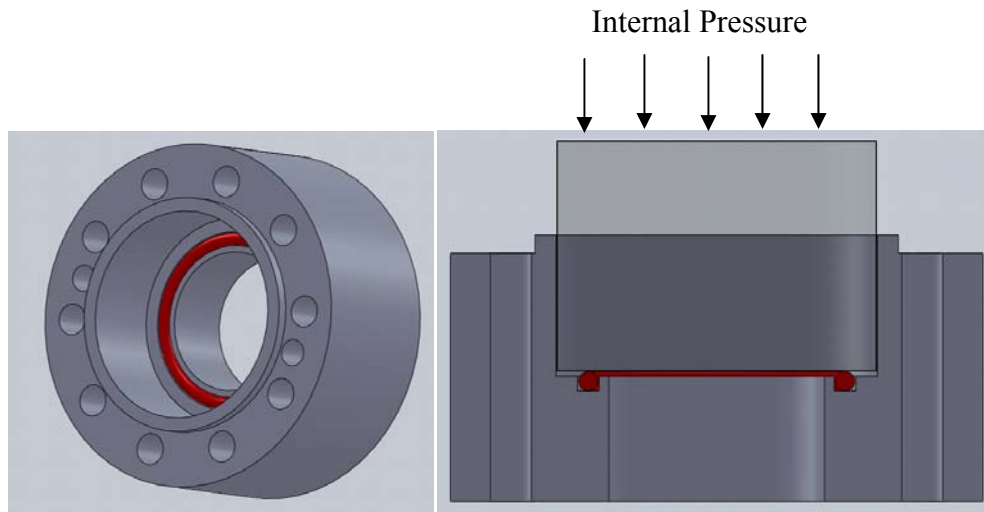


**Figure 3.15 - Window cap with redesigned o-ring seal isometric view (left) and cutaway view with quartz window (right).**

### 3.4.2 Premixed Combustion and Mixing Fan

The four gases were carefully selected for premixed combustion to elevate temperature and pressure inside the chamber prior to the diesel combustion. Researchers using a similar premixed combustion approach have used a wide variety of gases but mainly  $H_2$ ,  $C_2H_2$ ,  $C_2H_4$ ,  $O_2$ , and  $N_2$ . The gases composition ranges also varied as follow: 5.9-24.1%  $H_2$ , 3.05-5.1%  $C_2H_2$ , 0.8-5.0%  $C_2H_4$ , 27.1-36.2%  $O_2$ , and 45.3-69.3%  $N_2$ . After premixed combustion, both pressure and temperature were elevated and the products of combustion were similar to those of air. Such a wide range in gas composition was used with respect to each other to further simulate air heat capacity, viscosity, and conductivity (Baert et al., 2009).

In this study the selected four gases were as following 68%  $N_2$ , 28.5%  $O_2$ , 3.0%  $C_2H_2$ , and 0.5%  $H_2$ . This composition was the same as the one used by Naber and Siebers (1996). This composition was not only chosen because the product composition of  $O_2$  and the molecular

weight were similar to those of air, but also because of the specific heat, viscosity and conductivity closely resembled those of air. After complete premixed combustion, the product was calculated at 1200 K to have the following properties:  $\lambda=3.62$ ,  $C_p/C_{p,air}=1.03$ ,  $v/v_{air}=1.00$ ,  $k/k_{air}=1.03$  (Baert, Frijters, Somers, et al., 2009).  $C_2H_2$ , although more volatile than  $C_2H_4$ , was chosen because fewer hydrogen molecules would minimize water production and less heat on the chamber window would be required to prevent condensation (Oren, Wahiduzzaman, and Ferguson, 1984). Due to the assumption that the four selected gases were ideal gases, mixing of these gases was done using their partial pressures. This method was very similar to that of other researchers (e.g., Baert et al., 2009; Oren, Wahiduzzaman, and Ferguson, 1984).

Careful considerations were taken for the order of gas when filling the chamber. Due to its C-C triple bond, acetylene was unstable and can explosively dissociate at pressure above 200 kPa (Oren, Wahiduzzaman, and Ferguson, 1984). For that reason,  $C_2H_2$  needed to be added at the very beginning. However, purging the chamber at the beginning was very important to prevent contaminating the mixture. It was chosen to first purge the chamber using nitrogen before starting the filling process. After the purging procedure, nitrogen was filled to 20% of the desired mixture pressure. Next,  $C_2H_2$  was added until 23% (20%+3%) of the desired mixture pressure was obtained. Then  $H_2$  was added until 23.5% (20%+3%+0.5%) of the desired mixture pressure was obtained. Subsequently, the remaining  $N_2$  was added, 71.5% (20%+3%+0.5%+48%) of the desired mixture. Finally, to avoid going into the explosion region, oxygen was added last to the desired mixture pressure. The filling process was executed slowly so that the system could reach temperature equilibrium and the expansion of gas due to the heating process can be considered

negligible. Figure 3.16 is an image of the gaseous cylinders with the air actuated valves used for filling the chamber. Check valves were placed strategically to prevent backflows.



**Figure 3.16 - Gaseous cylinders with air actuated valves.**

Since gases will be inputted individually and temperature and gas homogeneity are essential, a mixing fan needed to be designed and implemented to the existing chamber. Careful considerations were given due to the extreme pressure and temperature that the chamber can endure during testing. Many vital options were judged in great detail. First a shaft, with a propeller blade at the tip penetrating into the chamber through an access port with a radial seal for sealing similar to that of Pickett (2007) was considered. After detailed investigations, this proved to have high cost and poor serviceability. Upon lengthy consultation with a manufacturer that would custom fabricate a radial seal suitable for this application, it was estimated that each

seal would cost approximately eighty dollars after the prototype trial period and would only last up to three combustion events. With such high cost for each seal and poor lifetime, the operational cost for running experiments would be costly. The second option was to utilize a magnetic couple drive mounted on the side of the chamber with a shaft and propeller penetrating into the chamber. Although an excellent option, the cost for purchasing a magnetic couple drive with the motor was too extravagant. The estimated cost would have exceeded seven thousand dollars.

Finally, it was decided to design and fabricate a housing, which would replace one of the optical assess to mount a brushless DC motor on the inside. This motor was used to rotate a mixing shaft. In addition, this housing was designed to mount the pressure transducer and two spark plugs, which will be mentioned in the subsequent section. A powerful, miniature brushless DC motor was chosen because of its size and the fact that it will not create any spark during operation, which could cause premature premixed combustion. The rotational speed of this motor could be varied by changing the pulse width of the required 50 Hz PWM input signal. This motor has a rated maximum rotational speed of 10,500 rpm if a 10 ms pulse width PWM signal was used. By mounting the motor on the inside of the chamber, the mixing fan could endure extreme pressure with zero leaks. However, cooling requirement was needed to prevent damaging the motor from extreme temperature. This was provided by a cooling coil constructed out of copper, wrapped uniformly around the motor. Copper was chosen because of its superior thermal conductivity property. As the coil enters and exits the chamber, ¼ inch NTP to tubing adapters were used to seal from leaks. Power was fed into the motor through a Conax power lead gland packaged with grafoil. This connection can withstand 41.3 MPa when installed properly. Figure

3.17 is CAD renderings of the multipurpose housing with cutaway views to show the motor, cooling coil, ball bearing, and shaft on the inside. Figure 3.18 shows the completed multipurpose housing installed on the chamber with notations to the components and the Conax power lead gland that was similarly used.

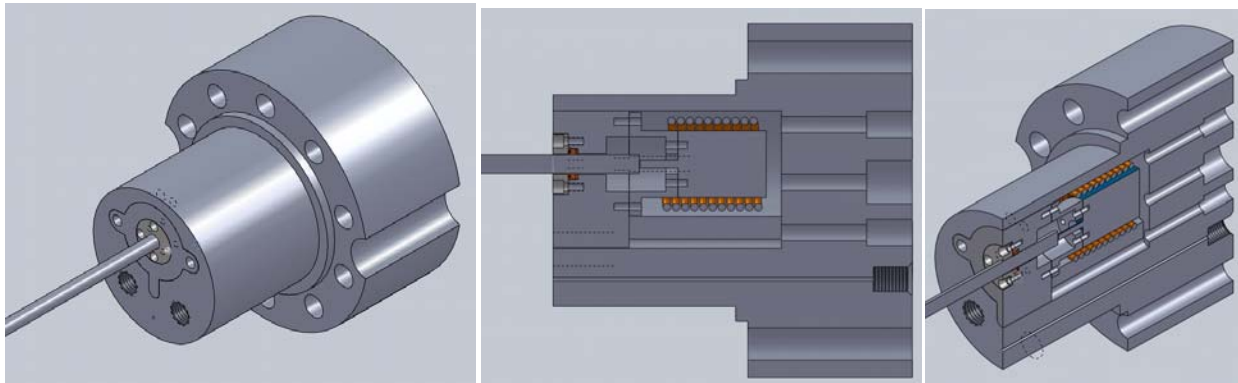


**Figure 3.17 - CAD renderings of the multipurpose housing assembly (left), cutaway view showing the motor, cooling coil, ball bearing, and shaft (middle), and isometric cutaway view (right).**

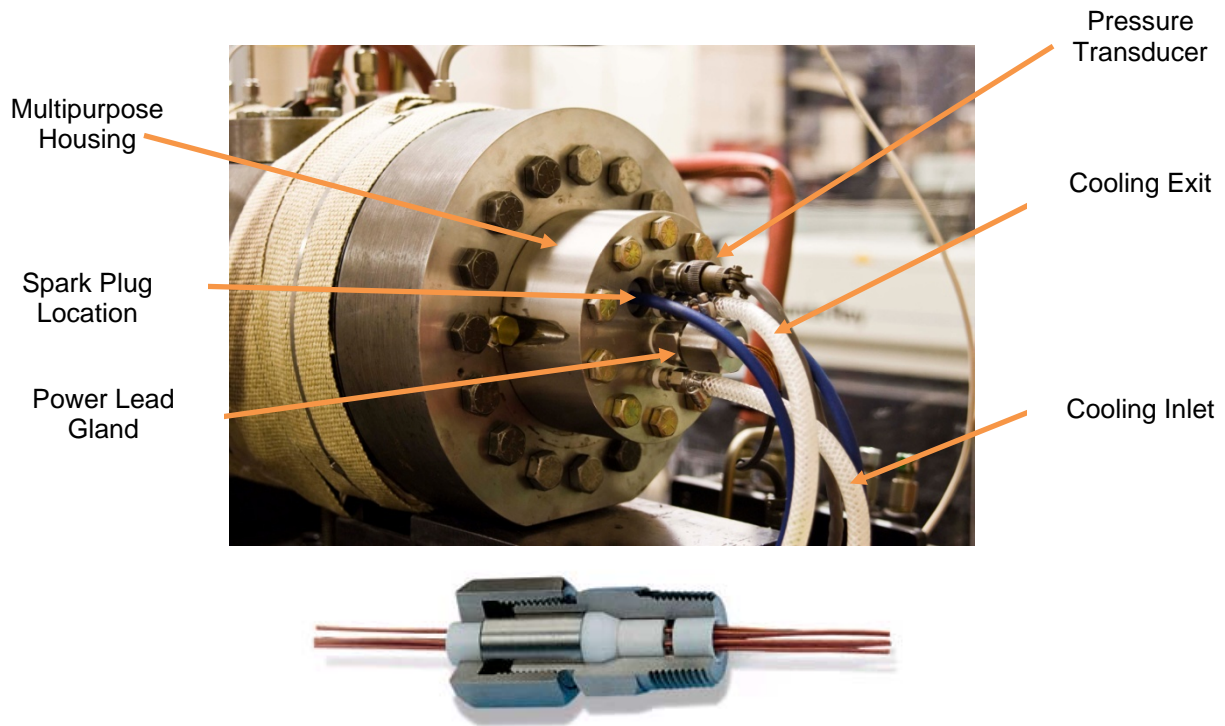


**Figure 3.18 - Multipurpose housing installed to the chamber with component notions (top) and Conax power lead glands (bottom).**

### 3.4.3 Spark Ignition System

In order to ignite the pre-combustion mixture, an ignition system was needed. Two ignition coils with a maximum of 45,000 volts were used to spark two automotive spark plugs. These spark plugs were mounted on the multipurpose housing. As 12 VDC electric current passes through the primary coils of the ignition coils a magnetic field was created. When this current is suddenly disrupted, the magnetic field would collapse which would create a high voltage pulse to develop across the secondary terminals through electromagnetic induction ("Induction coil," 2009). An electric arc can then be seen across the spark plugs. To trigger the

sparks in a timely matter and with the least amount of back electromotive force (back emf), a fast solid state relay (SSR) was used. Figure 3.19 shows the spark ignition system and SSR used.

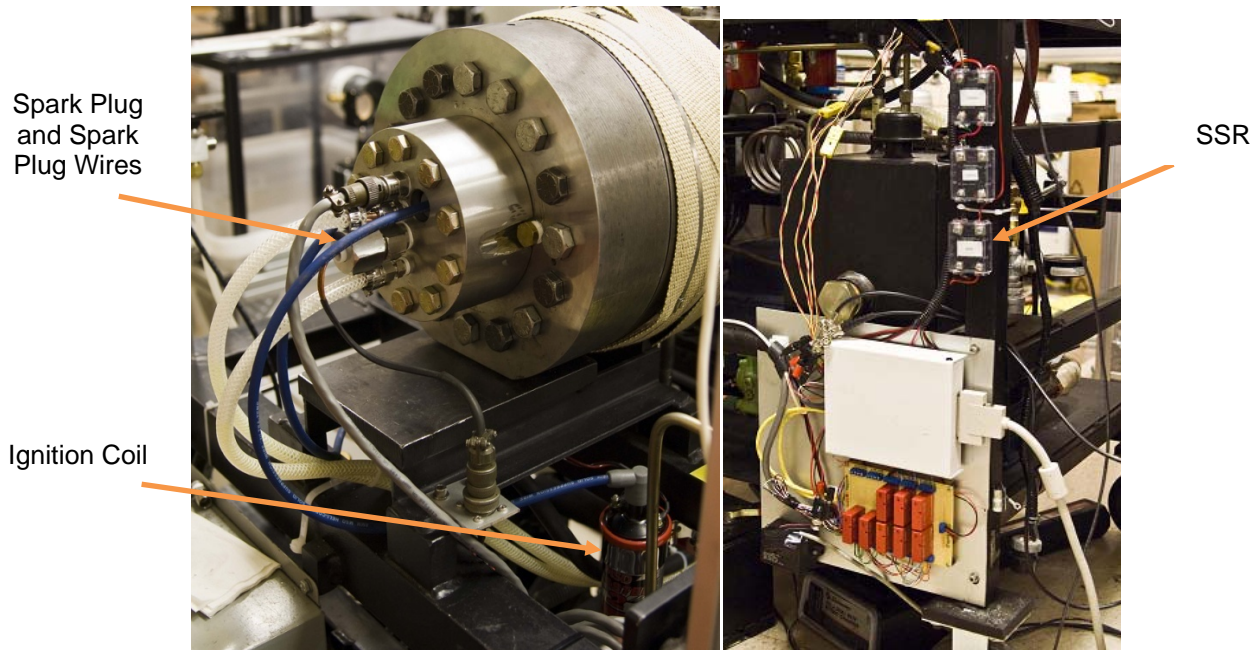


**Figure 3.19 - Spark ignition system: coils, ignition wires, and spark plugs (left) and fast SSR (right).**

### 3.4.4 Data Acquisitions and Controls

Temperatures on the surfaces of the chamber as well as the surface of the insert and internal temperatures were monitored using type K thermocouples. The range of these thermocouples is 273–1523 K with low limits of error. In order to accurately measure the internal temperature of the chamber it was necessary to have a low response time from the thermocouple used to measure the internal temperature. Following premixed combustion, pressure and temperature were elevated. After a short time (less than 2 seconds in some cases), the internal pressure and temperature decreased significantly due to heat transferred to the

chamber wall. In order to measure the temperature inside of the chamber, a thin 0.020 inches in diameter, 304 SS sheath, and grounded type K thermocouple was used. The response time for this thermocouple was less than 0.25 seconds. The tip of this thermocouple was placed at the center of the chamber, close to the tip of the injector.

Pressure measurement was also crucial in this study, thus two accurate pressure transducers were used. At first, a PCB 1704M02 strain gauge pressure transducer along with a PCB strain gauge signal conditioner was used to measure the gas filling process and combustion processes. This pressure transducer combination has a range from 0-68.9 MPa, very high accuracy (0.4% FS), very low thermal shift ( $\leq 0.018$  %/C), and great resonant frequency ( $>120$  kHz). However, more resolution was desired for the gas filling process. A Setra model 280E strain gauge pressure transducer was used for this purpose. This pressure transducer has a range of 0–689 kPa, output of 0–5 VDC, very high accuracy ( $\pm 0.11$ % FS), and low thermal shift ( $\leq 0.0135$  %/C). After the filling process was finished, a hand valve was closed to prevent the transducer from over pressuring. Both transducers underwent the same system calibration with a dead weight testing procedure mentioned previously. Figure 3.20 is the system calibration for the PCB pressure transducer and Figure 3.21 is the system calibration for the Setra pressure transducer. Both transducers have great linearity with low hysteresis. Although a full system calibration was not done for the PCB transducer because the dead weight tester could not simulate the full range, it was assumed to hold linearity throughout the full range because factory certificate on the transducer itself, without signal conditioning, prescribed so.

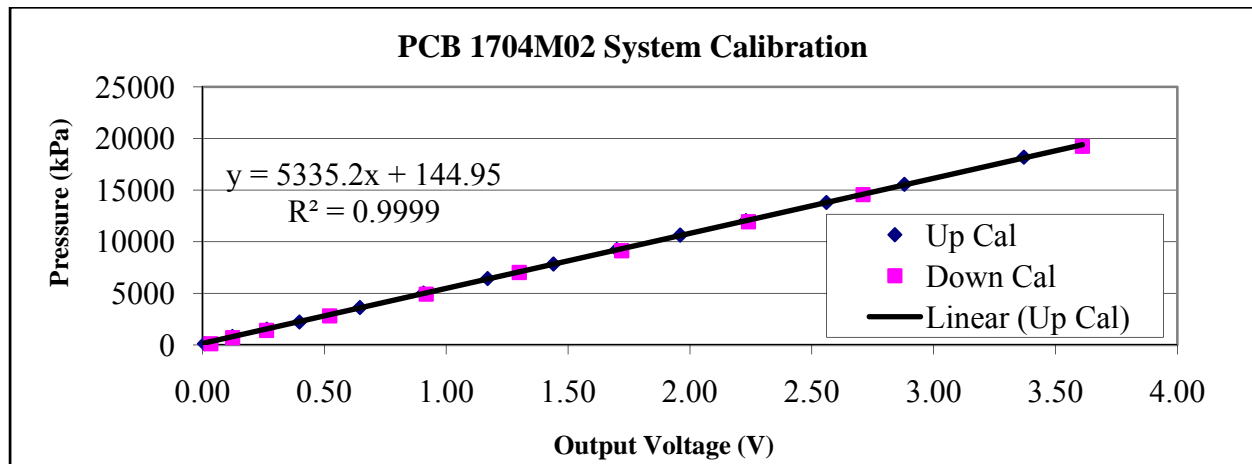


**Figure 3.20 - PCB 1704M02 system calibration.**

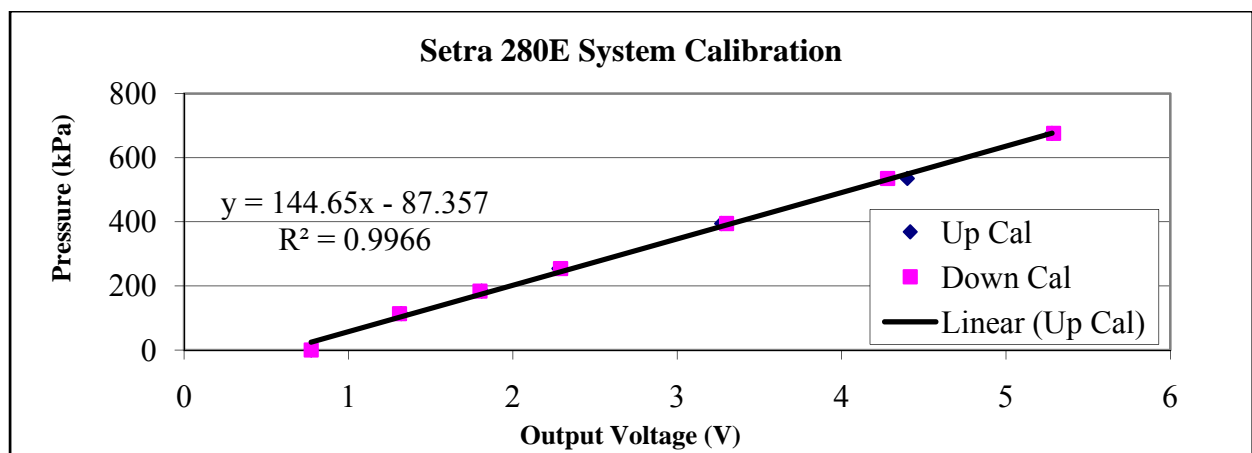


**Figure 3.21 - Setra 280E system calibration.**

To monitor and acquire temperature and pressure measurements, LabView 8.6 was installed on a PC and two National Instrument multipurpose data acquisition cards were used. The NI PCI 6115 and NI PCI-MIO-16XE-50, with the SCB 68 terminal box, provided more than sufficient channels and speed for this study. These data acquisition cards were also used to trigger the spark ignition system, camera, and diesel injection. In addition, they also controlled

relays for controlling the solenoid valves. These solenoid valves were used to provide air to the pneumatic valves for the filling of gases and to purge the chamber out after combustion. However, since the current requirement from these relays was too high for the DAQ card, an input/output (IO) module panel was designed and installed. When power was turned on and a 5 VDC (max 24 mA) was outputted to the IO module from the DAQ card, the relay was switched to provide 12 VDC (max 5 A) - either to power the solenoid valves or to trigger the spark ignition system or diesel injection. Figure 3.22 shows the terminal junction for the DAQ system along with IO module panel. The LabView system DAQ and control VI front panel can be seen in Figure 3.23. Not presented are the VI front panels to control the brushless DC motor speed and to acquire pressure over the entire mixing and combustion events.

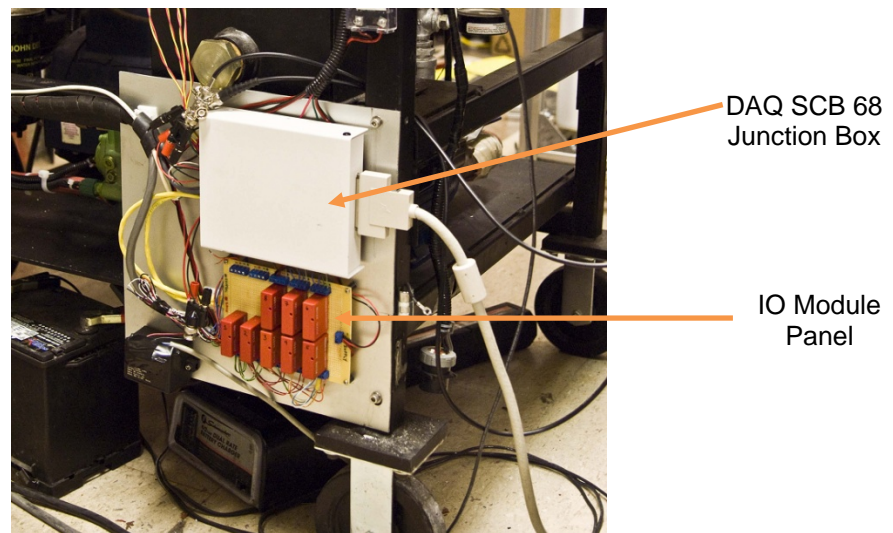


**Figure 3.22 - DAQ system and controls.**

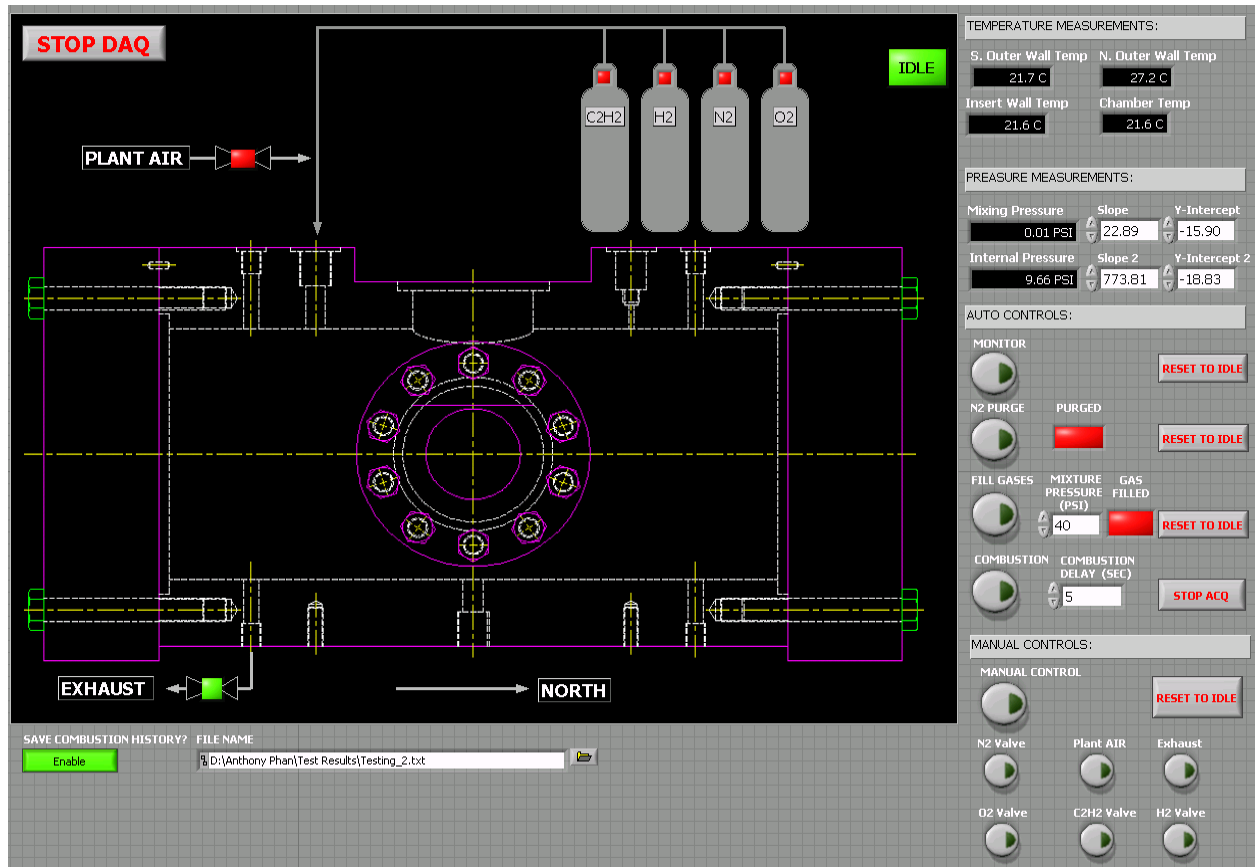


Figure 3.23 - Combustion vessel DAQ and control VI front panel.

## CHAPTER 4. RESULTS AND DISCUSSIONS

### 4.1 Introduction

This chapter presents the results obtained from performing experiments in the injection bench and in the constant volume chamber. The results will also be discussed. It will be divided into two subsections. First, the results and discussion for the rate of injection will be given. The second section will discuss the results and discussion for the combustion chamber will follow.

### 4.2 Rate of Injection Bench

#### 4.2.1 High Pressure Common Rail System Injection Delay

Before the use of the high pressure common rail system, fuel injections in a typical diesel engine occur by a mechanical injection pump driven by the engine cam or crank. Injection pressure was relatively low (approximated 15 MPa) and fuel quantity was adjusted using a mechanical throttle lever on the pump. Fuel timing was fixed and was subjected to the engine speed and load and the fuel fluid properties. As a result, when switching to alternative fuel from the typical diesel, injection timing changes were noticed. This was observed during engine experiments. For example, when switching to B100 (100% biodiesel) from diesel No 2, an advancement of approximately 2-3 CAD (crank angle degrees) was observed at fuel load condition. This advancement in timing was due to the differences in fluid properties and was detected using an engine timing detection tool made available by the engine manufacturer.

With the injection bench, conclusive results were obtained to quantify the injection delay of today's high pressure common rail system. An experiment was conducted to find the injection

delay for diesel and biodiesel blend injection operating at different injection pressure, injection quantity, and back pressures. The 6x133x800 (6 hole, 133 degree included spray angle, and 800 flow number nozzle) baseline injector was used at 1000 rpm engine speed. The definition of injection delay in this study was the time delay from the start of solenoid energizing to the start of the injection profile. This is illustrated in Figure 4.1. Also seen in Figure 4.1 are the energizing time and injection duration definitions.

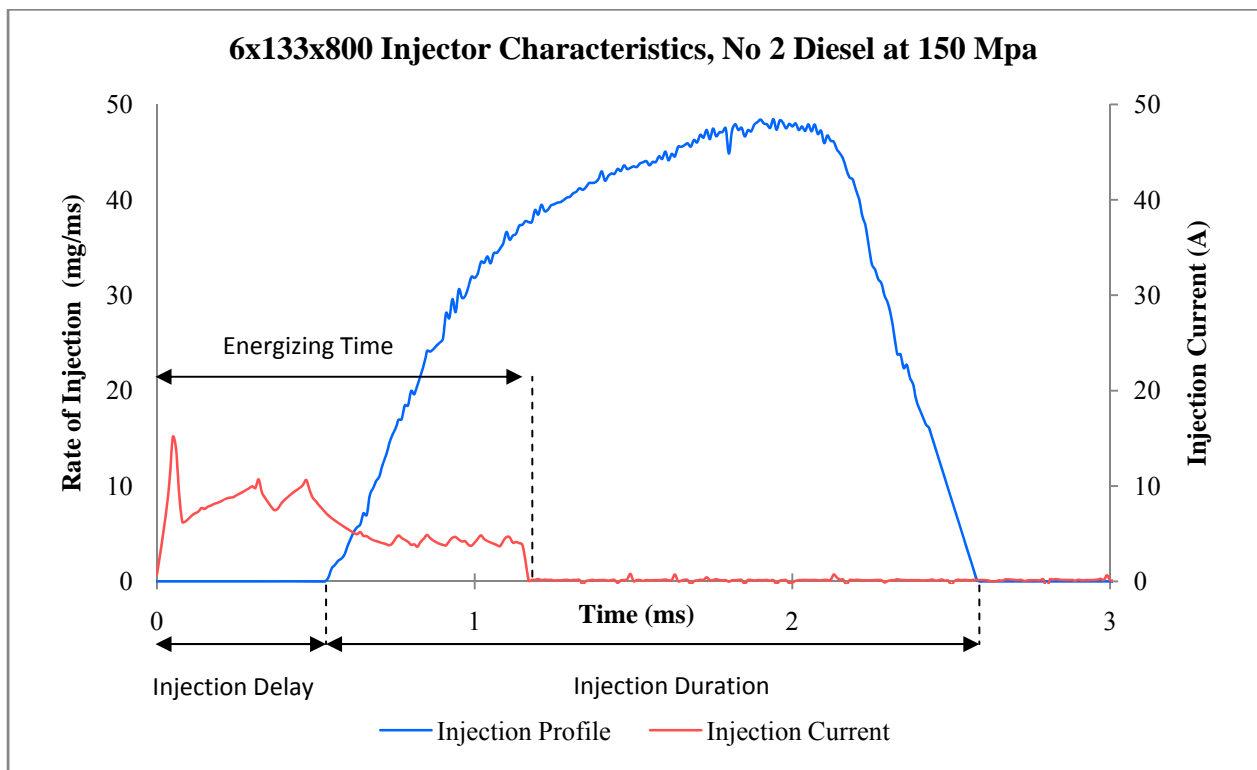


**Figure 4.1 - 6x133x800 injector characteristics with injection delay, energizing time, and injection duration definitions.**

Table 4.1 is a tabulated result of this study. Each case has an injection delay value that was averaged from at least 100 injection events to obtain a large sample statistical meaning with

a tolerance of less than  $\pm 1\%$  of the averaged value. It was observed that the injection delay for the typical diesel fuel spray from the high pressure common rail injection system was very minimal. Regardless of injection pressure, injection quantity, and back pressure, the injection delays have negligible differences among the different fuel used and have an average of 0.501 ms, 0.475 ms, and 0.475 ms injection delay for diesel No 2, B100, and B20, respectively. The standard deviations for the injection delays among the difference fuel used under difference conditions were close to zero, which meant that the results were conclusive. In addition, it was concluded that the injection delays for biodiesel were slightly earlier than that of diesel. However, with so little advancement in timing, this can be considered negligible. To put into perspective, the timing advanced from using biodiesel when compared to diesel No 2 was only about 0.153 CAD at 1000 rpm engine speed.

**Table 4.1 - Injection delay study results.**

Average Rail Pressure [Mpa]	Fuel Quantity [mg/injection]	Back Pressure [MPa]	No. 2 Delay [ms]	B100 Delay [ms]	B20 Delay [ms]
100	20	6.21	0.509	0.476	0.479
100	50	6.21	0.514	0.474	0.467
100	80	6.21	0.502	0.478	0.458
100	110	6.21	0.499	0.472	0.464
100	140	6.21	0.492	0.478	0.474
100	160	6.21	0.489	0.457	0.485
100	160	2.07	0.512	0.505	0.500
100	160	3.45	0.496	0.480	0.475
100	160	4.83	0.498	0.468	0.473
75	160	6.21	0.502	0.474	0.486
150	160	6.21	0.496	0.469	0.464
Average Delay [ms]			0.501	0.475	0.475
Standard Deviation			0.008	0.012	0.012

#### 4.2.2 Diesel Rate of Injections Using Baseline Injector

Using the baseline injector again, the effects of pressure, injection quantity, and injection pressure on the injection profiles were studied using diesel No 2. All cases were run under 1000 rpm engine speed. Before results are presented, it must be mentioned that in all test cases, the high pressure common rail system used in this study was not able to maintain a rail pressure at a completely constant value. As the electromagnetic valve of the supply pump opens and closes to adjust the amount of fuel going into the common rail to maintain a desired injection pressure, there are fluctuations. This system was originally designed for a four injectors operation. With only one injector injecting fuel and the other three common rail ports closed, imbalances in the originally control system was created and resulted in rail pressure variation that was higher than that seen in engine experiments. Figure 4.2 is the common rail pressure trace obtained from DevX 1.0 over five minutes to exemplify the fluctuations. It was seen that the rail pressure fluctuation was approximately  $\pm 10$  MPa from the desired 100 MPa. In engine experiment, only  $\pm 3$  MPa was observed. To alleviate this problem, injection profiles were ensemble averaged over many injection events (typically over 100 cycles) as mentioned previously.

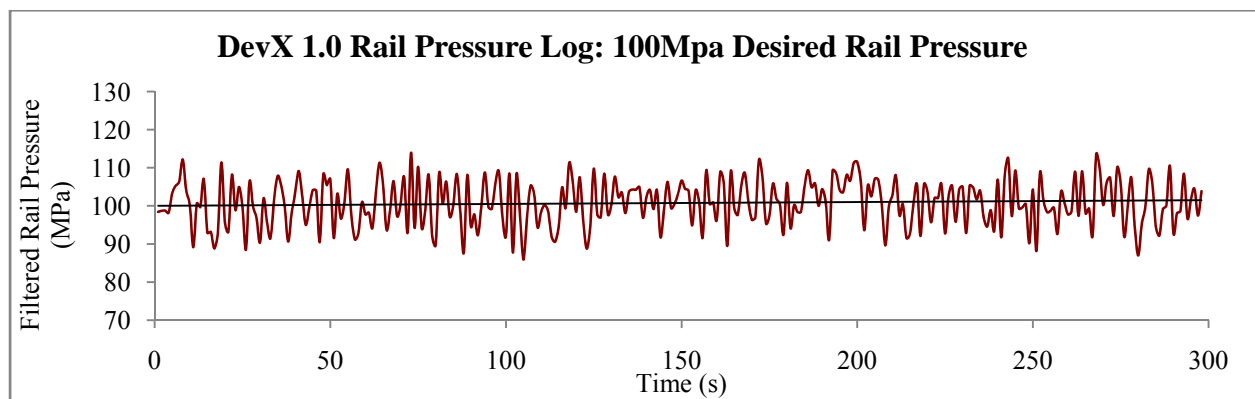


**Figure 4.2– Common rail pressure fluctuation.**

Figure 4.3 below plots the injection profiles to show the effects of backpressure on the injection profiles. From this figure, it was concluded that the variation in the injection rate was insignificant for back pressure ranging from 2.07 to 6.21 MPa. Although the injection profiles do not completely overlay one another to confirm this, the fluctuation in rail pressure was believed to have caused this. When fuel was injected at 100 MPa, the fuel exited with very high kinetic energy. With such a small change in pressure differences, the effects on the injection profiles were found negligible.

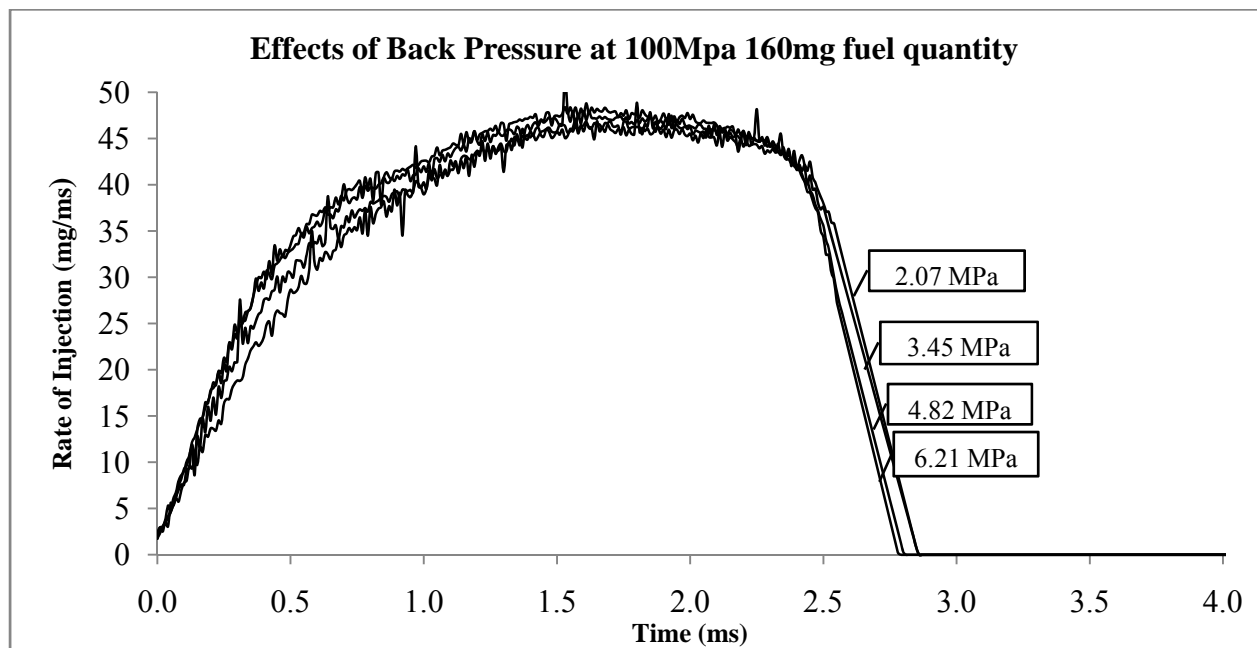


**Figure 4.3 – 6x133x800 injector characteristics, effects of backpressure.**

Next, a study on the effects of injector energizing time on the injection profile was done. This was done at 100 MPa injection pressure and 1000 rpm engine speed. Back pressure was kept constant at 6.21 MPa. Obviously, as the time energizing the injector solenoid increased, more fuel would be injected. This is shown in Figure 4.4. However, it was found that the time

energizing the injector did not affect the rise and fall of the rate of injections at the same injection pressure. Neither did it affect the magnitude of the maximum rate of injection.

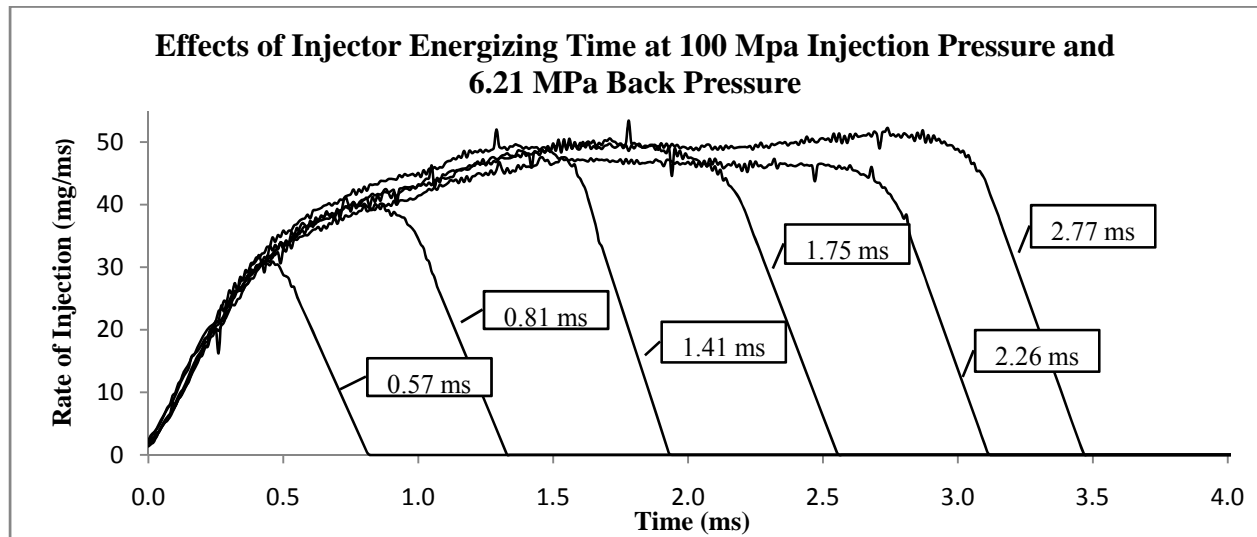


**Figure 4.4 – 6x133x800 injector characteristics, effects of injector energizing time.**

Figure 4.5 illustrates that the injection pressure was what governed the maximum magnitude of the rate of injection, if the same injector was used. In this experiment, approximately 160 mg of diesel were injected at 150 MPa, 100 MPa, and 75 MPa at 6.21 MPa back pressure. The Bernoulli equation could be used to theoretically calculate the maximum rate of injection. However, this was not done in this study because the detail characteristics of the injector were unknown. Although, the number of holes, spray angle, and flow number were known, it could only be used to relatively compare one injector to another. It does not quantify the exact size of each hole on the nozzle or the discharge coefficient. These characteristics must be known to a high degree of accuracy in order to calculate the maximum rate of injection. It can also be seen in Figure 4.5 that as the injection pressure was increased, fuel exited the nozzle at a

faster rate. Similarly, the rate of decay was faster. In addition, when the same injection quantity was desired, a higher injection pressure would yield shorter injection duration.

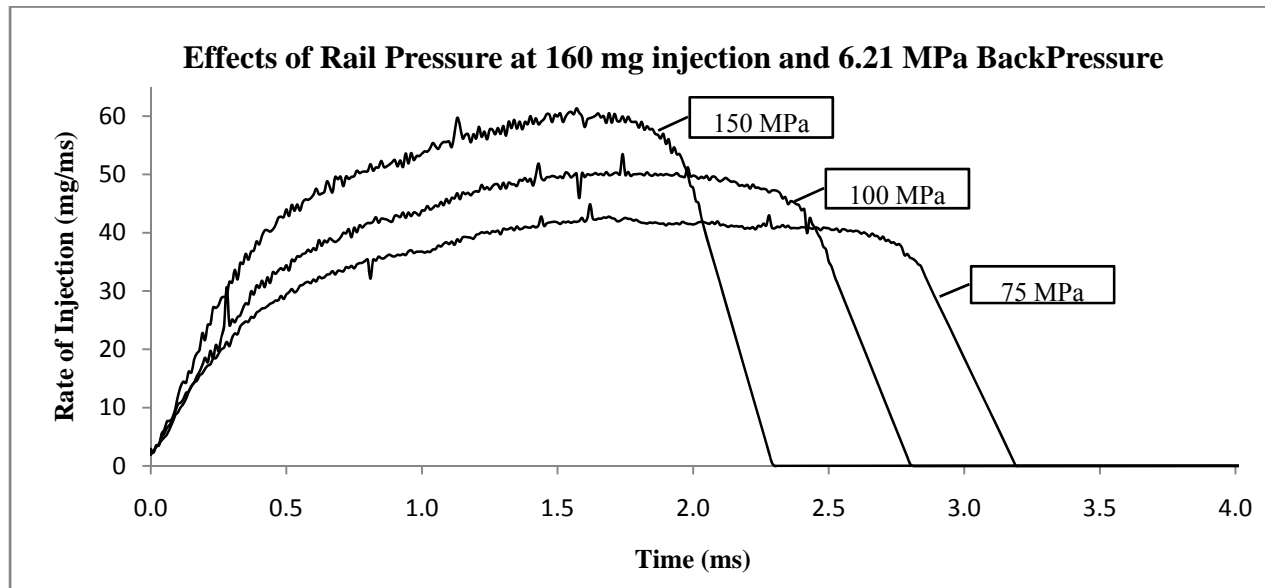
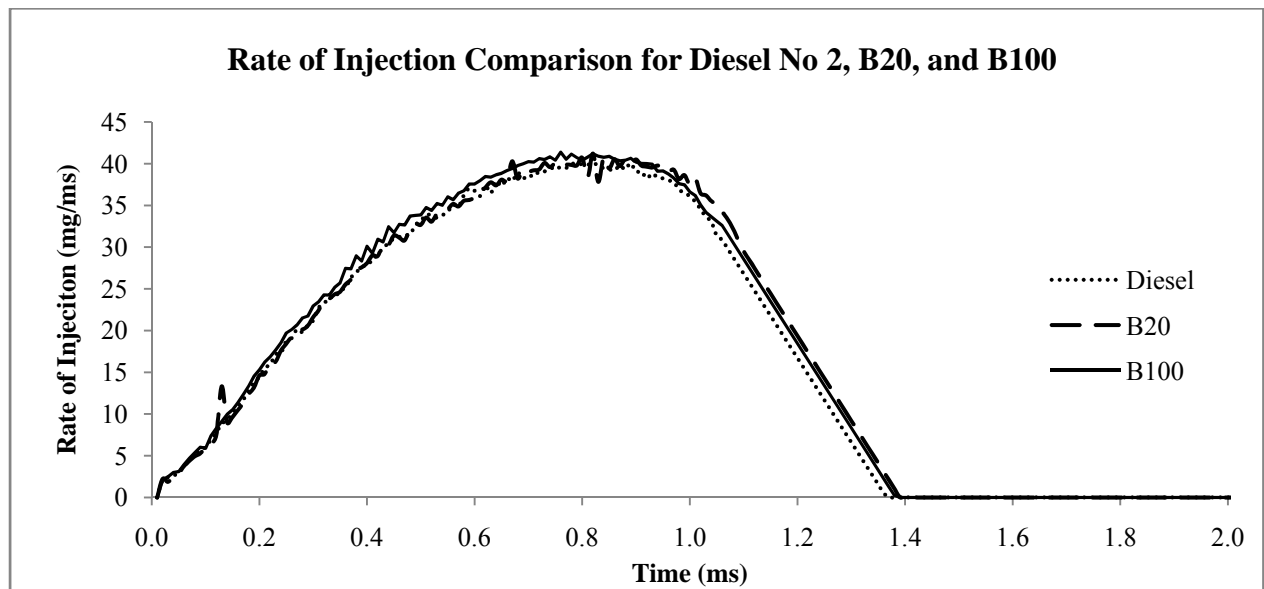


Figure 4.5 – 6x133x800 injector characteristics, effects of rail pressure.

#### 4.2.3 Biodiesel and Biodiesel Blend Rates of Injection

Using the baseline injector, No 2 diesel, B20, and B100 were used to compare the rates of injection for injection pressure of 100 MPa, 6.21 MPa back pressure, and 0.80 ms injector energizing time. Figure 4.6 shows the representative result from this study. It should be noted that after switching fuel, the injection bench ran for 15 minutes prior to the data collection to flush the system from any remains of the previous fuel residuals. The rates of injection were observed to be slightly different due to changes in fuel properties. Particularly of importance was density. No 2 diesel have a density of approximately  $850 \text{ kg/cm}^3$  and B100 have density of about  $880 \text{ kg/cm}^3$  (depending on feedstock) at room temperature. As the concentration of biodiesel was

increased, the rates of injection indicated that slightly more fuel was injected at the same injector energizing time. B100 have a higher maximum rate of injection because B100 density was slightly denser. Nonetheless, the injection profiles for the three fuel tested were very comparable. This was similarly seen with different injector energizing times but not presented here.



**Figure 4.6 – 6x133x800 injector rates of injection comparison using No 2 diesel, B20, and B100 with injection pressure of 100 MPa, 6.21 MPa back pressure, and 0.8 ms injector energizing time.**

#### 4.2.4 Rates of Injection for Different Injectors

Finally, a comparison in the rates of injection profile of the same type of injector with different hole-size and flow number was done using No 2 diesel. The included spray angle for all the injectors used in this study was 133 degrees. Five injectors were used and are as follow: 6x133x480, 6x133x800, 10x133x500, 10x133x800, and 16x133x800. The representative results

from this study are plotted in Figure 4.7. In addition, the integrated fuel masses are also given. The flow number quantifies the relative amount of fuel mass per injection. Consistently, the trend was that as the flow number increased, more fuel was injected. When comparing the injectors of the same 800 flow number (6x133x800 vs. 10x133x800 vs. 16x133x800), it can be seen that the 6-hole yielded the highest injected mass, followed by the 10-hole, then the 16-hole. However the difference in injected mass was very little. It was very interesting that although all of the injectors in this experiment have a relatively constant energizing time of 0.8 ms, the 6x133x800 injector had the highest rate of injection magnitude and the shortest injection duration. It was believed that this injector, out of the other 800 flow number injectors, would have the largest overall nozzle discharge area (if the discharge coefficients were constant among the injectors) or the highest overall discharge coefficient (if the discharge areas were constant among the injectors). In order to be more conclusive about this result additional information about the injector characteristics needed to be known.

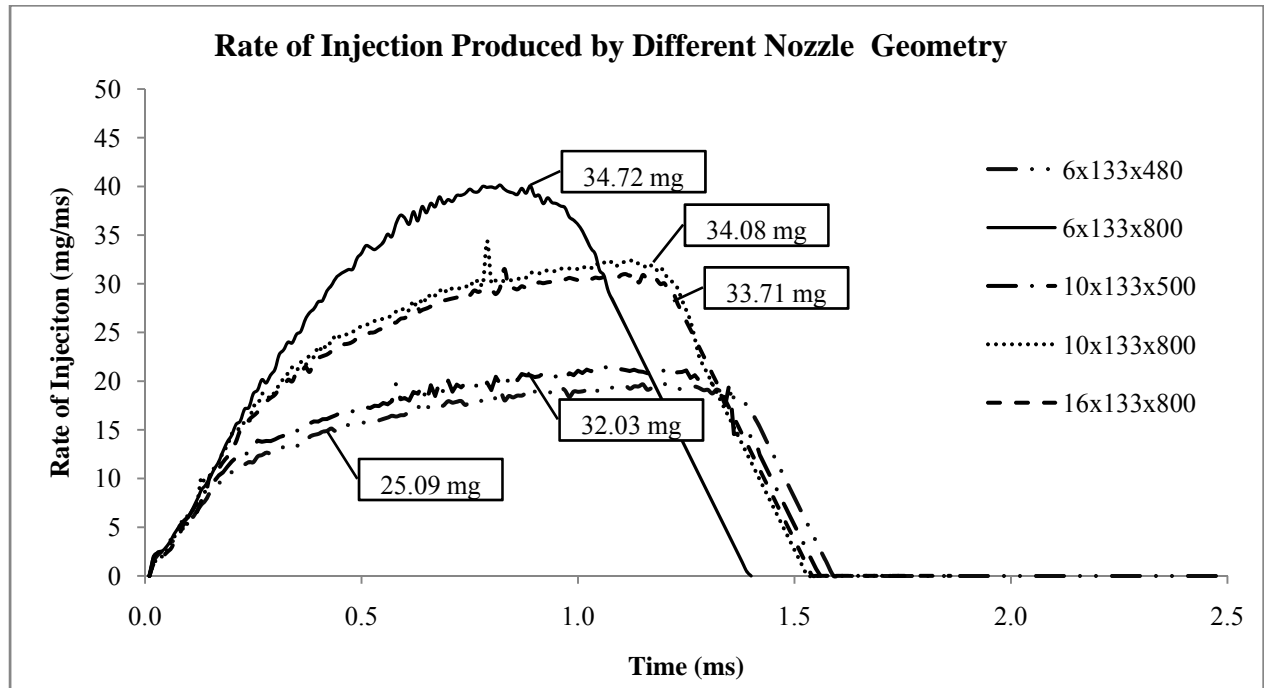


**Figure 4.7 – Diesel rate of injection comparison for different injectors at 100 MPa injection pressure, 6.21 MPa back pressure, and 0.8 ms injector energizing time.**

#### 4.2.5 Rate of Injection of Double Injection Scheme

The rates of injection using double injection scheme were also obtained. The 6x133x800 baseline injector was used again in this experiment. Injection pressure was 100 MPa; back pressure was 6.21 MPa; dwell time was 35 CAD (5.83 ms using 1000 rpm simulated engine speed). Figure 4.8 plots the results from this study. The trends observed were consistent with that seen in single injection events and demonstrated that this injection bench was capable of measuring multiple injection scheme. With the current injection system, up to five injections can be output in a single event. However, small injection quantity (< 5 mg) was subjected to

inaccuracy due to a fixed resolution of the bench. The resolution of the bench was governed by the inside diameter of the measuring tube.

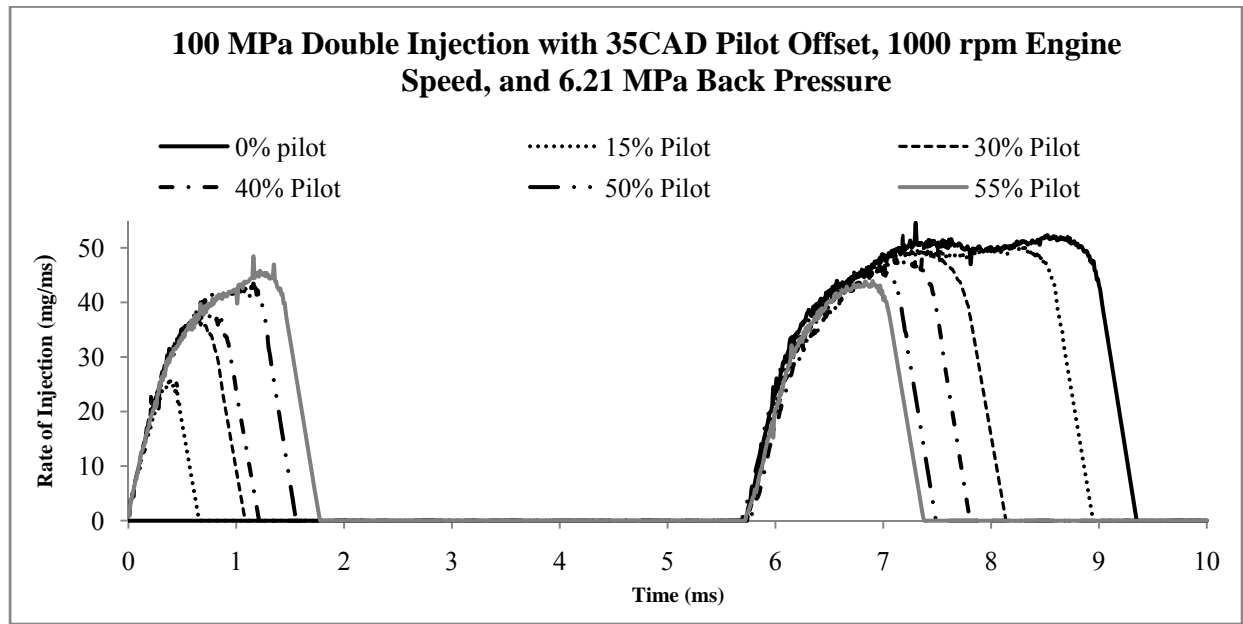


**Figure 4.8 – Diesel rate of injection of double injection scheme.**

### 4.3 Constant Volume Combustion Chamber

#### 4.3.1 Ultra Fast Frame Rate PLIF Diesel Spray Revisit

Before changes were made to the existing CVHC to become a CVPC, the work of Fuller (2009) was revisited. This work was brought upon due to the strange “glow” appearance around the diesel spray structure which looked unreal even though the image was corrected by subtracting the background and any scattering. Figure 4.9 are colorized diesel spray PLIF images collected at 10 kHz taken from Fuller (2009). A single-hole injector was used to inject fuel into the CVHC held at room temperature and 3.5 MPa pressure with an injection pressure of 100

MPa. The diesel spray was excited using a high-frequency laser operating in burst-mode. This experimental setup can be seen in Figure 4.10. Much work was performed to find out what caused this glow, seen clearly in Figure 4.9.

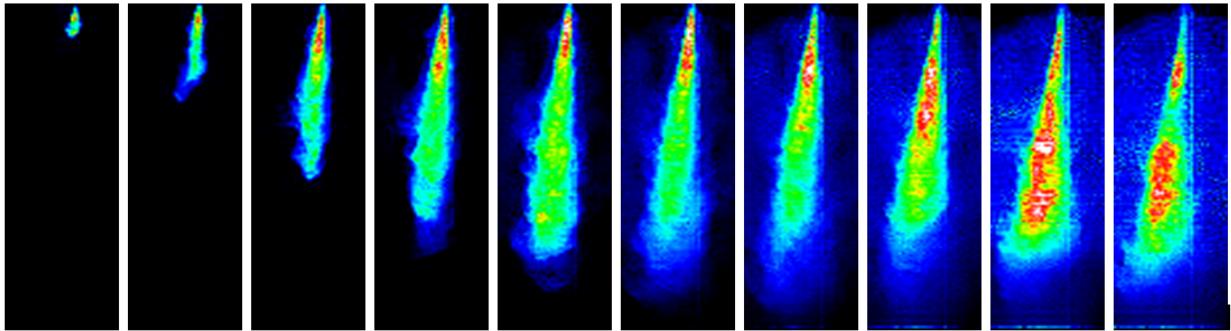


**Figure 4.9 – Scaled single-hole nozzle diesel spray PLIF images collected at 10 kHz with the CVHC temperature of 300 K and pressure of 3.5 MPa and with injection pressure of 100 MPa.**

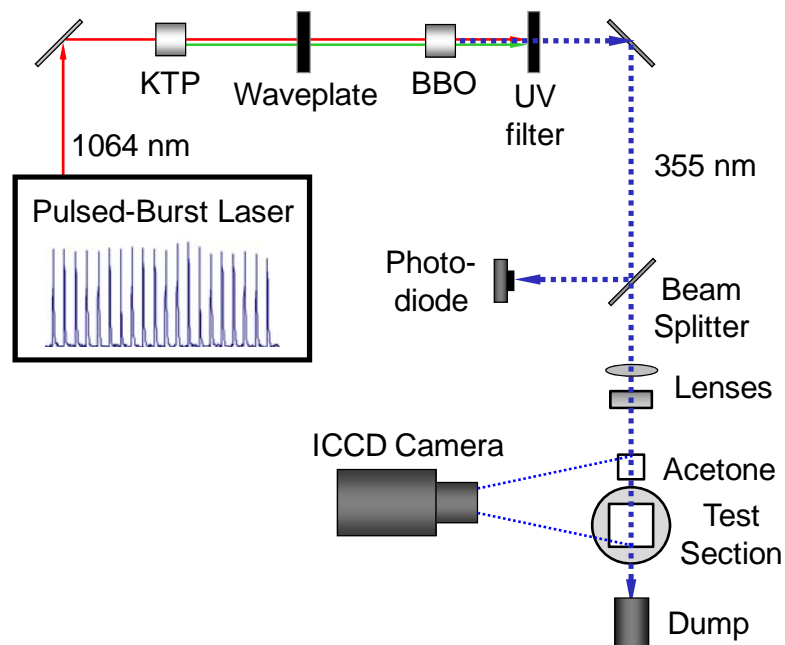


**Figure 4.10 - Optical layout for burst-mode laser imaging of diesel sprays.**

Fuller (2009) used the Olympus I-speed 2 high speed camera that was capable of 224 x 168 resolutions with 8 bit depth at 10 kHz rate to capture the PLIF images. After many experiments were carried out to confirm that the glow was not caused by diesel vapors or diesel aerosols, it was concluded that this camera was the reason why the unreal glow was seen. At such high acquisition speed, the camera lacked in performance. It could be reasoned that at high acquisition rate, the transfer mechanism for transporting the raw image to the internal memory was slowed down. Because the transfer mechanism was protracted, any subsequent images captured was affected by the previous images. To demonstrate, the Phantom V7 high speed camera was used to capture the diesel spray evolution once again. This 16 bit depth camera has a maximum resolution of 512 x 384 at 10 kHz. Seen in Figure 4.11 are corrected and colorized images collected using the Phantom V7 for a single-hole nozzle PLIF diesel spray at 10 kHz with the CVHC at 300 K and 1 bar. The injection pressure was 100 MPa. The glow was completely absent in these images.

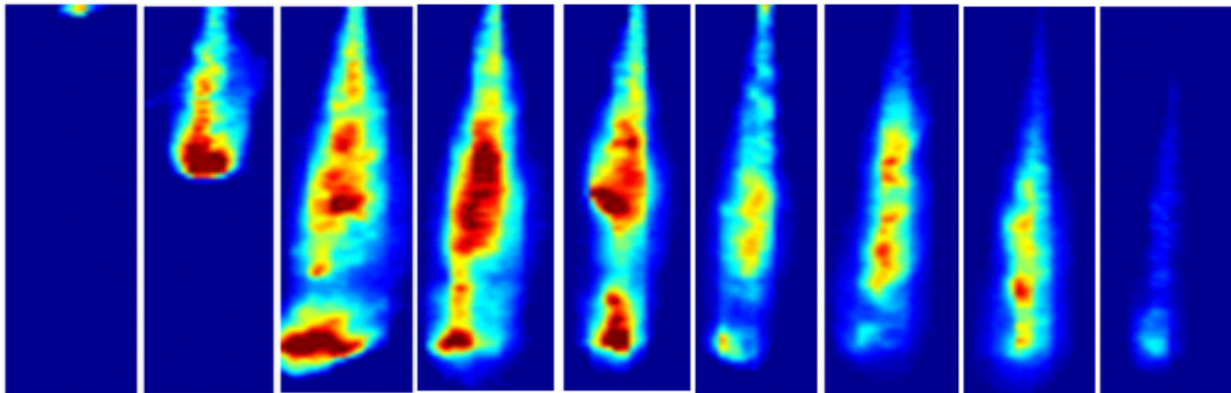


**Figure 4.11 - Scaled single-hole nozzle diesel spray PLIF images collected at 10 kHz with the CVHC at ambient condition and with injection pressure of 100 MPa.**

Due to the fact that energy from the laser sheet could vary spatially and temporally, it is notable to mention that images presented in Fuller (2009) and those presented here were corrected temporally and spatially with the use of a test specimen. In both studies, a quartz cell cuvette was placed in front of the laser sheet beam before going into the CVHC. This can be seen in Figure 4.12.

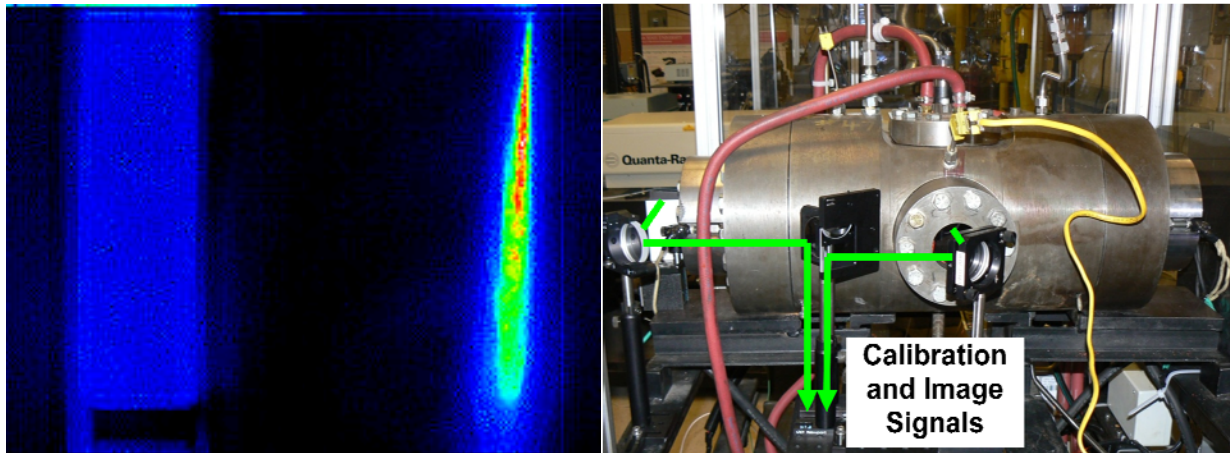


**Figure 4.12 - Colorized raw image showing cuvette and spray PLIF (left) and setup for simultaneously imaging cuvette and diesel spray (right).**

Fuller used both acetone and laser dye (Exciton LD 489) diluted in methanol inside the cuvette for recording the time-dependent laser sheet profile for image normalization on a shot-to-shot basis. Diesel diluted in acetone was used in this study. The reason for the switch was because Fuller (2009) used a 355 nm wavelength laser beam while wavelength used in this study was 266 nm. Noted by Fuller (2009), diesel at 266 nm absorbs less than at 355 nm. When the 266 nm wavelength was used, the laser sheet was allowed to completely pass through the diesel spray at the same laser energy seen in Figure 4.13.

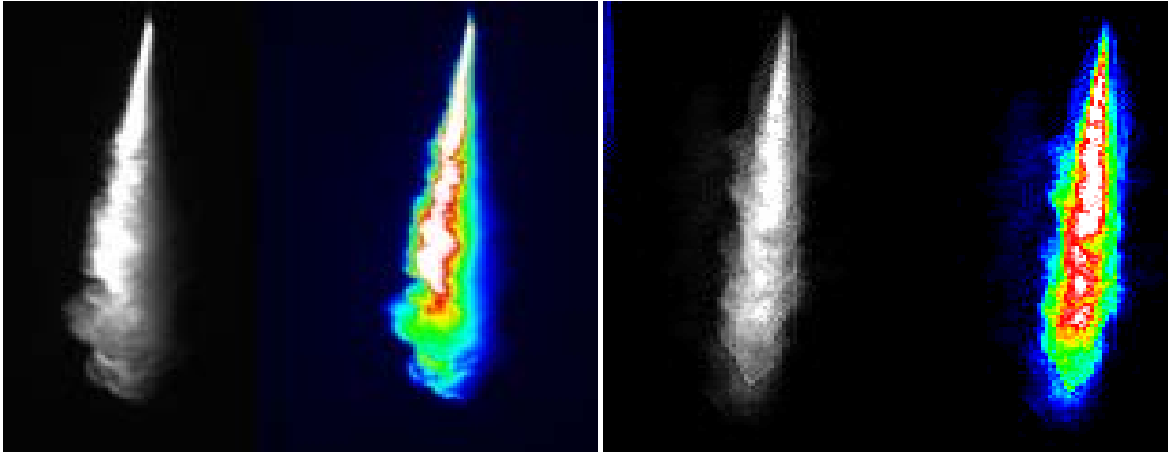


**Figure 4.13 - Raw and colorized diesel PLIF with 355 nm wavelength (left) and with 266 nm wavelength (right).**

When correcting the PLIF images with the use of the cuvette, it was assumed that diesel absorption was directly related to the laser power in a linearly matter. An experiment was setup to test this assumption. In this experiment, a 10 mm path length quartz cuvette filled with 5% diesel in acetone was made to exhibit fluorescence using the output of a frequency quadrupled a Nd:YAG laser. As different laser beam energy level was outputted by the laser, the energy was recorded by a laser power meter and the photodiode excitation voltage was recorded by an oscilloscope with and without the cuvette in front of the beam. At 266 nm wavelength, acetone would have negligible absorption. Only diesel would absorb the laser energy to fluoresce. Figure 4.14 and Figure 4.15 conclude that our assumption was valid and that absorption by diesel was directly proportional to laser power in a linearly fashion.

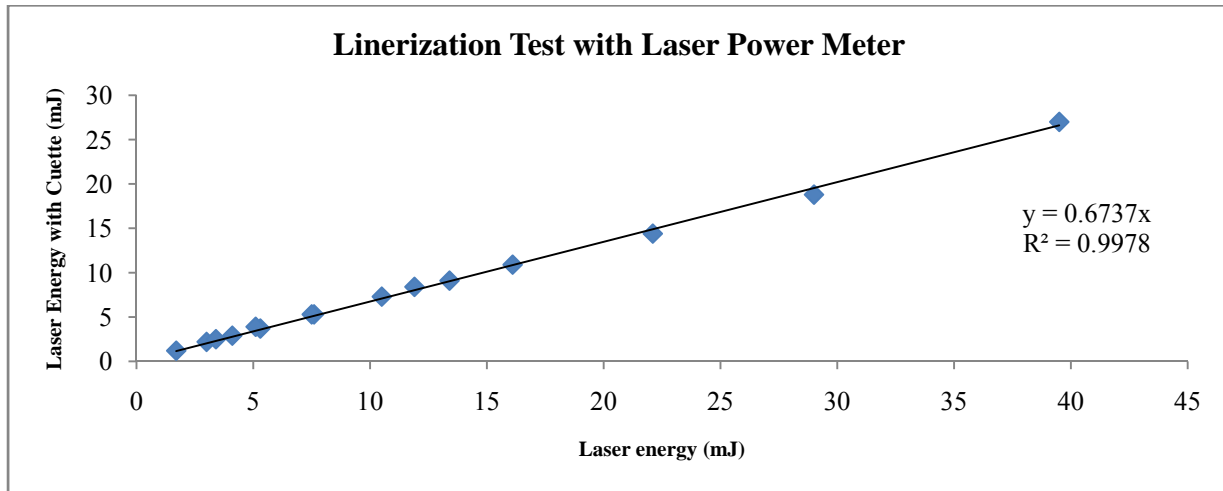


**Figure 4.14 - Linearization test using laser power meter detection.**

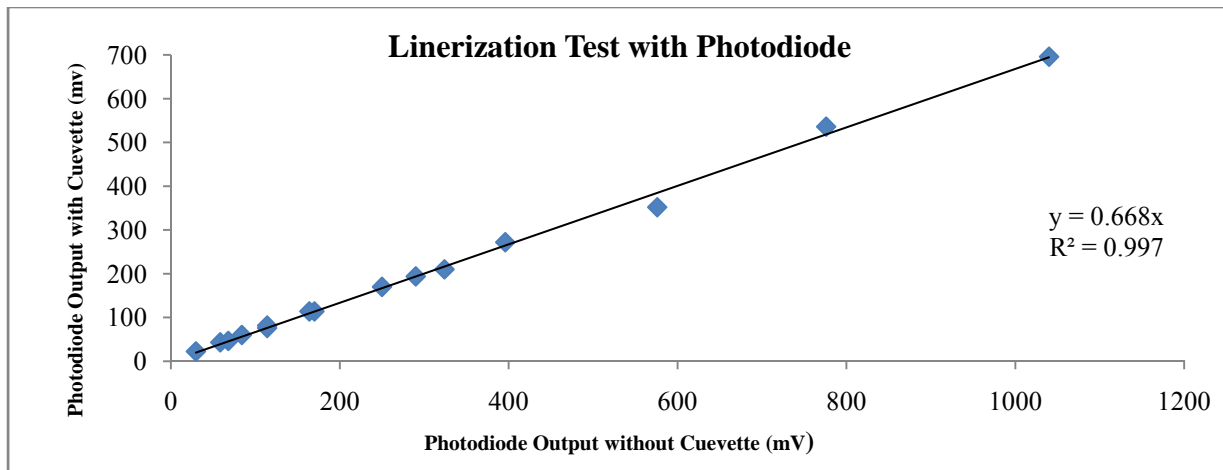


**Figure 4.15 - Linearization test using photodiode detection.**

### 4.3.2 Filling Process

After finishing experiments in the CVHC, it was desired to proceed for the conversion to become a CVPC with the changes mentioned earlier. As the seals for the windows and many

new components were implemented, it was important to make sure that during the filling and combustion processes, there were negligible leaks. If there were substantial leaks, mixing of gases during the filling process would not yield the correct desired mixture concentration. In addition, leaks during the combustion process would yield losses in initial mass, which would be problematic when calculations are performed. First, to make sure that leaks did not occur during the filling process, the sealed chamber was pressurized with nitrogen to approximated 689 kPa and the pressure trace from the Setra 280E pressure transducer was acquired over a period of ten minutes. Shown in Figure 4.16 is the pressure trace from this experiment. It can be seen that within a period of ten minutes, the chamber showed negligible pressure losses with an initial pressure of 689 kPa.

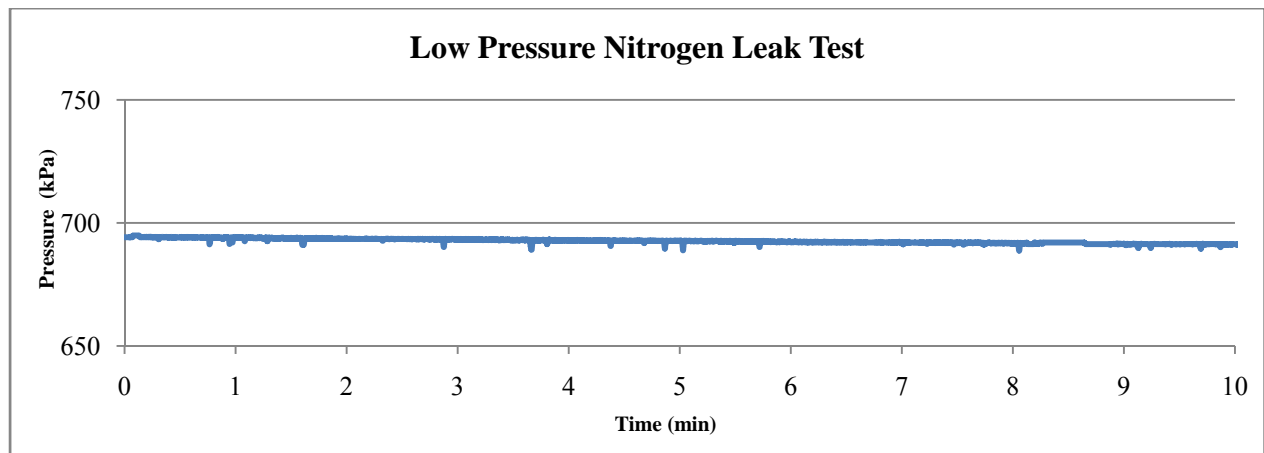


**Figure 4.16 - Low pressure leak test using nitrogen.**

Next, due to the fact that the internal chamber pressure will reach high pressure after premixed combustion, the sealed chamber was pressurized with nitrogen to approximately 3500 kPa to check for leaks. The pressure trace from the PCB 1704M02 pressure transducer was acquired over a period of ten minutes. After ten minutes, approximate 10% of initial pressure

was loss. Using soapy water, leaks did not seep out of the windows or the newly installed multipurpose housing. It was believed that nitrogen could have escaped from the injector seal or from the spark plugs seals. However, when scaled down into perspective, elevated pressure after premixed combustion would only last approximately 10-15 seconds. Immediately after premixed combustion, the internal pressure would decline as the heat is lost to the surrounding walls. Realistically, the chamber needs to hold high pressure for only up to 15 seconds. Results shown in Figure 4.17 confirmed that leaks during the high pressure test using pressurized nitrogen yielded negligible pressure loss up to 15 seconds. After premixed combustion, the product (simulated air) would have a molecular weight very similar to that of air (28.97 kg/kmol). As simulated air is denser than nitrogen, with a molecular weight of 28.01 kg/kmol, even fewer leaks would occur.

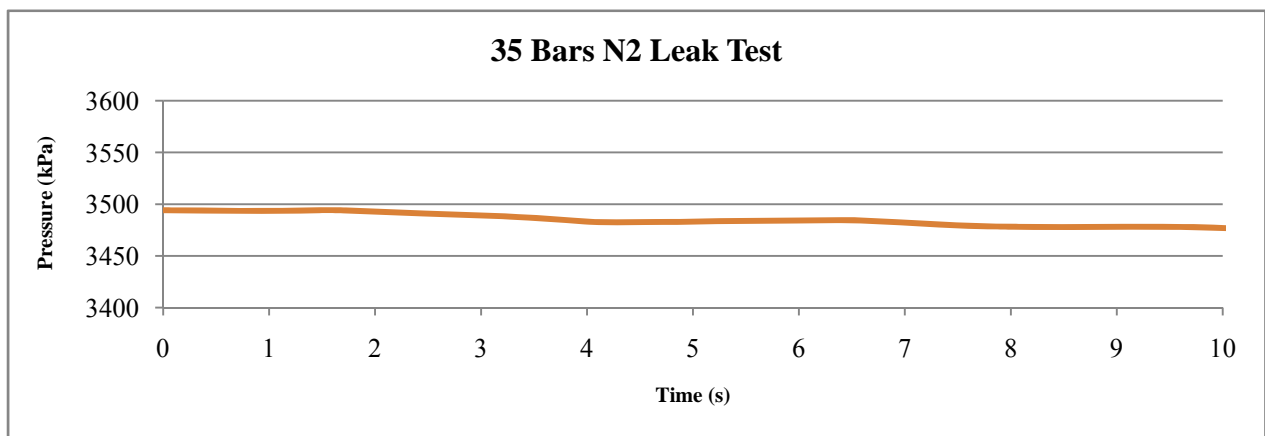


**Figure 4.17 - High pressure leak test using nitrogen.**

As mentioned previously, the filling of the four selected gases was done using its partial pressure assuming that gases behaved ideally. The gas purity level used in this study was all above 99.5%. Before the filling process, the chamber was purged with nitrogen, heated to 373 K,

and allowed to sit until the wall surface temperatures were uniformed. Heaters on the inside and outside of the chamber were controlled using a temperature controller in a PID feedback loop. This setup kept the chamber temperature constant within  $\pm 3$  K. Throughout the experiment the mixing fan was constantly rotating approximately 6000 rpm to help achieve uniform temperature distribution inside the chamber. Figure 4.18 is the pressure history of the filling process when 659 kPa mixture pressure was inputted. During the filling process, individual gases were slowly added in pulsation for better mixing and to allow time for temperature equilibrium and mixture homogeneity. Figure 4.18 shows that that the filling process was prolonged over nine minutes. By adding gases at a slow rate, the filling target pressures of individual gases were attained with high accuracy to ensure that the mixture composition was correctly achieved.

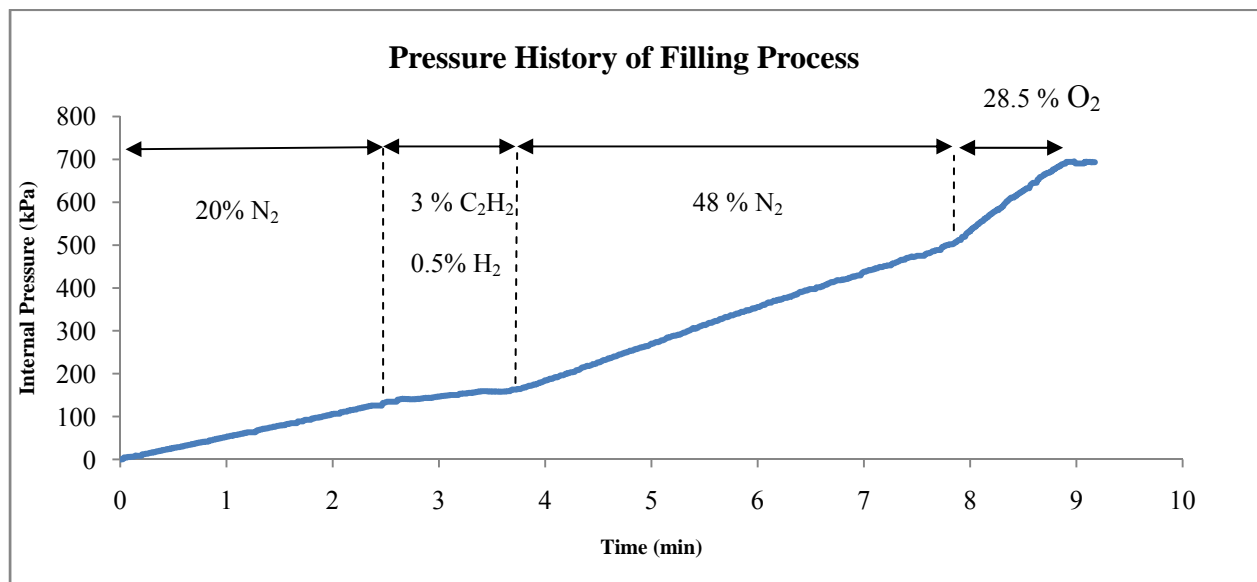


**Figure 4.18 - Pressure history of the filling process.**

### 4.3.3 Premixed Combustion

After filling of gases, time was allowed for the mixing fan to operate to further ensure gas homogeneity (typically 3-5 minutes). Then, the spark ignition system was triggered and premixed combustion was observed. Temperature and pressure trace were acquired and plotted in Figure 4.19. The pressure and temperature traces were very similar to other premixed combustion system. After ignition, pressure and temperature were elevated in a short period of time and the cool down stage was also noticed. When the selected gaseous mixture of 689 kPa was input and ignited, a peak chamber pressure of 2320 kPa and peak chamber temperature of 919 K was attained. The peak chamber pressure and temperature seen were subjected to the initial mixture pressure. A higher pressure and temperature could be attained from the current setup if a higher gaseous mixture pressure was inputted. Due to the limitation of the low pressure transducer (max 689 kPa) used for mixing, higher input pressure was not done in this study. The current system is also very flexible in terms of what gases mixture can be inputted. This means that it is flexible in simulating different environmental condition. For example, if the effect of EGR on diesel spray combustion was desired, CO<sub>2</sub> could be added as an input gas. It can also be recognized that the pressure transducer and thermocouple used in this study were very responsive and suitable for this study. While laser imaging and spectroscopy was not employed to studied spray combustion in this study due to time constraint, the CVHC and adjacent systems were demonstrated for readily studying spray combustion. From approximately 0.5 to 2.5 seconds in Figure 4.19, an injection of diesel spray will surely mark the event of diesel combustion. It can be noted that the small oscillations in the pressure and temperature traces were contributed from low speed acquisition rate (1000 S/s) and noise filtering. This was not

seen when high acquisition rate (100,000 S/s) was used in Figure 4.20. At this acquisition speed, pressure wave from the premixed combustion was also be detected by the transducer. This pressure trace was acquired from premixed combustion with only an input pressure of 344 kPa. However, at this speed, post processing was difficult due to the extremely large sample size.

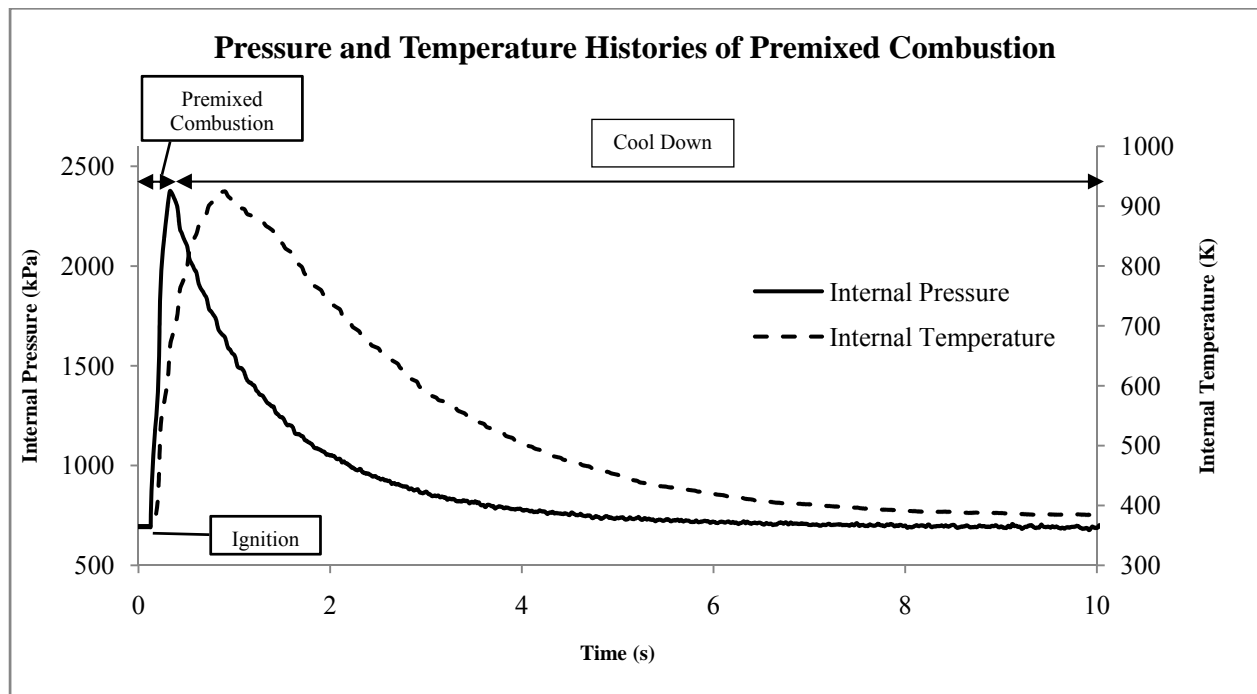


**Figure 4.19 - Pressure and temperature traces acquired during premixed combustion with an input mixture of 689 kPa.**

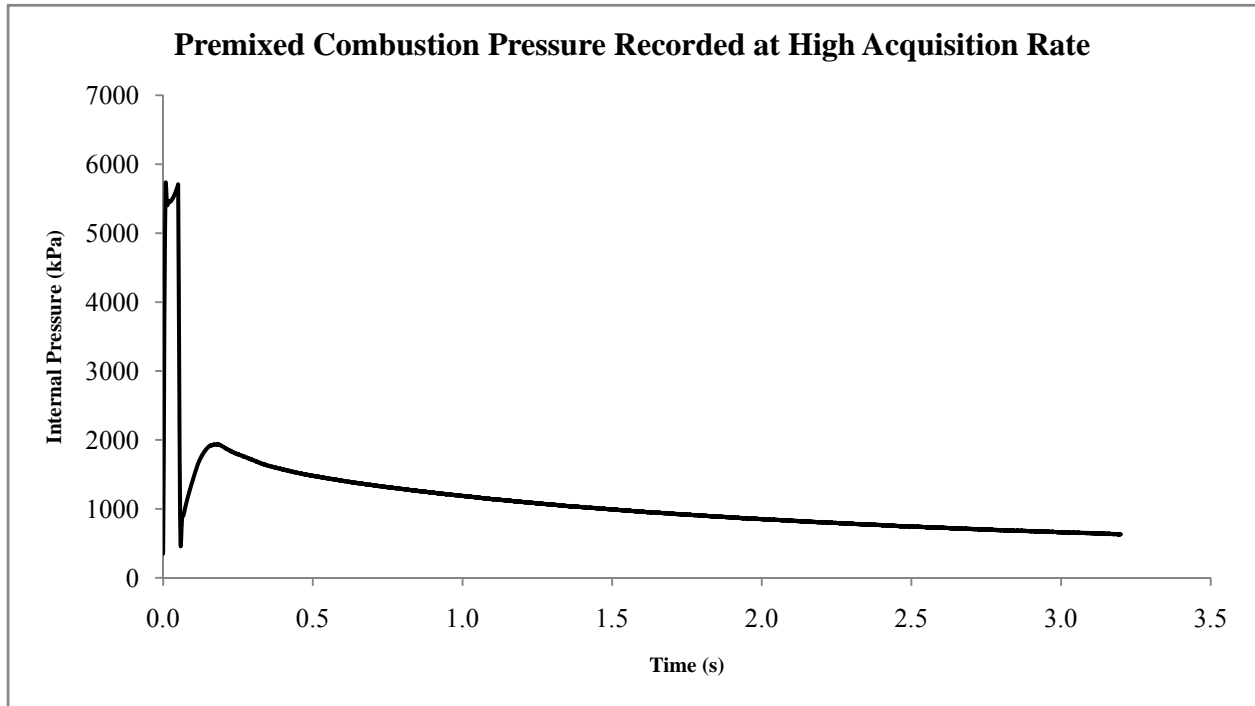


**Figure 4.20 - Pressure trace acquired during premixed combustion at high acquisition rate with an input mixture pressure of 345 kPa.**

## CHAPTER 5. CONCLUSIONS AND RECOMMENDATIONS

### 5.1 Conclusions

In completion of this study, a rate of injection bench was developed, validated, and demonstrated. Different injectors with various nozzle diameters and flow numbers were used with to study the rates of injection of both diesel and biodiesel blends under different operating conditions. It was discovered that the rate of injection trace had a slower than expected decay and correction was made based on the rate of decay. Validation of the bench was carried out by comparing the averaged integrated mass with measurement from a weight scale and the result showed that the bench consistently under-produced an average of 10% of the mass when compared to the actual injected fuel amount. This was consistent with findings from other researchers thus experiments were carried out to find the effects of backpressure, rail pressure, injector energizing time, and injection scheme with a 6x133x800 baseline injector. In addition, experiments were performed to learn if injection timing was an issue when switching from diesel to biodiesel. Rates of injection from five different injectors were also compared.

Test results showed that variation in the injection rate was insignificant for back pressure ranging from 2.07 MPa to 6.21 MPa. Also, when using the same injector energizing time to inject the same fuel, an increased in the injection pressure resulted in an increased in the peak injection rate and a decreased in the injection duration. The peak injection rate corresponded to the Bernoulli mass flow rate multiplied by the injector overall nozzle discharge flow coefficient. Moreover, for the same injection pressure, the rises and decays of the injection rates for different energizing times of the same injector have negligible differences. An increase in injector

energizing time only lengthened the peak injection rate duration. When comparing rates of injection between diesel and biodiesel blends, injection delays were negligible. This was concluded because only an advancement of 0.15 CAD was detected when biodiesel was used in place of diesel at an engine speed of 1000 rpm. In addition, the rates of injection of biodiesel were comparable to that of diesel. Because biodiesel have a slightly higher density, results from the injection bench indicated that an increase in biodiesel density yielded a slight increase in injected mass if injection conditions were matched.

Furthermore, the work of Fuller (2009) was revisited to analyze the unidentifiable glow around the diesel spray in the ultra fast frame rate PLIF images captured using the CVHC and a high frequency laser operating in burst mode. It was concluded that due to the camera's poor performance at high acquisition rate, artifacts from previous frames affected the followings and thus the unreal glow became apparent. To demonstrate, a similar experiment to that of Fuller (2009) was performed using a superior high speed camera. Images collected in this experiment showed no sign of the glow and were better in characterizing the spray structure.

After work was completed on the CVHC, implementations were made to the existing CVHC to become a CVPC. In completion, new O-rings replaced old copper gaskets for better sealing and a multipurpose housing was fabricated to house the pressure sensor, two spark plugs, and a mixing fan. A data acquisition system and control system was also employed and demonstrated. While the previous chamber was capable of achieving a fixed temperature of 600 K, the new chamber was demonstrated to attain up to 919 K while showing negligible leaks. Even higher temperature and pressure can be reached if more combustible gaseous mixture is inputted.

## 5.2 Future Recommendations

### 5.2.1 Injection Bench

It is recommended that a more conclusive study be done to better understand what caused the slow rate of decay seen in the raw pressure trace. The pressure sensor may be sent back to the manufacturer to qualify a system response time thus eliminating if the problem lies within the pressure sensor itself. In addition, to decrease fluctuation in the rail pressure when running experiments, it is suggested to increase the volume of the common rail. This will provide more dampening to the PID control system inside the ECU. Instead of the four cylinders common rail, it may also be beneficial to upgrade to the six cylinders common rail or even extend the current volume by adding another four cylinders common rail. Not only will this decrease rail pressure variations, but it will also decrease vibration seen when high injection pressure ( $>135$  MPa) is used. Strong vibration was experienced mainly because of an untuned PID which controlled the supply pump. As only one injector is injecting, it creates lows and highs in fuel demand from the supply pump. To also help decrease vibration, the motor support can be strengthened.

### 5.2.2 Constant Volume Pre-Combustion Cell

While running experiment with the CVPC, it was noted that the heater could be better controlled. Currently, two types of heater are controlled by only one temperature controller. One type was used to heat the wall temperature and another was used to heat the internal chamber temperature. Because the heaters have different performance characteristics and temperature of the wall and internal temperature at the start of the experiment were different, it is suggested to individually control each using two separate temperature controllers.

In addition, when using a combustible gaseous mixture of 689 kPa, it was noticed that two single sparks from the two spark plugs were not able to ignite the gaseous mixture in a consistent manner. A multi-spark scheme, with up to ten sparks, was used to ignite the mixture. It is recommended that even more combustible gaseous mixture should be used. When the input pressure is higher, gas molecules are closer together and the mixture should be more easily ignitable. Not only will the mixture be easier to ignite, but the duration interval at which diesel injection will yield combustion will also be lengthened. This will require another pressure transducer because the current one has a maximum pressure detection of 689 kPa.

Lastly, it is recommended that more windows be ordered and available before starting spray combustion experiments. It should be noted that the lead time for acquiring these windows was four to six weeks. Combustion is violent, which can cause the window to crack, and some test cases might yield soot, which can dirty the windows. Spare windows on hand will result in more seamless experiments.

## APPENDIX A1. INJECTION BENCH OPERATING PROCEDURES

This section provides a procedure for obtaining the raw injection profile from the injection bench. This is written with an understanding that the user knows how to monitor and control many injection parameters in DevX 1.0 (e.g., injection quantity, injection pressure and multiply injection timing).

### **Prerequisites:**

Before the rate of injection can be operated, the following items must be addressed (in no specific order):

- The fuel storage tank must have sufficient fuel. This tank stores fuel to be used in the injector. Unscrewing the black cap seen below allows access into the fuel tank where it is simple to do a visual check for fuel level. It is safe to unscrew the cap during operation of the bench.



- Plug in the fan for fuel cooling. The cooling fan can be seen in the following picture. Once plugged in, the fan will run until unplugged. The cooling fan needs to be operating during the experiment to ensure consistent test conditions and to prevent the supply pump from overheating.



- Turn on the power to the frequency inverter. On the back of the injection bench, there is a power disconnect switch. As power is provided to the frequency inverter, LEDs on the frequency control panel will be lit as seen below.



- There is enough capacity for any injected fuel in the fuel collection tank. This tank has a much larger capacity than the fuel storage tank and thus only needs to be emptied not as often as the fuel storage tank needs to be refilled.



- Turn on the power to the inductive pickup and connect the clamp onto the positive lead of the injector solenoid. When the injector is injecting, there should be a voltage trace capturing the current going into the injector. If this trace is not present, the battery is dead or the meter is disconnected. If this trace is negative (spiking down and then returning to zero) then the meter is connected improperly and must be moved to the other wire lead. It is important to turn off the inductive pickup off after every session as the battery will easily run down.



- Make sure the battery has sufficient charge.
- Launch DevX 1.0 and connect to the ECU. The password to DevX and ECU can be found in a file labeled “Passwords” found in the following location on the injection bench computer: E:\Injection Bench DAQ.

- Mount the injector onto the injector mount. This procedure is not outline in this document, however, similar procedure can found in the John Deere service manual when changing out the injector.



- Turn on the power to the charge amplifier.

### **Running an experiment:**

Once all the prerequisites have been met, it is ready to begin running a case. The following procedure outlines how to operate the bench and obtain the raw rate of injection:

1. In DevX, set all the injection parameters. This includes injection quantity, injection timing, and any double injection parameters. Regardless of the desired injection pressure, set the injection pressure to 30 MPa.
2. Launch LabView and the VI labeled “Injection Bench V1.1.vi.” In this VI, specify a running time and file location to which the pressure and current trace will be create and save. Also, select an engine speed file from the library.
3. Run the VI. Once the VI is ran, the crank and cam signal would be continuously generated. In DevX, confirm that the engine speed corresponds to the simulated engine

speed. Only when the ECU has detected an engine speed can the following procedures be continue.

4. Start the AC motor by depressing the “Run” button on the frequency inverter control panel. Monitor the frequency output and slowly increase the frequency to between 40 and 50. Increasing the frequency of the motor can be done with the potentiometer on the frequency inverter control panel. As the speed of the motor is increased, check for any leaks that may occur.
5. In DevX, set the manifold pressure. Increase the set point from 30 MPa to the desired injection pressure by adjusting it upward in 5-10 MPa intervals. After every adjustment, click the “commit to changes” button to change the pressure.
6. Press “Start Injection” in the LabView screen. Wait approximately ten seconds for the pressure inside tube to settle. Then set the back pressure by adjusting the pressure relief valve and monitoring it with the mechanical gauge.
7. Once the pressure trace is approximately constant and the desired back pressure has been obtained, log the pressure and current trace by depressing the “record data” button on the LabView screen. Fuel injection will continue and the pressure and current traces will be logged until the set stopping time has been reached.
8. Once the set stopping time has been reached and the injection has stopped, lower the injection pressure back to 30 MPa in the same way as the pressure was raised.
9. Turn the motor off by pressing the “Stop/Reset” button on the frequency control panel and turn off the VI stopping the signal generation.

## APPENDIX A2. INJECTION BENCH POST PROCESSING CODES

The following Matlab codes were for the injection bench preprocessing. A brief description is provided at the beginning of each code. Slight modifications may have been used due to changes within the experiment.

```
function filename=file_name(strin,i)
filename=strin;
filename=strcat(filename,int2str(i));
filename=strcat(filename, '.txt');

%Injection Bench Post Processing for Single Injection
%Author: Anthony Phan
%Written: Dec 23 08
%Version: 6.0
%Revised by: Justin Callies

%% Clear Matlab
clear all;
close all;
clc;

%% Prompt User for Sample Size and Input Delta Time Acq
Sample_Size=input('How many samples are there? ');
T=input('What is the mean fuel temperature (C)? ');
P=input('What is the backpressure (psi)? ');
del_T=0.01; %Data Acquisition Time in ms
Slope_Factor=.05;
clc;

%% Calculate Speed of Sound in Fluid
Percent=100; %Biodiesel Percentage
Start_From=1; %Start File Processing From File #)
P=900;

P=P*0.00689475728; %Convert to Mpa
% Constants
C1=-3.5972;
C2=4.6849;
C3=2.3682e-1;
C4=1.4412e-2;
C5=-3.9664e-3;
C6=-1.6236e-2;
C7=8.8429e-4;
C8=1.4570e3;
c=C1*T+C2*P+C3*Percent+C4*T*P+C5*P*Percent+C6*P^2+C7*Percent^2+C8; %Speed of
Sound in m/s

%% Calculation
```

```

for i=Start_From:Sample_Size
    %Reading File
    x=load(file_name('75Mpa_160mg_900psi_',i));
    [M(i) N(i)]=size(x);

    %Finding Start of Main Injection
    for j=1:M(i)
        if x(j,4)>0.3
            M_Inj_Start(i)=j;
            break
        end
    end
    %Finding Main Injection Duration
    for j=M_Inj_Start(i):M(i)
        if x(j,4)<=0.19
            M_Inj_Stop(i)=j;
            break
        end
    end
    M_Injection_Duration(i)=(M_Inj_Stop(i)-M_Inj_Start(i))*del_T;

    %Calculate Relative Time,Mass Flowrate, and Injection Current
    for j=(1):M(i)
        Time(j,i)=(x(j)-x(M_Inj_Start(i)))*1000;
        MassFlow(j,i)=((x(j,3)*210.91)-15.76)*6892.7*7.29659e-6)/c*1000;
        InjCur(j,i)=x(j,4)*10;
    end
end

Main_Injection_Duration_Avg=mean(M_Injection_Duration(1,Start_From:Sample_Size))

%% Compiling Profiles Matrix
for i=Start_From:Sample_Size
    for j=M_Inj_Start:M(i)
        if j<=4100 && MassFlow(j,i)<=1
            MassFlow_Star(j,i)=0;
        elseif j>M_Inj_Start(i)
            if j<=4100 && MassFlow(j,i)<=1
                MassFlow_Star(j,i)=0;
            else
                MassFlow_Star(j,i)=MassFlow(j,i);
            end
        else
            MassFlow_Star(j,i)=MassFlow(j,i);
        end
    end
end

end

%% Averaging Profiles
k=0;
[Q R]=size(MassFlow_Star);

```

```

for j=1:Q
    MassFlow_Average(j)=mean(MassFlow_Star(j));
    Time_ms(j)=j*del_T;
    if MassFlow_Average(j)>0 && k==0
        Ave_Shift = j;
        k=1;
    end
end

for j=1:Q-Ave_Shift
    MassFlow_Average(j)=MassFlow_Average(j+Ave_Shift);
end

%% Correcting Curves

%Find Slope using last and next Iteration
for i=6:length(MassFlow_Average)-5
    Slope(i)=(MassFlow_Average(i+5)-MassFlow_Average(i-5))/del_T;
end

%Find max negative slope Main
Max_Main_Slope=min(Slope(1:1500));

%Find Iteration Index of max negative slope Main
for i=1:1500
    if Slope(i)==Max_Main_Slope
        Max_Main_Slope_Iteration=i;
        break
    end
end

%% New Profile Average Using Slope

for i=1:length(MassFlow_Average)
    if i<Max_Main_Slope_Iteration
        Corrected_Profile(i)=MassFlow_Average(i);
    elseif i>=Max_Main_Slope_Iteration
        Corrected_Profile(i)=Corrected_Profile(i-
1)+Max_Main_Slope*Slope_Factor*del_T;
        if Corrected_Profile(i)<0
            Corrected_Profile(i)=0;
        end
    end
end

%% Integration over Corrected Curve

for i=1:1500
    Int_Sec(i)=(Corrected_Profile(i)+Corrected_Profile(i+1))/2*del_T;
end

Total_MassFlow=sum(Int_Sec)

```

```

%% Print to Text File
fname=('Output.dat');
fid = fopen(fname,'w');
fprintf(fid,'%g\t %g\t
%g\n',Corrected_Profile(1),Total_MassFlow,Main_Injection_Duration_Avg);
for i=2:2000
    fprintf(fid,'%g\n',Corrected_Profile(i));
end
fclose(fid);

%% Plotting Function
figure(1)
plot(Time,MassFlow,'k-',Time,InjCur,'r:')
xlim([0 15])
ymax=max(max(MassFlow))+2;
ylim([-5 ymax])
title('Injection Profile Relative to Injection Command')
xlabel('Time(ms)')
ylabel('Injection Rate (mg/ms)')
grid on

figure(2)
plot(Time,MassFlow_Star)
xlim([0 15])
ylim([-5 ymax])
title('Injection Profile Integrated Section')
xlabel('Time(ms)')
ylabel('Injection Rate (mg/ms)')
grid on

figure(3)
plot(Time_ms,MassFlow_Average)
xlim([0 15])
ymax=max(max(MassFlow))+2;
ylim([-5 ymax])
title('Averaged Injection Profile')
xlabel('Time(ms)')
ylabel('Injection Rate (mg/ms)')
grid on

figure(4)
plot(Time_ms,Corrected_Profile)
xlim([0 15])
ymax=max(max(MassFlow))+2;
ylim([-5 ymax])
title('Corrected Injection Profile')
xlabel('Time(ms)')
ylabel('Injection Rate (mg/ms)')
grid on

%Injection Bench Post Processing for Double Injection
%Author: Anthony Phan
%Written: Dec 23 08
%Version: 6.0

```

```

%Revised by: Justin Callies

%% Clear Matlab
clear all;
close all;
clc;

%% Prompt User for Sample Size and Input Delta Time Acq
Sample_Size=input('How many samples are there? ');
T=input('What is the mean fuel temperature (C)? ');
%P=input('What is the backpressure (psi)? ');
del_T=0.01; %Data Acquisition Time in ms
Slope_Factor=.05;
clc;

%% Calculate Speed of Sound in Fluid
Percent=100; %Biodiesel Percentage
Start_From=1; %Start File Processing From File #)
P=900;

P=P*0.00689475728; %Convert to Mpa
% Constants
C1=-3.5972;
C2=4.6849;
C3=2.3682e-1;
C4=1.4412e-2;
C5=-3.9664e-3;
C6=-1.6236e-2;
C7=8.8429e-4;
C8=1.4570e3;
c=C1*T+C2*P+C3*Percent+C4*T*P+C5*P*Percent+C6*P^2+C7*Percent^2+C8; %Speed of
Sound in m/s

%% Calculation
for i=Start_From:Sample_Size
    %Reading File
    x=load(file_name('100Mpa_140mg_900psi_40pi_35pa_',i));
    [M(i) N(i)]=size(x);

    %Finding Start of Pilot Injection
    for j=1:M(i)
        if x(j,4)>0.3
            P_Inj_Start(i)=j;
            break
        end
    end
    %Finding Pilot Injection Duration
    for j=P_Inj_Start(i):M(i)
        if x(j,4)<=0.19
            P_Inj_Stop(i)=j;
            break
        end
    end
end
end

```

```

P_Injection_Duration(i)=(P_Inj_Stop(i)-P_Inj_Start(i))*del_T;

%Finding Start of Main Injection
for j=P_Inj_Stop(i):M(i)
    if x(j,4)>0.3
        M_Inj_Start(i)=j;
        break
    end
end
%Finding Main Injection Duration
for j=M_Inj_Start(i):M(i)
    if x(j,4)<=0.19
        M_Inj_Stop(i)=j;
        break
    end
end
M_Injection_Duration(i)=(M_Inj_Stop(i)-M_Inj_Start(i))*del_T;

%Calculate Relative Time,Mass Flowrate, and Injection Current
for j=(P_Inj_Start(i)-10):M(i)
    Time(j,i)=(x(j)-x(P_Inj_Start(i)))*1000;
    MassFlow(j,i)=((x(j,3)*210.91)-15.76)*6892.7*7.29659e-6)/c*1000;
    InjCur(j,i)=x(j,4)*10;
end
end

Pilot_Injection_Duration_Avg=mean(P_Injection_Duration(1,Start_From:Sample_Size))
Main_Injection_Duration_Avg=mean(M_Injection_Duration(1,Start_From:Sample_Size))

%% Compiling Profiles Matrix
for i=Start_From:Sample_Size
    for j=1:M(i)
        if j<=4100 && MassFlow(j,i)<=1
            P_MassFlow_Star(j,i)=0;
        elseif j>M_Inj_Start(i)
            P_MassFlow_Star(j,i)=0;
        else
            P_MassFlow_Star(j,i)=MassFlow(j,i);
        end
    end
end

for j=M_Inj_Start(i):M(i)
    if j<=4100 && MassFlow(j,i)<=1
        M_MassFlow_Star(j,i)=0;
    else
        M_MassFlow_Star(j,i)=MassFlow(j,i);
    end
end

for j=1:M(i)
    MassFlow_Star(j,i) = P_MassFlow_Star(j,i)+M_MassFlow_Star(j,i);
end

```

```

end

end

%% Averaging Profiles
k=0;
[Q R]=size(MassFlow_Star);
for j=1:Q
    P_MassFlow_Average(j)=mean(P_MassFlow_Star(j));
    M_MassFlow_Average(j)=mean(M_MassFlow_Star(j));
    MassFlow_Average(j)=P_MassFlow_Average(j)+M_MassFlow_Average(j);
    Time_ms(j)=j*del_T;
    if P_MassFlow_Average(j)>0 && k==0
        Ave_Shift = j;
        k=1;
    end
end

for j=1:Q-Ave_Shift
    MassFlow_Average(j)=MassFlow_Average(j+Ave_Shift);
end

%% Correcting Curves

%Find Slope using last and next Iteration
for i=6:length(MassFlow_Average)-5
    Slope(i)=(MassFlow_Average(i+5)-MassFlow_Average(i-5))/del_T;
end

%Find injection end of pilot
for i=1:length(MassFlow_Average)
    if MassFlow_Average(i)<=0
        Avg_Pilot_Stop=i+10;
        break
    end
end

%Find max negative slope Pilot
Max_Pilot_Slope=min(Slope(1:Avg_Pilot_Stop));

%Find max negative slope Main
Max_Main_Slope=min(Slope(Avg_Pilot_Stop:1500));

%Find Iteration Index of max negative slope Pilot
for i=1:Avg_Pilot_Stop
    if Slope(i)==Max_Pilot_Slope
        Max_Pilot_Slope_Iteration=i;
        break
    end
end

%Find Iteration Index of max negative slope Main
for i=Avg_Pilot_Stop:1500

```

```

    if Slope(i)==Max_Main_Slope
        Max_Main_Slope_Iteration=i;
        break
    end
end

%% New Profile Average Using Slope

for i=1:length(MassFlow_Average)
    if i<Max_Pilot_Slope_Iteration
        Corrected_Profile(i)=MassFlow_Average(i);
    elseif i>=Max_Pilot_Slope_Iteration && i<Avg_Pilot_Stop
        Corrected_Profile(i)=Corrected_Profile(i-
1)+Max_Pilot_Slope*Slope_Factor*del_T;
        if Corrected_Profile(i)<0
            Corrected_Profile(i)=0;
        end
    elseif i<Max_Main_Slope_Iteration
        Corrected_Profile(i)=MassFlow_Average(i);
    elseif i>=Max_Main_Slope_Iteration
        Corrected_Profile(i)=Corrected_Profile(i-
1)+Max_Main_Slope*Slope_Factor*del_T;
        if Corrected_Profile(i)<0
            Corrected_Profile(i)=0;
        end
    end
end

%% Integration Over Corrected Curve

for i=1:Avg_Pilot_Stop
    P_Int_Sec(i)=(Corrected_Profile(i)+Corrected_Profile(i+1))/2*del_T;
end

for i=Avg_Pilot_Stop+1:length(Corrected_Profile)
    M_Int_Sec(i)=(Corrected_Profile(i-1)+Corrected_Profile(i))/2*del_T;
end

Pilot_Total_MassFlow=sum(P_Int_Sec)
Main_Total_MassFlow=sum(M_Int_Sec)
Total_MassFlow=Pilot_Total_MassFlow+Main_Total_MassFlow
%% Print to Text File
fname=('Output.dat');
fid = fopen(fname,'w');
fprintf(fid,'%g\t %g\t
%g\n',Corrected_Profile(1),Total_MassFlow,Pilot_Injection_Duration_Avg,Main_I
njection_Duration_Avg);
for i=2:2000
    fprintf(fid,'%g\n',Corrected_Profile(i));
end
fclose(fid);

%% Plotting Function

```

```

figure(1)
plot(Time,MassFlow,'k-',Time,InjCur,'r:')
xlim([0 15])
ymax=max(max(MassFlow))+2;
ylim([-5 ymax])
title('Injection Profile Relative to Injection Command')
xlabel('Time(ms)')
ylabel('Injection Rate (mg/ms)')
grid on

figure(2)
plot(Time,MassFlow_Star)
xlim([0 15])
ylim([-5 ymax])
title('Injection Profile Integrated Section')
xlabel('Time(ms)')
ylabel('Injection Rate (mg/ms)')
grid on

figure(3)
plot(Time_ms,MassFlow_Average)
xlim([0 15])
ymax=max(max(MassFlow))+2;
ylim([-5 ymax])
title('Averaged Injection Profile')
xlabel('Time(ms)')
ylabel('Injection Rate (mg/ms)')
grid on

figure(4)
plot(Time_ms,Corrected_Profile)
xlim([0 15])
ymax=max(max(MassFlow))+2;
ylim([-5 ymax])
title('Corrected Injection Profile')
xlabel('Time(ms)')
ylabel('Injection Rate (mg/ms)')
grid on

%Injection Bench Injection Delay Calculator for Signle Injection
%Author: Justin Callies
%Written: Apr 21 2009
%Version: 2.0

%% Clear Matlab
clear all;
close all;
clc;

%% Prompt User for Sample Size and Input Delta Time Acq
Sample_Size=input('How many samples are there? ');
del_T=0.01; %Data Acquistion Time in ms
clc;

```

```

%% Calculation
for i=1:Sample_Size
    %Reading File
    x=load(file_name('150Mpa_160mg_900psi_',i));
    [M(i) N(i)]=size(x);

    %Finding Start of Main Injection Current
    for j=1:M(i)
        if x(j+1,4)>x(j,4)
            if x(j+2,4)>x(j+1,4)
                if x(j+3,4)>x(j+2,4)
                    if x(j+4,4)>x(j+3,4)
                        if x(j+5,4)>x(j+4,4)
                            if x(j+6,4)>.5
                                M_Inj_Start_C(i)=j;
                                break
                            end
                        end
                    end
                end
            end
        end
    end

    %Finding Start of Main Injection Flow
    for j=M_Inj_Start_C(i):M(i)
        if x(j+1,2)>x(j,2)
            if x(j+2,2)>x(j+1,2)
                if x(j+3,2)>x(j+2,2)
                    if x(j+4,2)>x(j+3,2)
                        if x(j+5,2)>x(j+4,2)
                            if x(j+20,2)>1.5
                                M_Inj_Start_F(i)=j;
                                break
                            end
                        end
                    end
                end
            end
        end
    end

    %Calculate Injection Delay
    Inj_Delay(i) = (M_Inj_Start_F(i)-M_Inj_Start_C(i))*del_T;
end

% Calculate Average Injection Delay
Ave_Inj_Delay = sum(Inj_Delay)/Sample_Size

%% Print to Text File
fname=('Delay_Output.dat');

```

```
fid = fopen(fname, 'w');  
fprintf(fid, '%g\t %g\t %g\n', Inj_Delay(1), Ave_Inj_Delay, std(Inj_Delay));  
for i=2:Sample_Size  
    fprintf(fid, '%g\n', Inj_Delay(i));  
end  
fclose(fid);
```

## APPENDIX B1. DIESEL SPRAY IMAGING CODES

The following Matlab codes were for the diesel spray imaging studies. A brief discription is provided at the begining of each code. Slight modifciations may have used due to changes within the experiment.

```

%% Vapor Imaging
%   This script opens a string of *.tif files recorded from the iSpeed 2
%   camera and computed the average pixel intensity for each frame.
%
%% Initialize Code

clear; clc;

%% Select Files

home = cd; %Determine home directory
[nameFile,namePath] = uigetfiles; %Select files to open

%% Open Files

cd(namePath); %Make namePath the current directory
avgint = zeros(length(nameFile),1); %Preallocate avgint variable
load('Background.mat');
for ind = 1:length(nameFile)
    nameCurrent = nameFile(ind); %Convert nameFile to cell
    nameOpen = nameCurrent{1}; %Convert nameCurrent to string
    im(:, :) = imread(nameOpen, 'tif'); %Open tif image
    newimg = im-Background;
    avgint(ind,1) = mean2(im); %Find mean intensity value
    maximg(ind,1)=max(max(newimg));
end

%% Create Time Variable

time = [.0001:.0001:0.0001*length(nameFile)]; %Time variable [s]

%% Plot Resulting Mean Values

plot(time,avgint,'r');
xlabel('Time [s]');
ylabel('Mean Intensity [Arb Units]');
title('Aerosol Run 2');

%% Spray Imaging
%   This script opens a string of *.tif files, computes the normalization

```

```

% factor for the cuvette and applies it to the spray image.

%% Initialize Code

clear all;
close all;
clc;

%% Select Files

home = cd; %Determine home directory
[nameFile,namePath] = uigetfiles; %Select files to open

%% Open Files and Compute

cd(namePath); %Make namePath the current directory
avgint = zeros(length(nameFile),1); %Preallocate variable
avgint_cuvette = zeros(length(nameFile),1); %Preallocate variable
for ind = 1:length(nameFile)
    nameCurrent = nameFile(ind); %Convert nameFile to cell
    nameOpen = nameCurrent{1}; %Convert nameCurrent to string
    im(:, :) = imread(nameOpen, 'tif'); %Open tif image
    avgint(ind,1) = mean2(im); %Find mean intensity value
    if ind==1
        background(:, :) = im(:, :);
    end
    cor_image = im(:, :) - background(:, :);

    %Cuvette Matrix
    LC=108; %Left side Cuvette
    RC=152; %Right side Cuvette
    TC=102; %Top side cuvette
    BC=280; %Bottom side cuvette
    cuvette = (im(TC:BC, LC:RC));
    avg_cuvette = mean(transpose(cuvette));
    %avg_nor_cuvette = normr(avg_cuvette);
    max_cuv(ind) = max(avg_cuvette);
    avgint_cuvette(ind,1) = mean2(cuvette);
    avg_nor_cuvette = avg_cuvette / max_cuv(ind);

    %Spray Matrix
    LS=400; %Left side spray
    RS=475; %Right side spray
    TS=102; %Top side spray
    BS=280; %Bottom side spray
    spray = (im(TS:BS, LS:RS));

    %Spray Corrected With Averaged Cuvette (Normalized Beam)
    for i=1:(RS-LS)+1
        for j=1:(BS-TS)+1
            spray_cor(j,i) = spray(j,i) / avg_nor_cuvette(1,j);
        end
    end
end

```

```

figure(1)
clims = [ 1 65535 ];
subplot(3,length(nameFile),ind);
imagesc(cuvette,clims);
axis off
subplot(3,length(nameFile),ind+length(nameFile));
imagesc(spray,clims);
axis off
subplot(3,length(nameFile),ind+2*length(nameFile));
imagesc(spray_cor,clims);
axis off
end

max_max_cuv=max(max_cuv);
for i=1:length(nameFile)
    curvette_nor(i)=max_cuv(i)/max_max_cuv;
end

%% Plot Resulting Mean Values

figure(length(nameFile)+1)
plot(avgint,'r');
xlabel('Image Index');
ylabel('Mean Intensity [Arb Units]');
title('Image Average Intensity');

figure(length(nameFile)+2)
plot(avgint_cuvette,'r');
xlabel('Image Index');
ylabel('Mean Intensity [Arb Units]');
title('Cuvette Average Intensity');

```

## BIBLIOGRAPHY

- Baert, R. S. G., Frijters, P. J. M., Somers, B., Luijten, C. C. M., and Boer, W. d. (2009). Design and Operation of a High Pressure, High Temperature Cell for HD Diesel Spray Diagnostics: Guidelines and Results. *SAE 2009-01-0649*.
- Bosch, W. (1966). The Fuel Rate Indicator: A New Measuring Instrument for Display of the Characteristics of Individual Injection. *SAE 660749*.
- Bower, G. R., and Foster, D. E. (1989). Investigation of the Characteristics of a High Pressure Injector. *SAE 892101*.
- Bower, G. R., and Foster, D. E. (1991). A Comparison of the Bosch and Zuech Rate of Injection Meters. *SAE 910724*.
- Dec, J. E. (1997). A Conceptual Model of DI Diesel Combustion Based on Laser-Sheet Imaging. *SAE, 970873*.
- Dec, J. E., and Canaan, R. E. (1997). PLIF Imaging of NO Formation in DI Diesel Engine. *SAE, 980147*.
- Denso (2005). Common Rail System. *Automotive OEM Products* Retrieved May 26, 2009
- Elert, G. (2005). Ignition Temperature of Diesel Fuel Retrieved May 28 2009, from <http://hypertextbook.com/facts/2005/EileenTang.shtml>
- Espey, C., and Dec, J. E. (1993). Diesel Engine Combustion Studies in a Newly Designed Engine Combustion Studies Using High Speed Visualization and 2-D Laser Imaging. *SAE 930971*.
- Ferguson, C. R., and Kirkpatrick, A. T. (2001). *Internal Combustion Engines Applied Thermosciences*.

- Fuller, J. (2009). *High-Frame-Rate Planar Laser-Induced Fluorescence Imaging of Diesel Sprays using Pule Burst Diagnostics*. Iowa State University, Ames
- Heywood, J. B. (1988). *Internal Combustion Engine Fundamentals*.
- Higgins, B. S., Mueller, C. J., and Siebers, D. L. (1999). Measurements of Fuel Effects on Liquid-Phase Penetration in DI Sprays. *SAE, 199-01-0519*.
- Idicheria, C. A., and Pickett, L. M. (2005). Soot Formation in Diesel Combustion under High-EGR Condition. *SAE, 05FFL-127*.
- Induction coil (2009). Retrieved May 30, 2009, from [http://en.wikipedia.org/wiki/Induction\\_coil](http://en.wikipedia.org/wiki/Induction_coil)
- Karra, P., and Kong, S.-C. (2008). Diesel Emission Characteristics Using High Injection Pressure with Converging Nozzles in a Medium-Duty Engine. *SAE 2008-01-1085*.
- Kim, M. Y., and Lee, C. S. (2007). Effects of a Narrow Fuel Spray Angle and a Dual Injection Configuration on the Improvement of Exhaust Emissions in a HCCI Diesel Engine. *Science Direct, Fuel 86, 2871-2880*.
- Kobayashi, H., Kamimoto, T., and Matsuoka, S. (1981). A Photographic and Thermodynamics Study of Diesel Combustion in a Rapid Compression Machine. *SAE 810259*.
- Linne, M. A., and Parker, T. E. (2006). Ballistic Imaging in the Primary Breakup Region of Diesel Injector Sprays.
- Majewski, W. A., and Khair, M. K. (2006). *Diesel Emissions and Their Control*: SAE International.
- Marcic, M. (2003). Measuring Method for Diesel Multihole Injection Nozzles. *Science Direct (Sensors and Actuators A 107), 152-158*.
- Matsuoka, S. (1996). *The Measurement of Injection Rate* (Vol. 184 Part 3J): Proc. Instn. Mech. Engrs.

- Miller, J., Slipchenko, M., Meyer, T., Jiang, N., Lempert, W., and Gord, J. (2008). Ultrahigh-Frame-Rate OH Fluorescence Imaging in Turbulent Flames Using a Burst-Mode Optical Parametric Oscillator. *Optics Letter*.
- Mueller, C. J., Martin, G. C., Briggs, T. E., and Duffy, K. P. (2004). An Experimental Investigation of In-Cylinder Processes Under Dual-Injection Condition in a DI Diesel Engine. *SAE, 2004-01-1843*.
- Myong, K., Arai, M., Suzuki, H., Senda, J., and Fujimoto, H. (2004). Vaporization Characteristics and Liquid-Phase Penetration for Multi-Component Fuels. *SAE, 2004-01-0529*.
- Negus, C. R., Dale, B. W., Stenhouse, I. A., and McNiven, A. J. (1987). An Investigation of the Confined Combustion Properties of Residual Fuels Used in Marine and Industrial Engine. *CIMAC D-78*.
- Oren, D. C., Wahiduzzaman, S., and Ferguson, C. R. (1984). A Diesel Combustion Bomb: Proof of Concept. *SAE 841358*.
- Parker O-Ring Handbook ORD 5700 (2007). In P. H. Corporation (Ed.). Cleveland, OH.
- Pickett, L. (2007). Constant-Volume Diesel Combustion Retrieved January 30, 2009, from <http://www.ca.sandia.gov/ecn/cvdata/constantVol.php>
- Pickett, L. M., Kook, S., and Williams, T. C. (2009). Visualization of Diesel Spray Penetration, Cool-Flame, Ignition, High-Temperature, and Soot Formation Using High-Speed Imaging. *SAE 2009-01-0659*.
- Pickett, L. M., and Lopez, J. J. (2005). Jet-Wall Interaction Effects on Diesel Combustion and Soot Formation. *SAE, 2005-01-0921*.

- Pickett, L. M., and Siebers, D. L. (2004). Non-Sooting, Low Flame Temperature Mixing-Controlled DI Diesel Combustion. *SAE, 2004-01-1399*.
- Pickett, L. M., Siebers, D. L., and Idicheria, C. A. (2005). Relationship Between Ignition Processes and the Lift-Off Length of Diesel Fuel Jets. *SAE, 05-FFL122*.
- Rife, J., and Heywood, J. B. (1974). Photographic and Performance Study of Diesel Combustion with a Rapid Compression Machine. *SAE 740948*.
- Siebers, D. L. (1998). Liquid-Phase Fuel Penetration in Diesel Sprays. *SAE, 980809*.
- Takamura, A., Fukushima, S., and Omori, Y. (1989). Development of a New Measurement Tool for Fuel Injection Rate in Diesel Engine. *SAE 890317*.
- Tat, M. E., and Gerpen, J. H. V. (2002). Physical Properties and Composition Detection of Biodiesel-diesel Fuel Blends. *ASAE 026084*.
- Upatnieks, A., Mueller, C. J., and Martin, G. C. (2005). The Influence of Charge-Gas Dilution and Temperature on DI Diesel Combustion Processes Using a Short Ignition-Delay Oxygenated Fuel. *SAE 2005-01-2008*.